FINAL SUMMARY REPORT OF
FUEL-DYNAMICS TESTS H2 AND E4

by

R. C. Doerner, A. B. Rothman, A. De Volpi,
C. E. Dickerman, L. W. Deitrich,
D. Stahl, and W. F. Murphy

BASE TECHNOLOGY

UofC-AUA-USERDA

The facilities of Argonne National Laboratory are owned by the United States Government. Under the terms of a contract (W-31-109-Eng-38) between the U. S. Energy Research and Development Administration, Argonne Universities Association and The University of Chicago, the University employs the staff and operates the Laboratory in accordance with policies and programs formulated, approved and reviewed by the Association.

ANL-76-16

ARGONNE NATIONAL LABORATORY
9700 South Cass Avenue
Argonne, Illinois 60439

FINAL SUMMARY REPORT OF
FUEL-DYNAMICS TESTS H2 AND E4

by

R. C. Doerner, A. B. Rothman, A. De Volpi,
C. E. Dickerman, L. W. Deitrich,
D. Stahl,* and W. F. Murphy*

Reactor Analysis and Safety Division

February 1976

*Materials Science Division

TABLE OF CONTENTS

TABLE OF CONTENTS

Page

LIST OF FIGURES

LIST OF FIGURES

LIST OF FIGURES

8

LIST OF FIGURES

LIST OF TABLES

FINAL SUMMARY REPORT OF
FUEL-DYNAMICS TESTS H2 AND E4

by

R. C. Doerner, A. B. Rothman, A. De Volpi, C. E. Dickerman,
L. W. Deitrich, D. Stahl, and W. F. Murphy

ABSTRACT

Results of two failure experiments using LMFBR-type
fuel during simulated unprotected transient overpower acci-
dents are reported and analyzed. In both experiments, a single
fresh fuel pin in a Mark-IIA loop was subjected to a temperature-
limited, step-reactivity irradiation in the TREAT reactor. Total
energy was 490 MJ in Test H2 and 690 MJ in Test E4.

Except for their timing, the sequence of events in the
failure scenario was the same for both tests. Local coolant
boiling began 25-50 msec before failure. Significant upward
fuel flow in the center of the pin started as early as 100 msec
before cladding failure. Cladding failure was due to melting
after contact with molten fuel and occurred at the top of the fuel
column.

Formation of an outlet flow-channel blockage began about
10 msec after failure and was complete by 50 msec. Inlet block-
age began later and was less extensive. No significant amount
of fuel sweepout was observed.

Fuel remains separated into a small group of 50-1000-μm
fragments and a macroscopic group of chunks and clinkers. The
final distribution of fuel remains may have resulted from a de-
layed fuel/steel interaction in the inlet region.

I. INTRODUCTION

Data from two similar fuel-failure experiments (Fuel Dynamics
Tests H2 and E4) are studied and compared in an attempt to identify the fuel-
failure threshold and fuel-movement phenomena. Fuel compositions and ex-
perimental conditions for these tests were selected to simulate behavior of
fresh (zero-burnup) fuel during an unprotected transient overpower (TOP)
accident in the FFTF. Information used in the comparison includes the tran-
sient data recorded during the test, the hodoscope analysis of time-dependent
fuel motion, the posttest metallographic examinations, and the posttest thermal-
hydraulic calculations.

Both tests reported here used single pins in a flowing-sodium environment provided by a Mark-IIA loop. A double-walled evacuated ("adiabatic") fuel holder was used to provide a prototypic coolant-temperature profile at the time of failure. The experiments were performed in the TREAT reactor with step-reactivity inputs that produced temperature-limited transients of sufficient amplitude to cause cladding failure and extensive fuel motion in both experiments.

Test H2 was a failure-threshold test for which a TREAT energy of 490 MW-sec was attained, using a reactivity step of 1.99% Δk/k. A 40% more energetic transient (2.25% Δk/k; 690 MW-sec) was attained for Test E4 to enhance postfailure fuel-movement phenomena. Test fuel-heating rates were not sufficiently different for the two tests to unambiguously identify rate-dependent effects. However, the total energy in Test E4 was sufficient to produce significantly larger amounts of postfailure fuel movements than observed in Test H2.

Basic test data and thermal-hydraulic calculations reported when the tests were performed have been reviewed and reevaluated using methods and techniques learned by experience from the half-dozen loop tests conducted since Tests H2 and E4. Conversion of test signals to flow rates and temperatures, for example, is consistent in the present report, but may not agree in detail with earlier reported values. Identical thermal-hydraulic calculations (except for the appropriate flow, temperature, and power driving functions) allow a direct comparison of fuel, coolant, and cladding temperatures between the two tests up to the time of failure.

Descriptions of the tests, the initial evaluation of the test data and hodoscope results (hodoscope results for E4 are not available), and posttest metallographic examinations have been reported. (See Refs. 1-9 for Test H2 and Refs. 10-17 for Test E4.) The initial slug ejections in Test H2 have been analyzed by Cronenberg.[18] These and other TOP tests are summarized in the literature. (See Ref. 19 for H2 and Ref. 20 for E4 test analysis and summaries. Reference 21 compares various TOP tests.)

A. Overview

Thermodynamic conditions of the fuel and cladding at the threshold of failure are based entirely on calculations. Except for uncertainties in the specific heat and thermal conductivity of the fuel, these calculations provide an accurate thermal history of the fuel up to the time of flow-channel voiding and pin failure. Hodoscope results and flow and pressure data suggest a pattern for pre- and postfailure fuel motion. Certain details of the fuel motion are inferred from other in-pile tests, a number of out-of-pile experiments, and a likely sequence of events that could account for the observed posttest distribution of fuel.

Flow data, supported by posttest calculations, for Tests H2 and E4 suggest that mild boiling existed for 25-50 msec prior to failure; that significant amounts of upward fuel movement began as early as 100 msec before failure (H2 hodoscope observations); that blockage of the outlet flow channel began within ~10 msec after failure and was essentially completed by ~50 msec; that inlet blockage began later and was less dense than outlet blockage; and that the posttest fuel remains separated into (1) a fragmentation group size (50-1000 μ) and (2) a macroscopic group of chunks or clinkers that were deposited on the holder walls by a type of splattering or sputtering process. Fuel motion appears to have been caused by two identifiable mechanisms: an initial release of a small quantity of molten fuel at the failure threshold, and a redistribution of large quantities of fuel and steel several hundred milliseconds after the initial failure. (Delayed events in the S test series range from 2 msec, in S8, to 2420 msec, in S4, with an average of ~300 msec. In H2, a major event occurred 200 msec after failure; in E4, a secondary event occurred 65 msec after failure.) The initial release led to the observed interaction between molten fuel and two-phase coolant flow, and accounts for the fuel fragmentation. The delayed reaction may be a fuel-steel interaction that could account for the final distribution of macroscopic chunks. There was no evidence of significant fuel sweepout beyond the pin plenum during either the initial fragmentation or the delayed fuel redistribution. However, a large fraction of the available fuel moved above the original fuel region. Neither was there any evidence of massive and extensive fuel slumping or flow toward the inlet. No energetic fuel-coolant interactions (FCI's) occurred.

Prefailure boiling was identified by a greater volume of sodium flowing out of the channel than the volume that entered. Less then 1 cm^3 of this volume difference can be accounted for by expansion of the fuel pin and sodium on heating. Bubble collapse by vapor condensation was identified by small but measurable pressure pulses at the outlet.

Several factors have been identified that can play important roles in cladding failure. One of current interest is the behavior of the liquid film left on the cladding surface during boiling. The film may vaporize or be swept upward with the liquid-vapor flow. Fauske estimated[22] that it takes 20-30 msec to dry out a local region of the cladding, depending on the film drag characteristics. Work by Henry and Grolmes[23] supports this estimate. Overheating and meltthrough immediately follow cladding dryout. Because of the upward flow of coolant vapor, the region where boiling is initiated is near the top of the fuel column and possibly just behind (downstream) or under the spacer wire where a stagnation region may exist.

Both the test data and posttest calculations for H2 and E4 suggest the prefailure boiling time was ~50 msec and not strongly dependent on the rate of fuel-pin heating. In both tests, ~30 cal of heat energy were transferred to the coolant per centimeter of pin length from the time boiling began to the time of failure. During this same time, more than three times as much heat energy

was generated in the E4 test fuel, accounting for the much higher fuel temperature and melt fraction at failure. A large thermal gradient was produced in the outer surface layers of the fuel during the test as failure conditions were approached. Some radial gradient is expected during rapid transient heating due to the finite thermal-relaxation time characteristic of the low conductivity of fuel and gap, and the high thermal conductivity of the cladding and sodium. A significant portion of the temperature gradient is caused by power spiking at the fuel surface in these tests (caused by the partially filtered thermal-neutron spectrum of the TREAT reactor and the high self-shielding of the test fuel). Because of the power depression at the center of the fuel, initial fuel melting in the test transient began in radial nodes that were 10-20 mils in from the surface and propagated inward toward the center. Only in E4 was there sufficient energy to melt the fuel pellet completely before failure.

During the early stages of prefailure melting, the cladding and outer shell of solid fuel formed an effective container that limited radial fuel motion. Consequently, the prefailure fuel motion after melting began was upward against or around the insulator pellet, spacer tube, and plenum spring. In H2, melting began 180 msec before failure, the time at which upward fuel motion was first observed in the hodoscope data. Melting began 110 msec before failure in E4, but there are no hodoscope data to confirm upward fuel motion at this time.

Thermodynamic calculations and the posttest examinations suggest that, during the early stages of fuel melting and upward flow, cracks in and between the fuel pellets were "healed" or sealed, and the major escape path was at the cold interface with the insulator pellet. Molten fuel flowed against and around the insulator pellet, moved upward, and caused cladding melting from the inside. Sufficient heat energy was transferred to the cladding to initiate local coolant boiling in the flow channel. About 30 msec after boiling began, the liquid-sodium film on the cladding dried out, the cladding melted and molten fuel was released into the flow stream. Posttest findings in E4 of once-molten fuel (that did not contain any steel diluent) in the pin-plenum region suggest fuel movement prior to cladding melting.

Current analytical FCI models[26-30] require empirical adjustment of parameters to obtain reasonable predictions of the magnitude of pressure pulses and velocities of the ejected sodium slugs. Most analytic models of the FCI process assume a series of equilibrium thermodynamic states. Recent improvements include pressure and temperature gradients in the mixing zone, and the effects of vapor blanketing of fragmented fuel. Various models assume that the mass and temperatures of released fuel are known, that the heat-transfer rate (or heat-transfer surface) increases in some known way with time; that all released fuel instantaneously fragments and is swept out of the mixing zone with the coolant flow; or that the mixing zone is bounded by rigid walls and the sodium vapor pressure is the sole driving force for slug ejection.

As suggested by Cronenberg[18,31] violent transition boiling during the initial fuel release is another likely cause of fragmentation. (Other mechanisms, such as excess strain energy in the surface layer of the fuel globules as they freeze, have also been considered.) The process of boiling and fragmentation lasted 5-10 msec, after which the flow channel was effectively voided and possibly increased in volume by $2\frac{1}{2}$ times as the walls of the fuel holder ruptured. (A small amount of noncondensable bond gas may be released from the fuel pin that serves to retard rapid heat transfer to coolant, and to "cushion" vaporization pressure pulses and thus prevent an energetic FCI.) The fragments, especially the smaller and lighter ones, were carried with the liquid-vapor flow and tended to freeze on the cold surfaces in the upper regions of the flow channel to start flow blockage at the outlet. Blockage without accompanying sweepout has been demonstrated in some out-of-pile tests by Ostensen et al.[32] A certain amount of mechanical packing was evident in the posttest examination.

Fuel released after channel voiding interacted with the vapor stream and a thin liquid film on the holder-wall surfaces. Subsequent fragmentation and vapor production were limited accordingly. Fuel ejected from the pin melted the inner holder wall locally and froze on the outer wall, accounting for the observed porous structure found in the posttest examinations. Some liquid reentry occurred, but did not produce an energetic secondary FCI. Residual vapor and some noncondensable gas prevented a sodium hammer during reentry.

Fuel blockages of a porous nature were found at the inlet, and, although they contained a higher concentration of steel than the outlet blockage, there was no evidence that they were caused by extensive cladding or fuel flow (slumping).

No measurable quantity of fuel fines could be reclaimed from the main loop sodium in either Test H2 or E4, suggesting that most of the small-fragment movement was upward, with freezing on the upper structure and packing, possible in layers, to complete the outlet blockage, similar to the results observed by Ostensen et al.[32] in out-of-pile tests. Large-fragment motion was limited by the small size of the flow channel, especially in the region of the spacer wire and (near the top of the flow channel) of the thermocouple lead.

B. Relation to Hypothetical FFTF Accident

A number of power histories are available for the hypothetical FFTF unprotected overpower accident, depending on the Doppler and void coefficients used, and the magnitude of the reactivity coefficients for fuel and coolant movements. Tests H2 and E4 were performed before the programmable TREAT control system was available. Transient shapes for these tests were bursts specified by the total energy release rather than by the rate of energy addition. Consequently, rates of fuel-pin heating cannot be directly identified with FFTF heating rates during reactivity ramp accidents.

HEDL has provided calculated fuel energy and cladding-temperature histories for a hypothetical $3/sec unprotected transient overpower accident in FFTF.[33] Figure 1 compares these calculations for a high- (12.3 kW/ft) and a low-power pin (9.1 kW/ft) to those of the experiments. Conditions at the time of failure are reasonably prototypic, but the prefailure rates of change are more characteristic of $6-10/sec accidents. Equilibrium conditions were being approached at the time of failure in Test H2 and, hence, it is characteristic of a scram-protected accident. Test E4 is clearly in the unprotected-accident class at the time of failure.
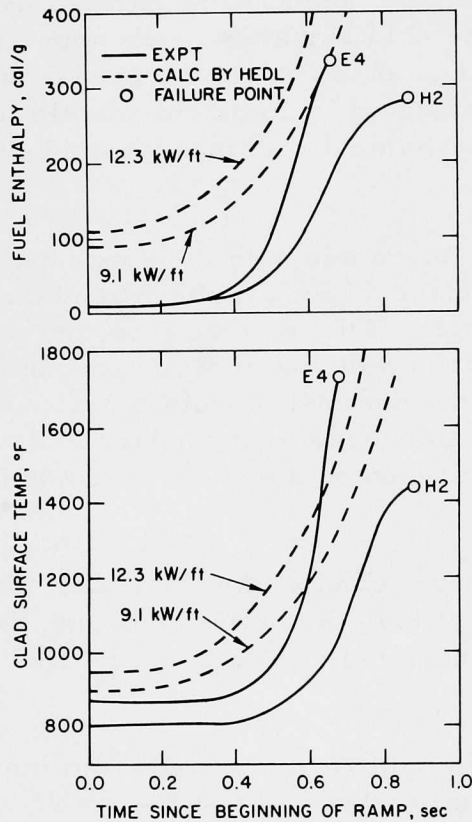
Fig. 1

Thermal-history Comparison between Experiments and Calculated $3/sec Unprotected TOP Accident in FFTF. Calculations were performed by HEDL.[33] Fuel enthalpy and cladding temperature for the experiments were calculated by the COBRA-III code using the measured test geometry and flow conditions, and the TREAT power as a driving function. "Zero" time for the experiments is taken as the time when the reactor power reaches 1 MW (see Figs. 4 and 5).

II. TEST SPECIFICATIONS

Tests H2 and E4 were conducted in Mark-IIA loops at the TREAT facility on June 11 and November 17, 1970, respectively. Extensive descriptions of TREAT[34-37] and the loop[38-40] have appeared in the literature. Only the particulars relevant to the two tests are given here.

A. Experiment Description

For each test, a single fuel pin was supported in the Mark-IIA loop by an adiabatic fuel holder. The loop fits into a 4 x 8-in. secondary-containment can having an inner liner of B_6Si filter material.[41,42] The entire assembly replaces the two central fuel elements in the TREAT core. Test signals are amplified and recorded on magnetic tape in the instrument room of the reactor building, and on strip charts and visicorders in the TREAT control room. Final adjustments of the sodium flow and the loop temperature are made just before the test, as are the loop instrument response and calibration measurements. The tests were performed remotely from the TREAT control room. During the test, the loop heaters were turned off.

B. TREAT Loading

For Test H2 (Transient 1317, Loading 554), the 19 x 19-in. TREAT core array was loaded with 277 standard fuel elements, 16 control-rod elements, 9 slotted fuel elements, 2 slotted aluminum-clad reflector elements, 23 Zircaloy-clad reflector elements, and 32 aluminum-clad reflector elements, as shown in Fig. 2. Each TREAT control or transient rod shown in Fig. 2 consists of a pair of control elements driven as a single unit.
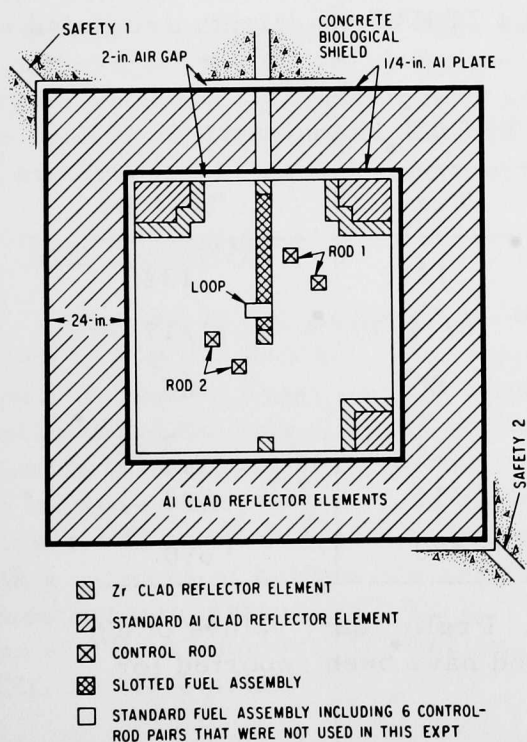
Fig. 2

TREAT Core Loading for Test H2 (Transient 1317). Control rods (rods 1 and 2) are moved as a pair. In this loading, the cold critical position of rod No. 2 was 26.88 in. with all the other rods in their most reactive state (completely withdrawn). With rod No. 2 in its most reactive position (full in) the critical position of rod No. 1 was 16.00 in.

The core loading for Test E4 (Transient 1346, Loading 588) is shown in Fig. 3. In this loading, there were 285 standard fuel elements, 16 control elements, 9 slotted fuel elements, 2 slotted aluminum-clad reflector elements, 21 Zircaloy-clad reflector elements, and 26 aluminum-clad reflector elements.
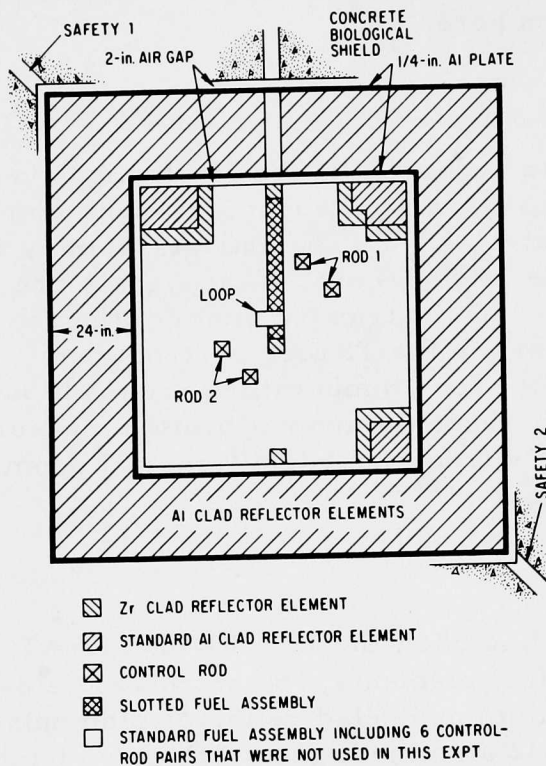
Fig. 3

TREAT Core Loading for Test E4 (Transient 1346). In this loading, the cold critical position of rod No. 2 was 13.57 in. with all the other rods in their most reactive state (completely withdrawn). With rod No. 2 at 40 in., the critical position of rod No. 1 was 15.9 in.

C. TREAT Transient

Summary results for the H2 and E4 TREAT transients are listed in Table I.

TABLE I. Summary of TREAT Transients

	Test H2	Test E4
Transient No.	1317	1346
Date	6/11/70	11/17/70
Initial Period,[a] msec	80	66
Reactivity, % $\Delta k/k$	1.99	2.25
Core Temp Rise, °C	115	143
Integrated Power,[b] MW-sec	490	690

[a]Determined from Figs. 4 and 5. Preliminary values of 69 and 58 msec for the initial period have been reported for H2 and E4, respectively.

[b]Numerical integration of power.
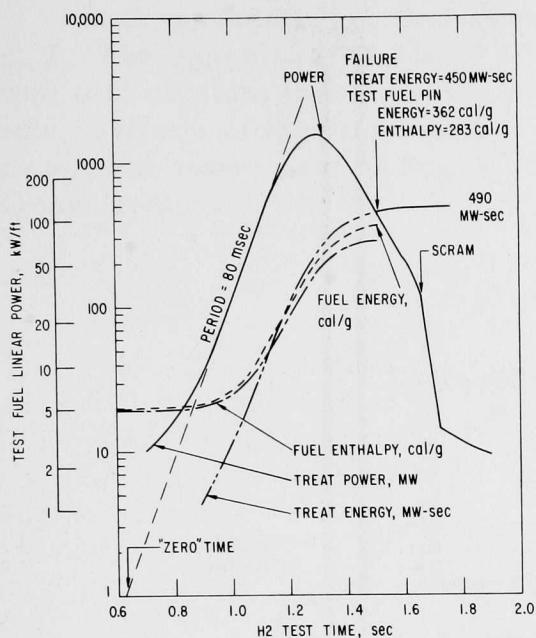
Fig. 4. Power and Energy History for Test H2. TREAT energy is the integral of the power, and fuel energy from fission is the product of the TREAT energy and the calibration factor. Test–fuel enthalpy was calculated by the COBRA-III code using the power history as a driving function. The left scale is the fuel power in kW/ft at the hottest axial node.
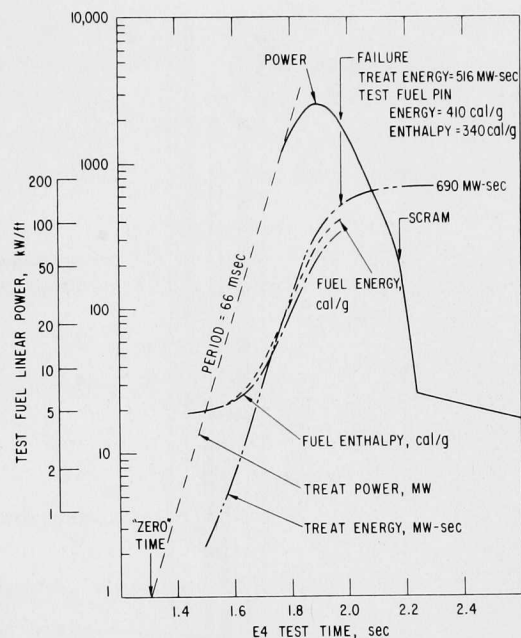
Fig. 5. Power and Energy History for Test E4. TREAT energy is the integral of the power, and fuel energy from fission is the product of the TREAT energy and the calibration factor. Test–fuel enthalpy was calculated by the COBRA-III code using the power history as a driving function. The scale on the right represents the test–fuel power in kW/ft at the hottest axial node.

Values for the integrated power as reported by TREAT operations are averages recorded on the TREAT strip chart (determined from the OSCAR graph reader) for "Integrator #1." These values are within 5% of the integrated power recorded on the data tape, but 13% (E4) and 18% (H2) lower than obtained by numerical integration of the power trace. To be consistent, the power history as recorded on the magnetic tape and the numeric integral of this history are used in all the posttest calculations. Power and energy histories for the H2 and E4 transients are shown in Figs. 4 and 5.

D. Test Geometry

A view of the loop with an exploded view of the fuel pin and holder is shown in Fig. 6. Sodium flow is controlled by an electromagnetic Annular Linear Induction Pump (ALIP) whose pumping capacity is manually or program controlled at the loop control console. Flow is downward through the pump and upwards through the test section and fuel holder. An overflow pipe located 2.5 in. above the pump return leg maintains a constant sodium head in the upper plenum. The approximately 525-cm^3 volume of gas above the plenum is filled with a mixture of helium and argon gas at ~0.9 atm at STP and at ~2.1 atm at operating temperature (~800°F). (The fueled test section was loaded into the loop at TREAT under a flowing argon atmosphere. Atmospheric pressure at INEL is ~12.8 psia.)

18
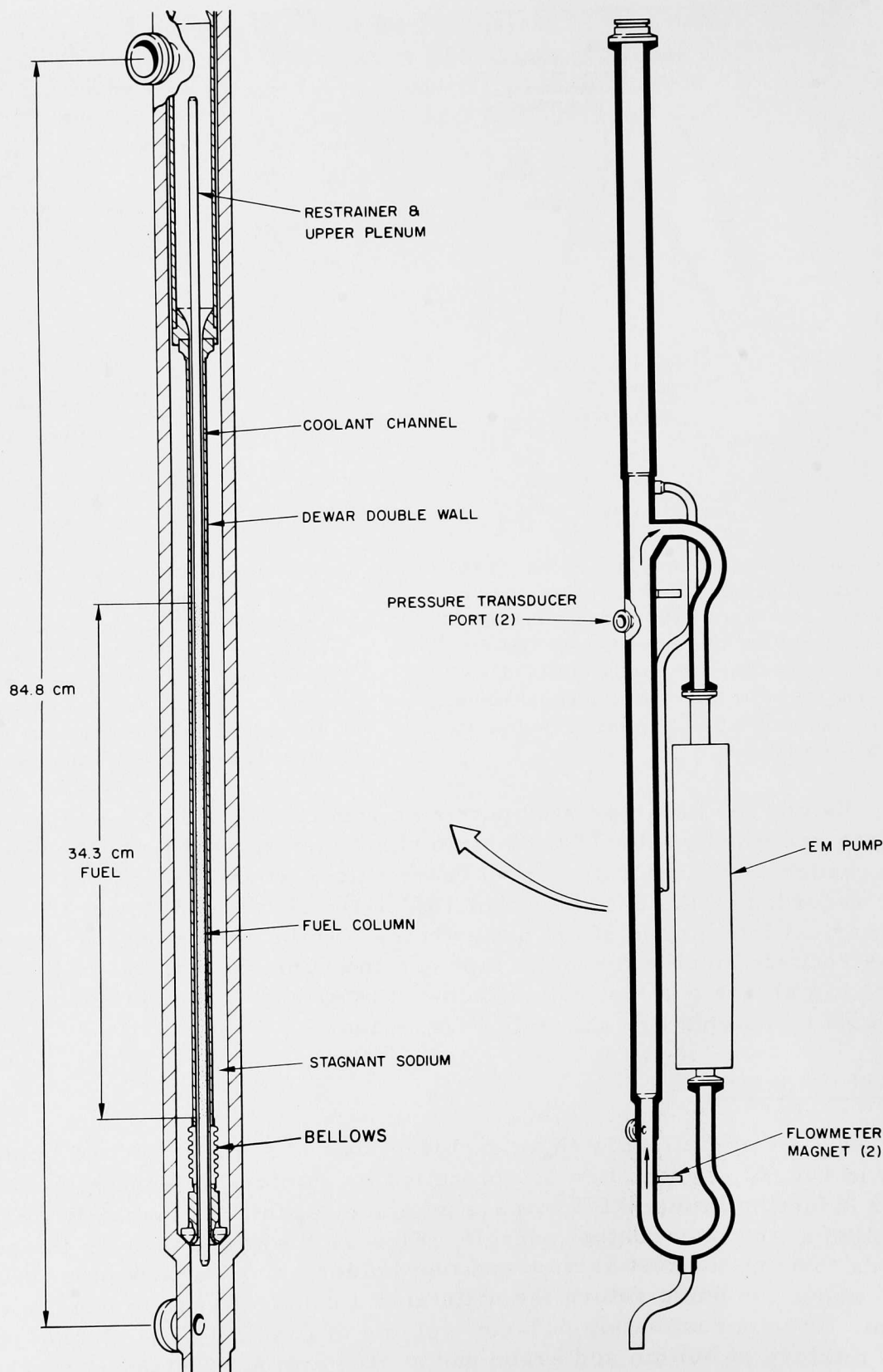
Fig. 6. Mark-II Loop for TREAT Tests. Sodium flow is upward inside the evacuated double-wall Dewar. The upper flowmeter is just above the upper pressure–transducer port, and the lower pressure port is just above the lower-flowmeter magnet. The restrainer and upper plenum refer to the spacer tube and holddown spring above the fuel pellets within the pin cladding. ANL Neg. No. 900–436.

A cross-sectional view of the test at the TREAT midplane is shown in Fig. 7. The upper part of Fig. 7 illustrates the general arrangement of the pump, test section, thermal-neutron filter, and the adjacent TREAT fuel elements. Details of the test section, filters, and secondary containment can are shown in the lower part of Fig. 7. The outer sodium annulus is a region of stagnant sodium.
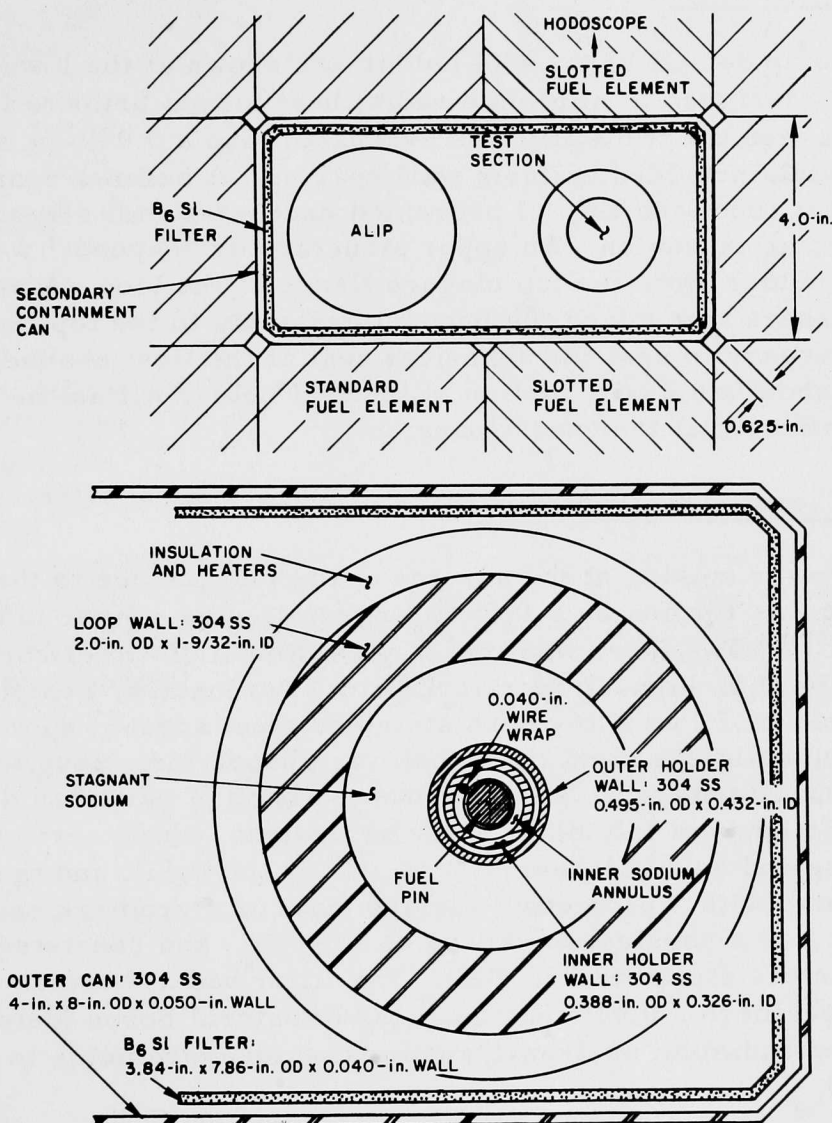
Fig. 7. Cross Section of Loop in TREAT at Axial Centerline. Top view shows relative locations of the test section, the sodium pump (ALIP), the B_6Si thermal-neutron filter, and the adjacent TREAT fuel elements. Details of the secondary containment can, the filter, and the test-section cross section are shown in the lower figure.

A dump tank connected through a nickel burst disk to the bottom of the loop (not shown in Fig. 6) provides an expansion volume if loop pressures should become excessive. The disk rupture rating is 2800 psi at 500°C. A

severe FCI with peak pressures ~250-500 atm lasting several microseconds would rupture the burst disk even though such an event may go undetected by the pressure transducers due to their finite time response. Since the disk did not rupture in either Test H2 or E4, it is concluded that a severe FCI approaching the thermodynamics limit did not occur.

1. Fuel Holder

Some details of the fuel holder are shown at the lower part of Fig. 7. It was designed to minimize radial heat losses prior to fuel failure. The space between the two walls was evacuated, and a 0.040-in. spiral wire between the walls provided uniform wall spacing. A bellows near the lower end of the outer tube (see Fig. 6) prevented excessive wall stress due to differential thermal expansion. An upper structure or "bayonet" was used to hang the fuel holder from the top closure flange of the loop. A series of Belleville washers that joined the bayonet assembly to the top flange provided the force necessary to seat the spherical seal at the flow-channel inlet. They also allowed about a 0.25-in. motion of the fuel holder within the loop to accommodate differential thermal expansion.

2. Thermal-neutron Filters

Power spiking at the surface of the fuel pin due to thermal-neutron self-shielding was limited by a B_6Si filter installed as a liner in the outer containment can.[41,42] The filter was made by painting a 50-50 mixture of B_6Si and Pyromark Type H.E. high-temperature paint (Trademark, Tempil Division, South Plainfield, N.J.) on a 16-mesh stainless steel screen, spot-welded to a 0.025-in.-thick stainless steel liner that was shaped for a snug fit inside the secondary containment can. After the base coating of paint had dried, the surface was polished evenly down to the grid wires (which served as a thickness reference and as a mechanical support for the B_6Si), and the shield was baked and coated with a protective surface layer of Pyromark paint. The finished filter has a physical thickness of 0.040 in., and consisted of 25% Type 304 stainless steel and 75% B_6Si. The filter had a thermal-neutron absorption equivalent to a 0.019-in. thickness of natural boron (determined by thermal and epicadmium neutron-transmission measurements in plane geometry[41,42]).

E. Fuel Pins

Fuel used in the tests were taken from a group of pins fabricated for EBR-II irradiation in the PNL-17 subassembly. The physical properties of the pins are listed in Table II. Small differences in composition and pellet densities were neglected in the neutronics calculation. Isotopic enrichments and atom densities are listed in Table III.

TABLE II. Properties of the Fuel Pins

	H2	E4
Pin Identification	PNL-17-42	PNL-17-43
Density		
Smeared, % TD[a]	88.94	88.04
Pellet, % TD[a]	93.25 ± 0.29%	92.84 ± 0.28%
Fuel Pellets		
Weight, g[a]	68.512	67.628
Length, in.	13.560	13.523
Diameter, in.	0.197	0.197
Composition		
wt % plutonium	22.1	22.0
wt % uranium	66.0	66.2
Off-gas[b] at 1600°C, cm^3/g	0.035 ± 0.005	0.05 ± 0.02
H_2O at 800°C, ppm	11 ± 5	9 ± 2
Carbon, ppm	<50	<50
Oxygen-to-Metal (O/M) ratio	1.9640	1.9612
^{235}U in U, %	65.2 ± 0.2	65.5 ± 0.2

[a]TD = 11.09 g/cm^3.
[b]3 wt % carbowax binder added from 20 wt % solution sintered in argon-8% hydrogen atmosphere.

TABLE III. Fuel-pellet Enrichment and Atom Density

Isotope	Enrichment, wt %	Atom Density, 10^{20} atoms/cm^3
^{234}U	0.665 ⎫	0.74
^{235}U	93.18 ⎪ in UO_2	114.8
^{236}U	0.262 ⎪	0.32
^{238}U	5.89 ⎭	58.48
^{238}Pu	0.035 ⎫	0.02
^{239}Pu	86.56 ⎪	49.56
^{240}Pu	11.61 ⎬ in PuO_2	6.62
^{241}Pu	1.65 ⎪	0.94
^{242}Pu	0.146 ⎭	0.08
^{16}O		458.8

Before TREAT exposure, two modifications were made to the pins. The original 0.054-in. spiral wire wrap was removed and replaced by a 0.040-in. Type 316 stainless steel wire in order to provide a prototypic ratio of fuel-to-coolant cross section. The pins were also shortened to fit into the Mark-IIA test section. Pins were clad with 0.015-in.-wall Type 316 stainless steel tubing (ASTM A-213 as modified; 20% cold-worked) of (0.230 ± 0.001)-in. OD. Fill gas was helium of 1 atm plus 1 cm^3 of xenon tag gas. The total volume of the pin plenum, including the gap gas, was 5.19 ± 0.10 cm^3. A schematic assembly of the fuel pin in the flow channel is shown in Fig. 8.

F. Power Calibration

A calibration factor of 3.3 W/g of oxide per MW of TREAT power was used for both tests. A somewhat lower value (3.1 W/g-MW) was measured previously for Test H1.[43] Excellent agreement has been reported between measured coolant temperatures for that test and SAS-1A calculations.[44] Corrections for differences between the pin used in H1 and the PNL-17-type FFTF pin gave the higher (3.3 W/g-MW) value for the present tests. Later transport calculations supported the 3.3-W/g-MW value for Tests H2 and E4.

G. Instrumentation

Instrumentation for detecting outlet pressure and flow velocity was attached to the loop body just below the pump return. A corresponding instrumentation section was located at the lower end of the test section. Locations of the test instrumentation are shown in the schematic view of the flow path (Fig. 8).

Three Chromel-Alumel grounded-junction type of thermocouples were located as shown in Fig. 8. They were of 0.040-in. OD and had Type 316 stainless steel sheaths. The reference junction temperature was held at 150°F. During both tests, thermocouple TC-3, at the top of the fuel column, failed by meltthrough when molten or hot fuel was first deposited on the junction. The expected temperature at failure was 2550°F and the thermocouple characteristic response time was ~30 msec.

Sodium flow velocity was monitored by electromagnetic sensors operated with 1.0 A of magnet current. The output signals for a fixed pipe size, magnetic field strength, and resistivity ratio of fluid to wall material were linearly proportional to the flow velocity. Flow detectors were calibrated by passing a known weight of sodium through a mockup of the inlet-flow detector region of the loop during a measured time interval. Results of these calibrations for the lower detectors corrected for density gave a flow-volume sensitivity of 630 cm^3/sec-mV of output signal. The upper flow detector was calibrated against the lower detector during steady-state flow conditions. A volumetric flow calibration was used to avoid the problems of varying cross-sectional flow areas in different regions of the flow path. Flow-signal amplifiers were set for full-scale readings of 1260 and 1050 cm^3/sec for the H2 and

A. Lower end cap of fuel pin, Type 316 SS.

B. Spherical seat of fuel holder. This defines the inlet to the flow channel.

C. Locking pin to fix test fuel in holder; 0.070-in. diameter, Type 304 SS.

D. Inner–fuel–holder wall; 0.388-in. OD x 0.326-in. ID, Type 304 SS.

E. Outer–fuel–holder wall; 0.495-in. OD x 0.432-in. ID, Type 304 SS.

F. Evacuated wall cavity.

G. Fuel-pellet stack; 0.194-in. OD x 13.5 in. long; See Tables II and III for fuel properties and composition.

H. Insulator pellets; natural UO_2, 0.194-in. OD x 0.5 in. long.

I. Spacer tube; 0.187 ± 0.002-in. OD x 0.014 ± 0.001-in. wall, Type 316 SS.

J. Spacer–tube end cap; 0.062-in.-dia hole, 0.187 in. long, Type 316 SS.

K. Compression spring; 0.194 ± 0.002-in. OD x 0.025-in.-dia wire, 7-in. full length, 112 coils, Type 302 SS.

L. Top end cap of fuel element; 0.812 in. long, Type 316 SS.

M. Flow–channel cross-sectional area above TC3 is 0.0407 in.^{2} (0.262 cm^2).

N. Flow–channel cross-sectional area above TC3 is 0.0394 in.^{2} (0.254 cm^2).

O. Inlet flow area is 0.4418 in.^{2} (2.85 cm^2).

P. Outlet flow area is 0.7438 in.^{2} (4.80 cm^2).

Q. Plenum flow area is 0.7854 in.^{2} (5.07 cm^2).

Fig. 8. Schematic Flow Path and Pin–assembly Diagram

E4 tests, respectively. During the E4 test, the outlet-flow detector signal exceeded full scale of the recording channel during the initial slug ejection and during the first reentry event. Flow rates during these periods were estimated from the time derivatives of the measured data on either side of the flow peak.

Pressures at both ends of the flow channels were monitored by unbonded strain-bridge-type Statham transducers mounted on the ends of NaK-filled standoff tubes. Space limitations did not allow mounting the pressure transducers directly on the loop. The NaK coupling also served to thermally isolate the strain bridge from the loop body. Full-scale settings were 300 and 1830 psi for Tests H2 and E4, respectively.

H. Initial Conditions

Steady-state flow velocity through the flow channel was set at 6.3 m/sec in H2 and at 5.4 m/sec in E4. Initial sodium temperatures were 800°F for H2 and 850°F for E4. In the subsequent analysis of the transient flow and temperature data, it was assumed that the thermocouples, pressure transducers, and flow detectors were not radiation-dependent, even though some later tests suggest this not to be the case. An apparent shift in the pressure-data baseline appears to be due to a thermal sensitivity.

III. TEST DATA FOR H2

The original digitized flow data for Test H2 were processed through a low-pass filter, and the rapid flow transients were filtered out. The 60-Hz signal superimposed on the dc flow signal was removed by a least-squares fitting routine. In the absence of the magnetic tape with the analog test signals, the flow data during rapid flow changes were read point by point from the visicorder record and superimposed on the digitized data.

Pressure pulses were generally too short (~1 msec) to be recorded in the digitized data. Pulse amplitudes and shapes were read from the visicorder record and hence have an estimated error of ±5 msec in timing. Shifts in the base line ("zero setting") due to temperature effects introduced an estimated ±25-psi uncertainty in the pressure-pulse amplitude.

A. Flow and Pressure Data

Only data for the lower (inlet) pressure transducer are available for H2, since the channel for the upper transducer was inadvertently left connected to the calibration test signal during the transient.

Figure 9 shows inlet and outlet flow rates (with the 60-Hz signal removed) and lower pressure data (not including the base line shift). Test-section velocity is the volume flow rate divided by the cross-sectional flow area (0.262 cm^2) below TC3 (see Fig. 8). Small apparent differences between inlet and outlet flow up to 1.46 or 1.47 sec may be due to a temperature- and/or radiation-dependent change in upper-flow-detector sensitivity. (Some of this difference results from fuel-pin and coolant expansion due to heating.)
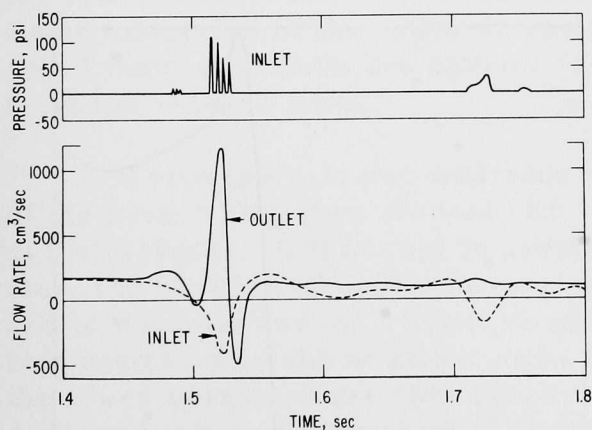
Fig. 9

Flow and Pressure Data for Test H2. Steady-state flow at 1.40 sec is 165 cm^3/sec, and velocity through the test section is 629 cm/sec. Shift in baseline of pressure data has been removed. Outlet pressure data was lost. The small oscillations in the postfailure flow (~20 cps) are characteristic responses of the loop to boiling. The inlet ejection from 1.71 to 1.74 sec is possibly due to a fuel-steel interaction.

Figure 10 shows the integrated inlet and outlet flow volumes since zero test time. For a well-defined vapor bubble, the integrated flow is a measure of the position of the liquid-vapor interface with time. Differences between the liquid volumes into and out of the test section constitute the void (see Fig. 11).
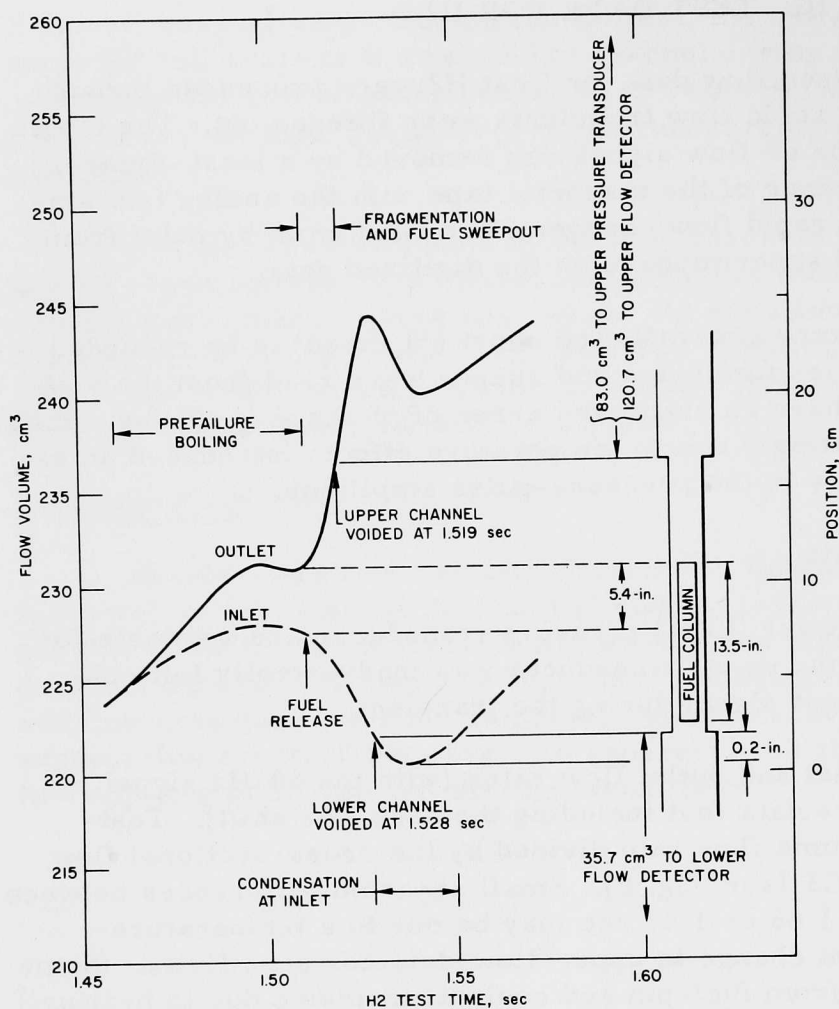
Fig. 10

Integrated Inlet and Outlet Flows for Test H2. For a well-defined vapor separating the liquid in the flow channel into an upper and lower head, these curves represent the position of the liquid-vapor interface. The relative locations of the fuel column and flow channels are shown on the right side of the figure.

Fig. 11

Void-growth Curve. The apparent negative void before boiling begins is a measure of fuel-pin and sodium expansion on heating.
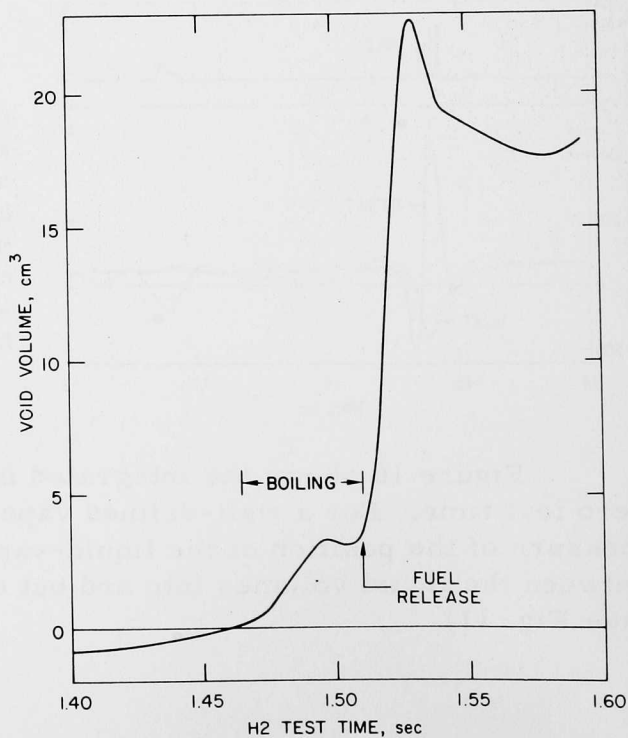
A definite change in the void-growth rate between 1.46 and 1.47 sec
is noted in Fig. 11. This is attributed to mild boiling at the cladding surface
in the region of the upper insulator pellet and is consistent with the cladding
temperatures calculated at 1.465 sec. As the boiling region grew radially and
axially, the void grew (see Fig. 11) at an approximately linear rate of 133 $cm^3/$
sec from 1.47 to 1.495 sec (that is, for 25 msec). During the period of pre-
failure boiling, the flow was two-phase, and the integrated flow volume of
Fig. 10 does not represent the mixing-zone interfaces. Differences between
the two integrated flow volumes, however, do correctly measure the total void.

At 1.50 sec, the bottom liquid-void interface no longer moved upward
(see Fig. 10), indicating that the vapor fills the complete cross-sectional flow
area. At the same time the inlet flow (see Fig. 9) reversed direction.

From 1.48 to 1.502 sec, the sodium vapor, carried upward with the
flow stream, condensed, accounting for the decrease in outlet flow (see Fig. 9).
Vapor-bubble collapse is evident by the small (<10 psi) but observable re-
sponse in the pressure trace from 1.485 to 1.495 sec.

The simultaneous occurrence of a large pressure pulse (120 psi) and
sodium ejection from both ends of the flow channel as slugs at 1.51 sec is
taken as the time for initial cladding failure and release of molten fuel.
A thermal interaction between the molten fuel and the two-phase coolant flow
(or, if the channel is voided at the point of fuel release, between the fuel and
the liquid film on the holder walls) is a mechanism for fuel fragmentation and
coolant ejection as a slug. Cronenberg's analysis[18] of fragmentation due to
transition boiling may not be directly applicable in this case, since he studied
molten-fuel ejection into a homogeneous liquid-flow channel. Nevertheless,
the transient thermal interaction leads to fragmentation and vapor expansion.
Rapid expansion of the vapor drives the upper and lower liquid-sodium slugs
out of the test section and carries (sweeps) the freezing fuel fragments away
from the release point.

From the void and interface curves of Figs. 10 and 11 only one-fourth
of the 23-in.-long flow channel (3.6 cm^3 of void) is filled with vapor at the time
of fuel release. If this void is assumed to be near or at the top of the fuel col-
umn, the position of the liquid-void interface relative to the fuel-release point
and to the inlet and outlet sodium plena can be determined. A sketch of the
test geometry is shown at the right of Fig. 10. The figure also indicates that
the lower portion of the flow channel is voided at 1.528 sec. After this time,
further downward movement of the mixing-zone interface is restricted by
condensation as the vapor mixes with the relatively cold sodium at the inlet
plenum.

Fragmentation and the major amount of upward postfailure fuel
motion probably occurred during the 10-msec period from 1.51 to 1.52 sec.
After that time, not enough liquid remained for an FCI to cause fuel fragmen-
tation. Downward fuel movement and slumping can occur up to 1.55 sec, when
liquid reenters the flow channel.

Four pressure pulses of decreasing amplitude were recorded between 1.515 and 1.53 sec. They probably correspond to a single event in the mixing zone at the time of fuel release. Transducer response to a single pressure pulse is known to exhibit characteristic damped oscillations.[45] Each pulse may also represent separate sequential coolant-vapor events that decrease in magnitude because of the decrease in available liquid in the mixing zone. An apparent 5-msec delay between the first pulse (at 1.515 sec) and the fuel-release time (1.510 sec) can be accounted for by the ±5-msec timing error and by the finite propagation velocity of the compressional wave front through the ~44 cm of two-phase coolant separating the mixing zone (assumed centered 1.75 in. below the top of the fuel) and the lower pressure transducer. From 1.528 till 1.550 sec, the entire fuel-column length is blanketed with vapor. There are no data from which the downward progression of cladding melting can be inferred directly. Probably, cladding melting also propagated downward at the same rate as the voiding, but delayed by ~20 msec to allow for film dryout.

Mixing-zone pressures during the 10-msec fragmentation time (1.51-1.52 sec) retarded fuel release during initial failure. After the slugs began to leave the flow channel, the mixing-zone pressures dropped and more fuel was ejected. Some molten-fuel deposits on the inner holder wall produced the meltthroughs near the top of the fuel column as observed in the posttest examination. This would have occurred at ~1.520 sec. With rupture of the holder wall, the mixing-zone volume increased ~2.5 times, and the pressure would suddenly be reduced to some low value. This could account for the relatively large reverse acceleration of the outlet coolant from 1.522 to 1.534 sec.

B. Mechanical Work

The mixing-zone pressures have been estimated using a model of the loop developed by Deitrich.[46] In this model, the work done in slug ejection is calculated by the momentum and continuity equations based on incompressible fluid flow. The total work done by the expanding vapor bubble is the sum of the change in the fluid kinetic energy, the work done in compressing the 525-cm^3 plenum gas, the work done against the pump in moving sodium backward, the energy dissipated by friction, the change in potential energy, and the energy change due to area changes in the flow path. Some of the major results of Deitrich's model are shown in Fig. 12. A peak bubble pressure of 92 psi was calculated at 1.515 sec. The agreement between measured and calculated pressure pulses is encouraging, but probably fortuitous. These calculations show that less than 10 J of useful work was done by the bubble. [Useful work is defined as the integral of P dV and is not necessarily the same as the work done by the bubble. In this case (H2), frictional losses were small and the work done by the bubble (10.1 J, max at 1.526 sec) was nearly equal to the P dV work (9.7 J).] At 1.526 sec (maximum bubble work), the total energy into the test was 1×10^5 J. Accordingly, the efficiency for conversion of thermal to mechanical energy is 10^{-4}, the same order of magnitude as found in other loop tests.
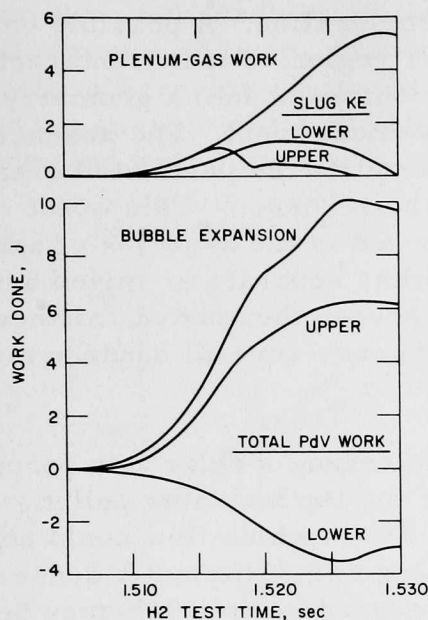
Fig. 12

Components of Work and Energy in Test H2 as Determined from the Flow Dynamics. A vapor bubble is assumed to expand and push sodium out of the flow channel. The kinetic energy of the upper and lower sodium slugs are shown at the top. Work is done in compressing the 525 cm³ of plenum gas (also shown at the top), in overcoming frictional losses, in moving liquid backward through the pump, and in changing the potential energy at the sodium head. The total work done by the expanding bubbles and the total P dV work on the upper and lower sodium slugs is shown at the bottom.

C. Postfailure Flow and Pressure Data

Except for the inlet event at 1.72 sec, postfailure flow was a periodic variation of about 20 cycles superimposed on a steady approach to zero flow. The almost steady postfailure outlet flow of ~100 cm³/sec compared to the prefailure flow of 165 cm³/sec is evidence that the outlet blockage accounted for the decrease and occurred during the initial failure sequence from 1.51 to 1.55 sec. The fragmentation process is presumed to be essentially complete by 1.522 sec, the time when the outlet-slug velocity reaches a maximum. Fuel sweepout occurred only during time of positive (upward) flow (t < 1.528 sec). This leaves the 20-msec period between 1.51 and 1.53 sec as the time during which the outlet blockage was formed. That part of the blockage formed by compacted fuel particles probably occurred in the ~10-msec period from 1.52 to 1.53 sec.

In some studies of the loop response to boiling, Carter[47] has shown that flow variations of the amplitude and period observed in Test H2 were characteristic of moderate boiling. The observed 20-cycle oscillations were associated with boiling. They decreased in amplitude, and ultimately disappeared as the flow plugs and mixing zone cooled.

The inlet event beginning at 1.70 sec corresponded to an average acceleration of ~6 x 10⁴ cm/sec² for the slug; that associated with the initial-failure slug was ~8 x 10⁴ cm/sec², suggesting that mixing-zone pressures for the two events were comparable and that possibly the events themselves were of the same type and had the same magnitude of interaction. Both the amplitude and shape of the pressure pulses for this event were quite different from those observed in the initial failure sequence. The large increase in mixing-zone volume caused by holder-wall meltthrough would account for a reduced

pressure, but not for the relatively large slug acceleration. A possible cause
of the event is a steel-fuel interaction in the inlet region. Such an interaction
could lead to a secondary or delayed fuel-movement event into a geometry
quite unlike that at the time of the first fuel-movement event. The absence
of any significant outlet response to this event supports the postulated crea-
tion of the outlet blockage during the initial failure sequence. This event
probably corresponded to the delayed event observed in the S-series of auto-
clave tests. Large quantities of molten steel, either separate or mixed with
the fuel, would exist during the transition time between thermodynamic heat-
ing and cooling in the mixing zone. Such a time occurs several hundred msec
after peak power.

During the posttest disassembly and examination, a relatively porous
plug was observed in the outlet region just above the top insulator pellet.
Comparisons between this plug and that found in E4 (in which flow could not
be established after the test) indicated that the plug was sufficiently dense to
stop all outlet flow. The fact that the flow was reduced by only 40% may be
due to such causes as a finite bypass flow, vapor in the region of the flow de-
tector, turbulence in the flow-detector region due to boiling, or a change in
flow-detector calibration. Possibly several or all of these factors combined
yielded the indicated net positive flow. It is also possible that the final block-
age as observed in the posttest examinations was not formed until after 1.9 sec
and that finite flow actually existed during the earlier (than 1.9 sec) stages.
There are no recorded data beyond 1.9 sec, and later flow activity is unknown.

The apparent inlet flow (~75 cm^3/sec) after 1.75 sec seems to indicate
there is a finite flow through the flow channel, despite the possible presence
of an outlet plug.

D. Temperature Data

TC3, the thermocouple 1 in. below the top of the fuel column, burned
out within 30 msec of the initial time of fuel release. This is the estimated
lag in thermocouple response due to its finite time response. Figure 13 com-
pares measured and calculated temperatures. Calculations were made using
the Argonne version IIIC of the COBRA code.[48,49] This version allows an
inlet-flow and temperature-forcing function (both taken from the experimental
data) and a power-driving function. (Additional details are given in the appen-
dix.) Since the code used does not explicitly treat boiling heat transfer, these
calculations were run assuming that heat transfer was to a single-phase liq-
uid coolant only. This produced an overestimation of heat loss from the pin
after vapor was produced in the channel. Thus the calculations underesti-
mated both the fuel and mixing-zone temperatures. Up to the time of failure
these differences may be small, but growing rapidly. Heating of the pin after
initial failure is probably more nearly adiabatic with little or no heat trans-
fer out of the pin until fuel-pin-holder wall-temperature differences are
large enough for significant radiative heat transfer. According to the calcula-
tions, the peak cladding-surface temperature (located in the top axial node of
the fuel column, the same location as TC3--see Figs. 8 and 13) reached the

saturation temperature at 1 atm at 1.422 sec and the saturation temperature at 2 atm at 1.483 sec. Observed prefailure boiling began at 1.465 sec, in excellent agreement with the calculation. At this time, calculation indicated that the surface of the fuel pellets began to cool. (This cooling may be overestimated due to the single-phase heat-transfer model.)
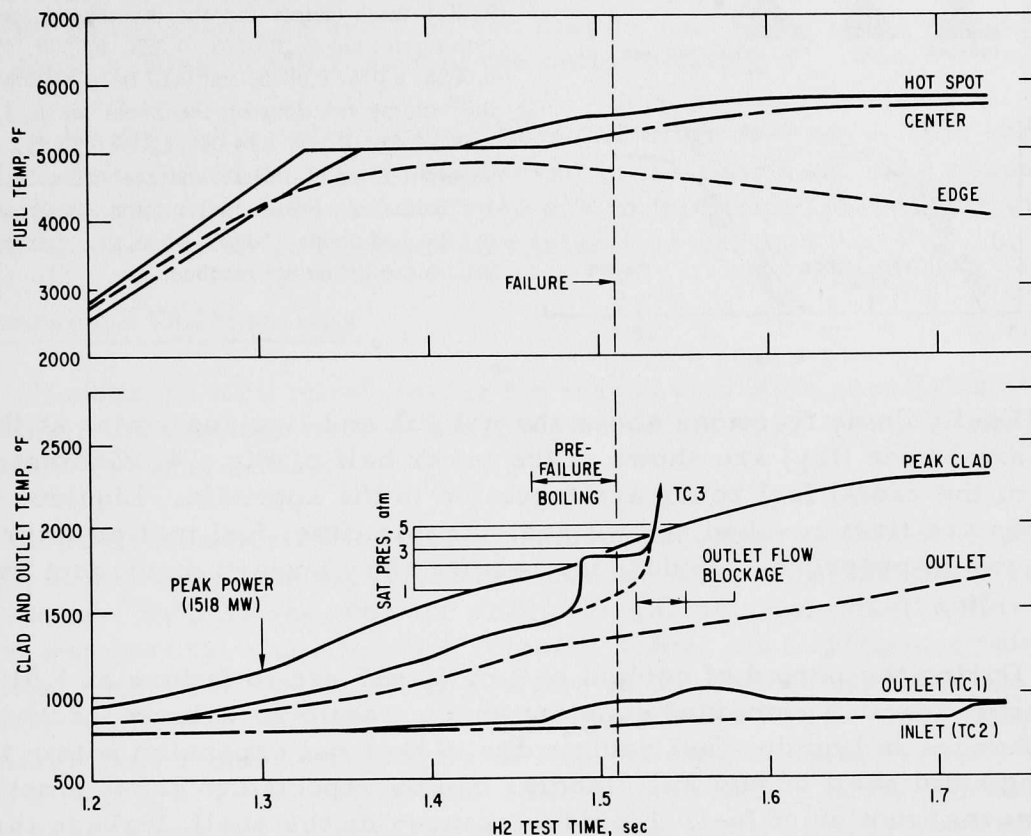
Fig. 13. Calculated (top figure) and Measured (lower figure) Temperature Histories for Test H2. Calculations are reliable up to the time of prefailure boiling and measureable at failure. Peak cladding temperature is for hottest axial node, 1.5 in. below the top of the fuel column. Sodium-saturation temperatures are shown for pressures up to 5 atm.

Calculations shown in Fig. 13 indicate that the rate of thermal-energy addition during the overpower portion of the transient exceeded the heat-energy loss rate by thermal conduction through the fuel pellet and cladding into the sodium flow stream. As melting began near the edge of the pin (at 1.33 sec), the melt front rapidly propagated inward, leaving a thin shell (0.0125 in. thick) on the outside of the fuel pellets. In these calculations, the solidus was defined as the state of the fuel when the melting temperature (5000°F) is first reached, and the liquidus as the state (at the same temperature) after the latent heat of fusion (118 Btu/lb; 247 J/g) has been added. The inward propagation rate of both states is shown in Fig. 14 for a pie-shaped sector of the fuel pellets.

ABOVE SOLIDUS
ABOVE LIQUIDUS
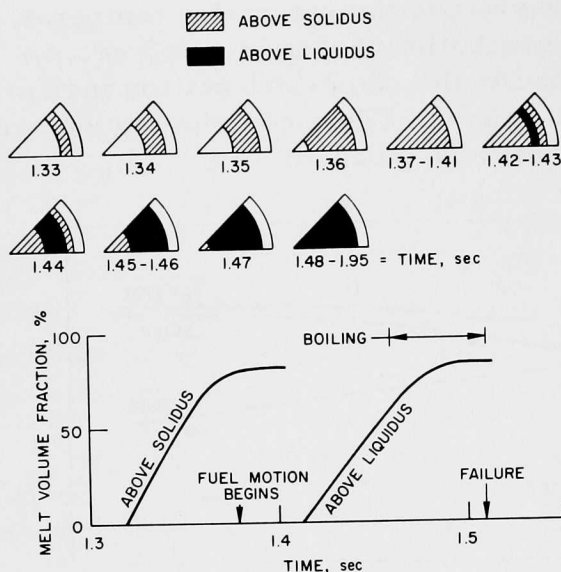
Fig. 14

Melting History by Radial Zones and by Volume Fraction (Lower Figure) of Hottest Axial Node. Radial mesh points for the pie-shaped sectors (top figure) are 0, 0.0125, 0.025, 0.0375, 0.05, 0.0625, 0.075, 0.0875, and 0.10 in. Corresponding volume fractions of the zones are 0, 1.56, 4.68, 7.81, 10.94, 14.06, 17.19, 20.31, and 23.44%. Time of failure and prefailure boiling are indicated. Initial fuel motion, as observed by the hodoscope, begins when the maximum solidus conditions are reached.

Fuel volume fractions above the solidus and liquidus states at the hottest axial node (top) are shown in the lower half of Fig. 14. Geometric details of the radial fuel zones are tabulated in the appendix. Liquidus temperatures are first reached at 1.42 sec. At this time, fuel motion internal to the pin was in progress. (Hodoscope results show upward movement beginning at 1.36 sec.)

During the period of coolant boiling (1.465 sec to failure at 1.51 sec), the liquidus fraction remained constant at the maximum volume fraction of 77%. Changes in liquidus fuel volume due to thermal expansion within the confining solid shell of fuel and cladding can be expected to cause a net upward internal motion of fuel. Liquid pressures on the shell, leakage through cracks in the fuel shell, and cladding melting were the causes of failure.

After the initial failure, only ~130 J/g of thermal energy was added in the test. At most, this would (adiabatically) increase the fuel temperature by 100°F, well within the uncertainties of the calculations. Thus, the post-failure results for Test H2 are believed to be reasonable.

Measured data for TC3 were somewhat erratic between 1.49 and 1.52 sec, and seemed to vary between the saturation temperatures and the dashed curve shown in Fig. 13. This may be the result of passage of a vapor bubble during prefailure boiling. (Thermocouples of the type used, with an ~30-msec time response, are not expected to respond to alternating vapor and liquid temperatures during the 30-msec boiling period, since "response time" is defined in terms of response to a step change in boundary conditions. Because of the finite heat capacity of the immediate environment during this boiling period, the effective response is much slower.) At 1.53 sec, TC3 failed, indicating contact of hot fuel/cladding fragments with the junction. When corrected for the finite response time of TC3, this corresponds to the beginning of outlet flow blockage. Average mixing-zone temperatures were

expected to be ~1700°F and higher (sodium-vapor temperatures) during and after initial slug ejection. Since temperatures of this magnitude were not measured at the inlet, the bottom of the flow channel probably never became blanketed with vapor. The slight rise in outlet temperature from 1.54 to 1.58 sec possibly reflects heating of the sodium in the outlet plenum, resulting from cooling of the outlet blockage plug. The slight dropoff in outlet temperature (~80°F) between 1.56 and 1.60 sec may be the result of turbulent mixing due to local boiling in the region of the outlet blockage.

A slight heating of the inlet was noted after 1.71 sec. This correlates well with the delayed interaction observed in the flow data. The absence of inlet heating between 1.53 and 1.55 sec due to inlet-flow reversal is evidence of vapor condensation as suggested by inlet-flow recovery in Fig. 10.

E. Hodoscope Observations

Hodoscope film speed during the test gave a time resolution of 6.7 msec per frame, and the data were averaged over two frames for an overall 13-msec increment in event timing.

The first indication of fuel movement occurred at 1.32 sec: a slight bending or bowing of the top of the fuel column away from the pump side of the test section. By 1.34 sec, bowing within the geometrical constraints of the test section was general along the fuel column. Initial pin bowing was coincident with attainment of the solidus temperature in the hottest region of the fuel pin. A definite indication of upward fuel movement began at 1.36 sec. The initial fuel motion was from the region about 1 in. below the top of the fuel, leaving behind a region of little (or no) fuel. The amount of fuel partaking in the upward motion appeared to increase almost linearly with time (constant rate) until 1.51 sec (the failure time). Almost all the fuel-density decrease occurred in the top several inches of the fuel column, with only minor depletion in the midregion and no statistically significant fuel-density change in the lower portion of the pin. After failure, there was some evidence of fuel entering the flow channel.

It is difficult to distinguish radial fuel motion within the flow channel that is due to pin bowing from that due to fuel release. Nonetheless, no abrupt increases of fuel were found in the flow channel at the time of failure.

From the available data, fuel-motion activity seems to be complete by 1.56 sec, some 50 msec after failure. The statistical significance of the data after 1.7 sec is too poor to verify the type and amount of fuel-motion activity that may be associated with the inlet flow ejection observed at 1.72 sec.

Fuel motions seen by the hodoscope in this test were among the largest observed in any test and therefore have a high degree of relative accuracy.

F. Posttest Examination

The H-2 tests exhibited upward fuel motion that melted part of the upper insulator pellet without commensurate melting of the upper cladding. No measurable quantity of fuel fines were found outside the test section, and substantial masses of large fuel chunks or clinkers were found on the fuel-holder walls. The portion of the fuel pin above the failure point had moved upward and was held in the elevated position by frozen debris in the upper flow channel. Independent of this motion, the upper insulator pellet and spacer tube moved upward inside the cladding, probably before actual failure.

The experiment disassembly and part of the macroscopic examination were performed by the Reactor Analysis and Safety Division in a high-purity nitrogen-atmosphere glovebox. The rest of the macroscopic examination and the microscopic examination were performed in the Materials Science Division's Alpha-Gamma Hot Cell Facility (AGHCF). The loop sodium was recovered at the HFEF and sent to MSD for fines retrieval by sodium dissolution. This operation was performed in the high-purity nitrogen-atmosphere glovebox by a joint RAS-MSD force.

1. Disassembly

The test train was removed from the shipping container, and the test section was separated from it at the T-joint. The lower portion of the test section is shown in Fig. 15. A radiograph of the entire test section is shown in Fig. 16. It can be seen that the top of the fuel element has moved upward by about 1.75 in. (see Figs. 6 and 8). The spacer tube located beneath the spring has moved up about 0.75 in. producing some additional spring compression. After the exposed sodium from the test section was cleaned, the surfaces were found to be clean and bright. The pin holding the fuel element in the spherical seal and the clip that joined the test section to the upper adapter tube were easily removed. The exposed portion of the fuel-element plenum appeared fairly clean and straight. However, as made evident by the radiograph, the fuel element was fused to the adiabatic holder tubes and could not be withdrawn.

2. Macroscopic Examination

The spherical seal, the expansion bellows, and the upper collar were first removed by circumferential cutting. Sodium was removed from
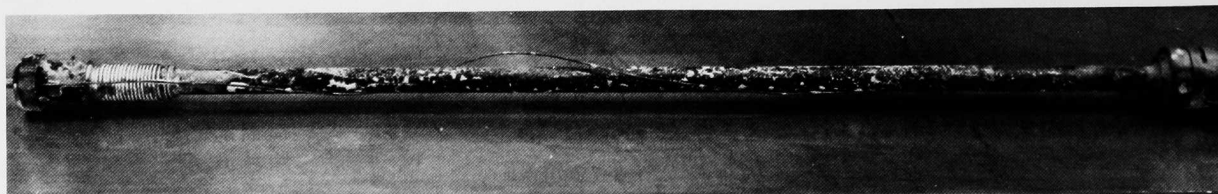
Fig. 15. Lower Portion of Test Section. Mag. 0.25X. ANL Neg. No. 900-1151.

TOP OF
FUEL PIN

POST-
TEST

1-3/4-in.

PRE-
TEST

BOTTOM OF
FUEL PIN
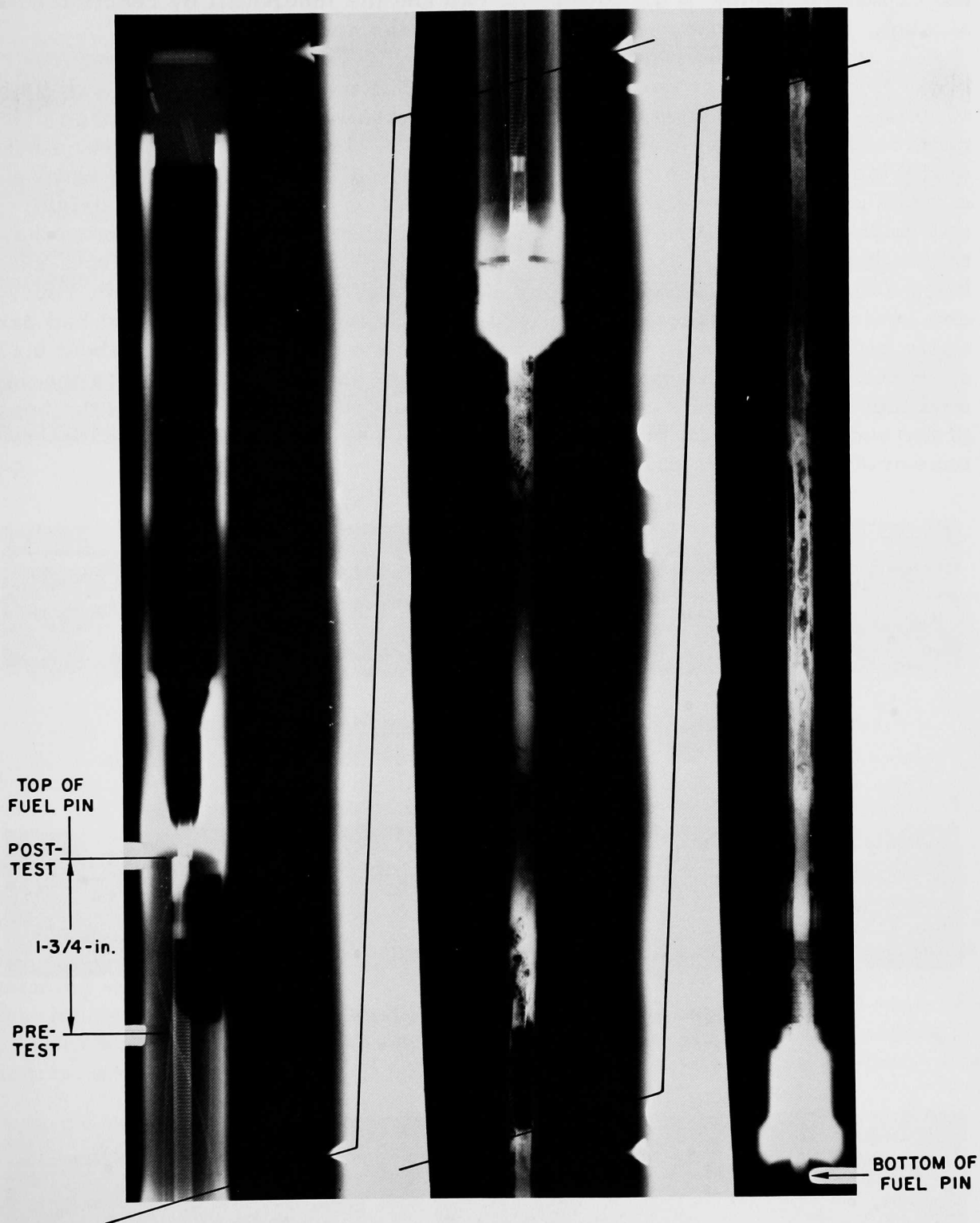
Fig. 16. X-radiograph of Entire Test Section, in Three Portions. Mag. 0.5X. ANL Neg. No. 900-732A.

the exposed portions of the lower end cap and the inner wall by reaction with alcohol. These portions were found to be clean and bright.

The entire outer wall was then longitudinally slit in two places, ~180° apart, using a small, abrasive cutoff machine. One-half was then pried off to expose the inner wall, which is shown in Figs. 17-19. The outer surface of the inner wall and the inner surfaces of the outer-wall segments, when cleaned of sodium by reaction with alcohol, were found to be clean, bright, and relatively straight, except for two areas. The first was adjacent to the top of the original fuel column, which was located about 17.375 in. from the bottom of the rod. As shown in Fig. 20, several holes had been burned out and several short cracks were in evidence. Some once-molten steel had partially filled the region between the separator-wire convolutions at about 0.17 in. from the bottom of the rod. A small amount of debris was evident on the adjacent inner surfaces of the outer wall. The second area, ~8 in. from the bottom of the rod, was a small blister ~0.5 in. long. The area probably represents once-molten stainless steel.
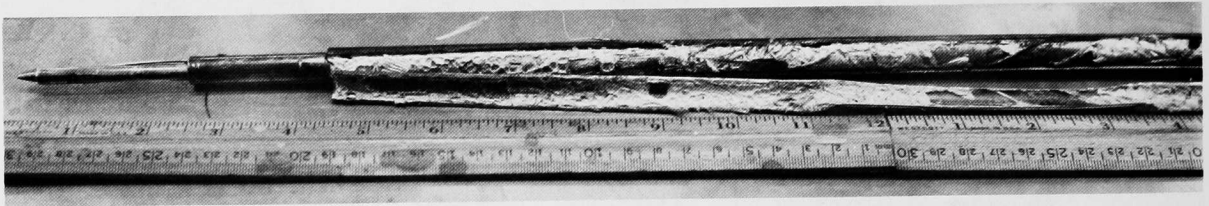
Fig. 17. Exposed Portion of Lower Section of Inner Wall after Longitudinally Slitting Outer Wall. ANL Neg. No. 900-1156.
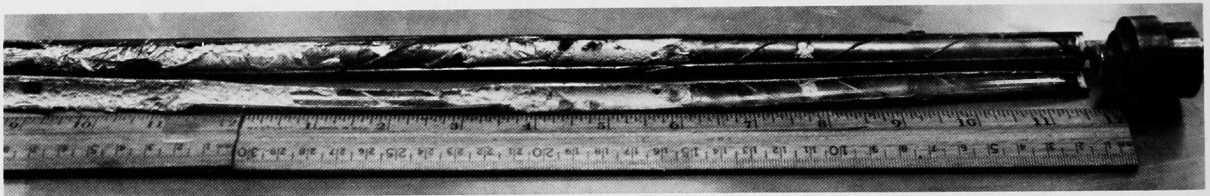
Fig. 18. Exposed Portion of Middle Section of Inner Wall after Longitudinally Slitting Outer Wall. ANL Neg. No. 900-1157.
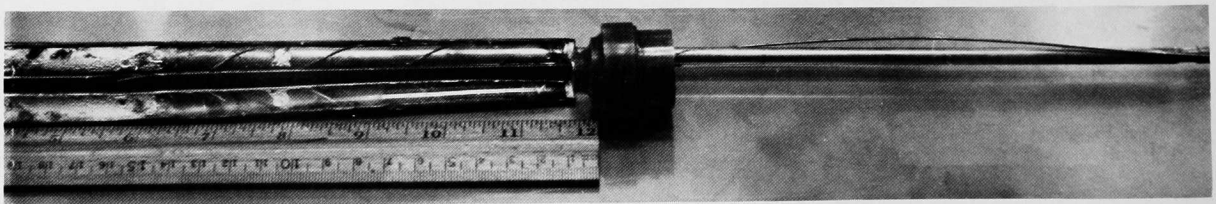
Fig. 19. Exposed Portion of Upper Section of Inner Wall after Longitudinally Slitting Outer Wall. ANL Neg. No. 900-1158.
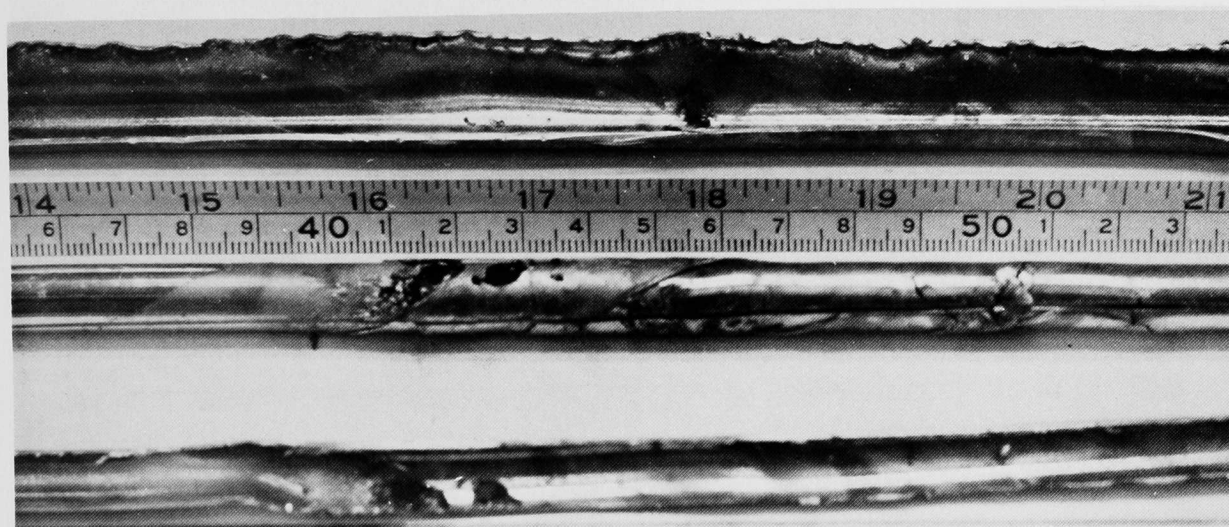
H-2

14-1/2" — 15-3/4"
POSTTEST FUEL VOID

17-3/8" PRETEST
TOP OF FUEL

Fig. 20. Exposed Portion of Inner Wall after Sodium Removal,
Showing Interaction Zone. ANL Neg. No. 900-731.

The entire length of the inner wall was next slit longitudinally in two places, ~180° apart. The lower end was pried up and the lower end plug was found to be easily removable, as seen in Fig. 21. Loose and adherent debris were found, along with once-molten cladding that had dropped down from the region immediately above. The latter is more clearly seen in Fig. 22. The lower 4.75 in. of one of the slit halves were cut off transversely. The remaining section was slit a little deeper to open the halves of the inner wall. One inner surface is shown in Figs. 22 and 23. An enlarged internal view of this surface in the interaction zone is shown in Fig. 24. Fuel and cladding debris, as well as the charred upper portion of the element, are evident. Fuel
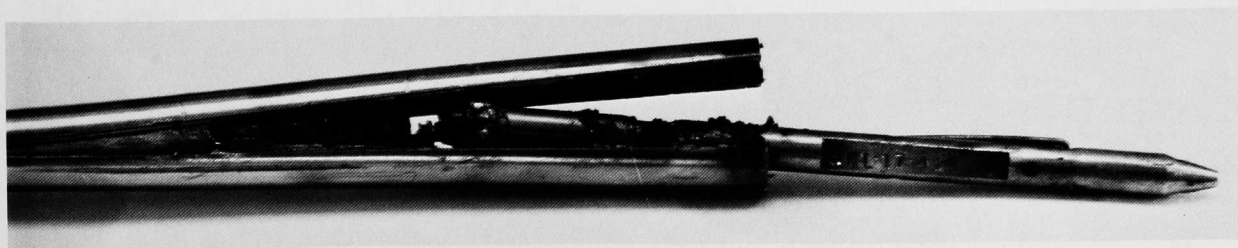
Fig. 21. Slit Inner Wall, Showing Free Lower End Plug. Mag. 0.975X. ANL Neg. No. 900-1171.
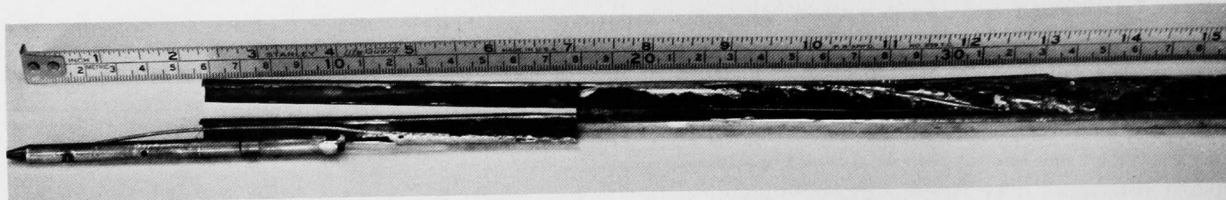
Fig. 22. Exposed Lower Section of Inner Wall after Slitting and Opening. ANL Neg. No. 900-1172.
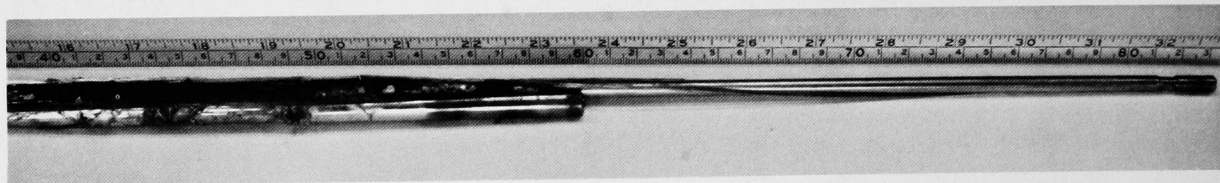
Fig. 23. Exposed Upper Section of Inner Wall after Slitting and Opening. ANL Neg. No. 900-1173.
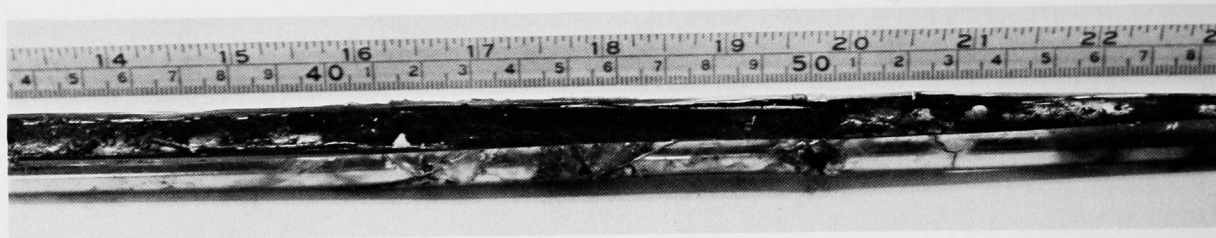
Fig. 24. Enlarged View of Inner Wall at Interaction Zone. ANL Neg. No. 900-1178.

and cladding debris, loosened as a result of the cleaning operation, were collected, washed free of sodium, and set aside for characterization. A total of 64.40 g of particles was retrieved. The original fuel and total rod weights were 68.51 and 190.68 g, respectively.

The two halves of the inner wall were then separated completely and photographed. Both halves are shown in Figs. 25-29. Clearly evident are the lower end plug and cladding with some fuel still present, scattered fuel and cladding, the remains of the wire wrap and frozen cladding, the remains of upper insulator pellets, and the unaffected upper part of the element with its wire wrap and thermocouple. Metallographic sections, both longitudinal and transverse, were taken from various regions starting at the lower end plug and insulator pellets, and ending in the plenum portion above the upper insulator pellets. Positions can be located by referring to Figs. 25-29.

3.   Microscopic Examination

The lowest longitudinal section examined was taken at about the interface between the bottom fuel pellet and the insulator pellet below it. This
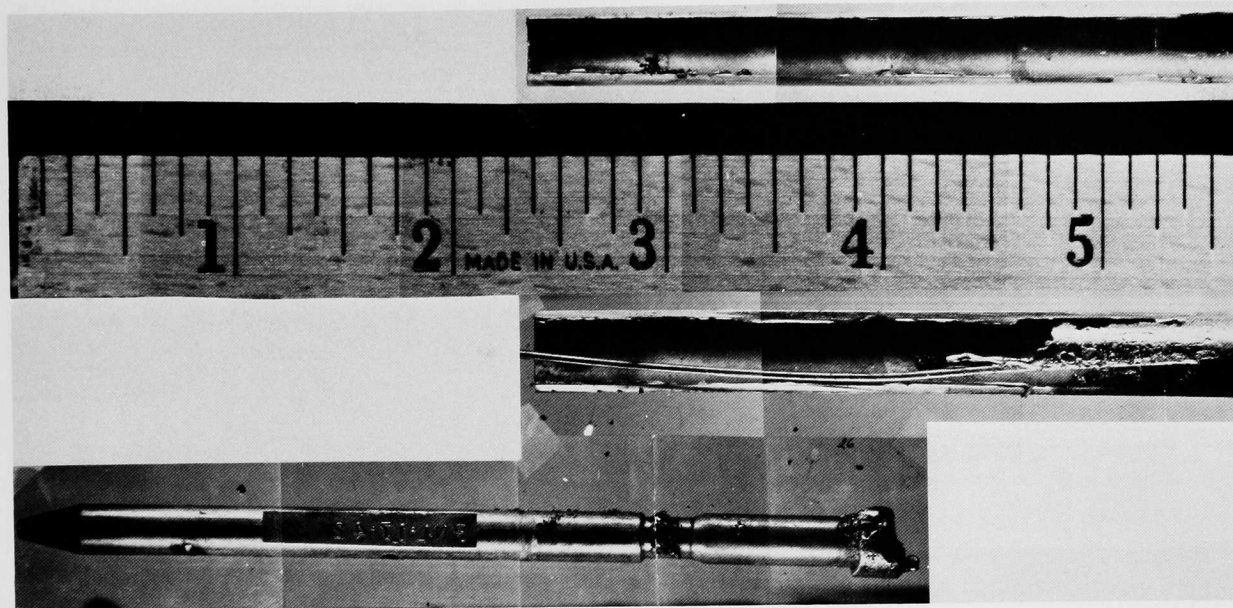
Fig. 25. Inside Surfaces of Inner Wall, 0–5 in. from Bottom End Plug. Neg. No. MSD–168134.
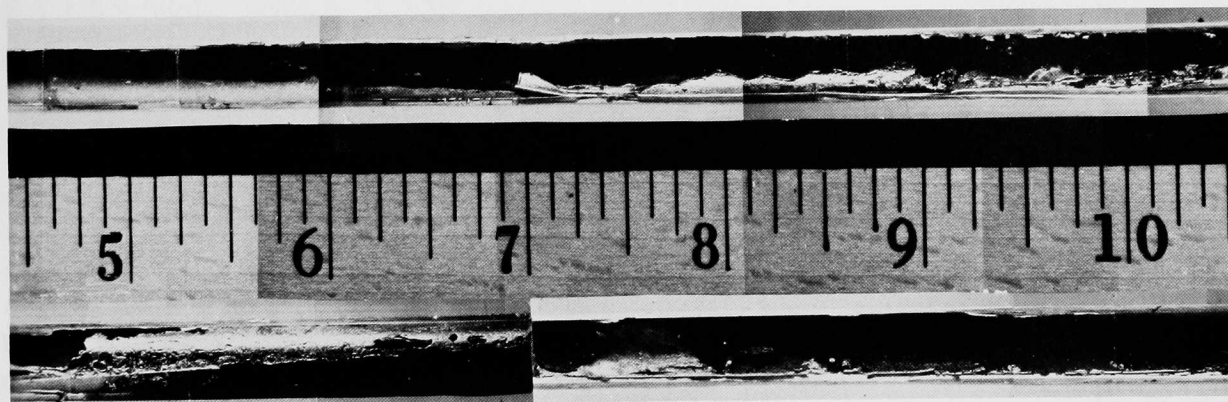
Fig. 26. Inside Surfaces of Inner Wall, 5–10 in. from Bottom End Plug. Neg. No. MSD–168135.
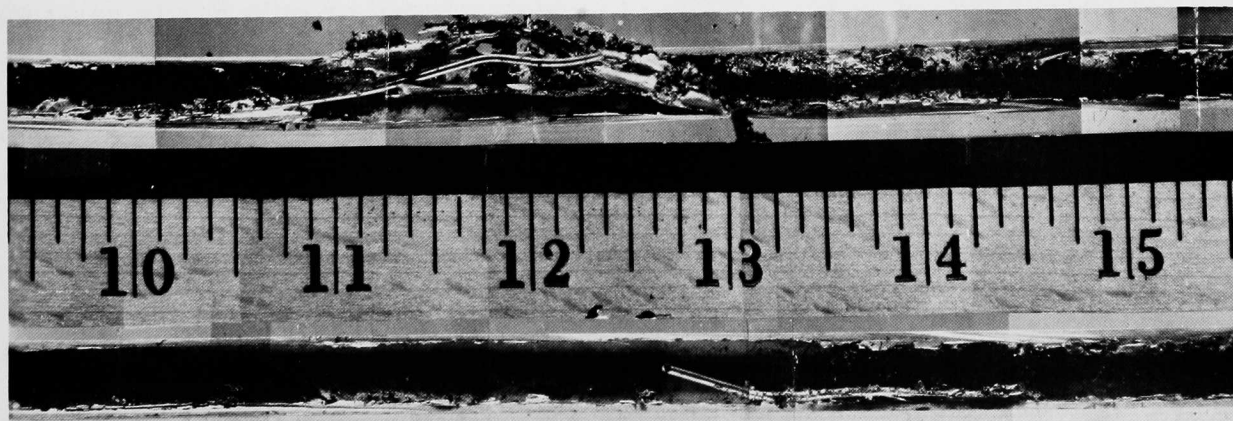
Fig. 27. Inside Surfaces of Inner Wall, 10–15 in. from Bottom End Plug. Neg. No. MSD–168136.
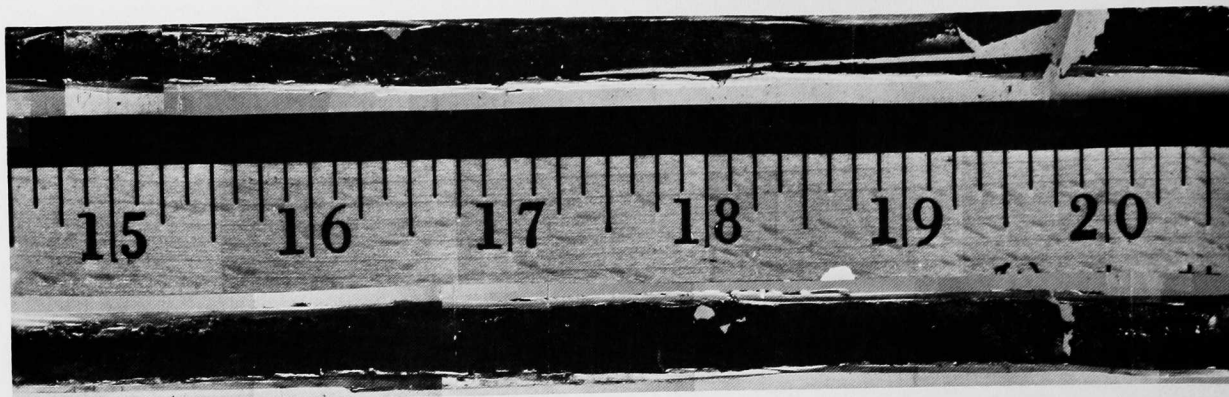
Fig. 28. Inside Surfaces of Inner Wall, 15-20 in. from Bottom End Plug. Neg. No. MSD-168137.
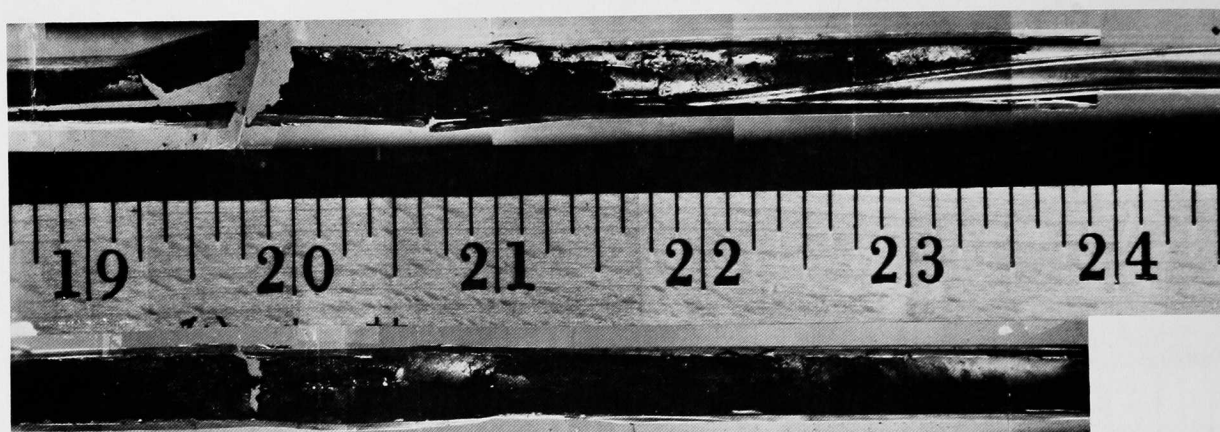
Fig. 29. Inside Surfaces of Inner Wall, 19-24 in. from Bottom End Plug. Neg. No. MSD-168138.

interface was about 3.875 in. from the bottom of the rod. The bottom of the fuel column is shown in Fig. 30. Fusion had occurred (within the cladding) between the resolidified fuel and the UO_2 insulator pellet almost across the entire interface. In the region of the junction of the cladding, fuel, and insulator pellet, the fuel appeared to have molten. Directly above the region of the juncture, a 9-12-mil-thick layer of unrestructured or only partly restructured fuel occurred. The fuel at the juncture of fuel, insulator pellet, and cladding appeared to have been hotter (approximately at the solidus) than the fuel directly above it. The layer of unrestructured fuel against the cladding is similar to that observed in Test E2. The pattern of columnar grains is indicative of the solidification pattern, and at the top of the photograph is what appears to be the bottom of a central void in the columnar grains of fuel. The insulator pellet experienced grain growth to an average depth of ~30 mils, increasing slightly toward the center. The stainless steel that flowed down and froze appeared (see Fig. 22) to have blocked ~60% of the channel over an axial distance of 0.1-0.2 in. Dispersed fuel and cladding particles from above could temporarily bridge this gap to cause a flow blockage.
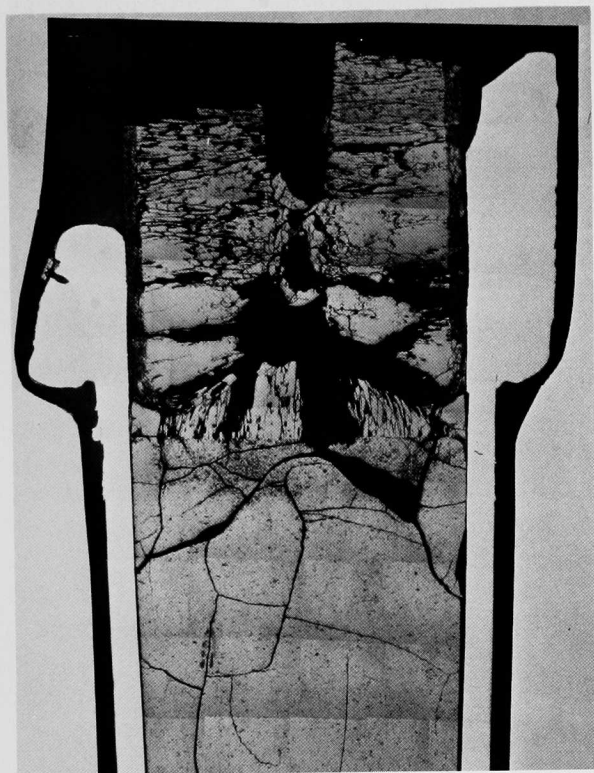
Fig. 30. Fuel and Insulator Pellet at Bottom of Fuel Column. Mag. 7.75X. Neg. No. MSD–161691.

The next section was taken transversely at a position ~6.5 in. from the bottom of the rod (see Fig. 31). Portions of the inner wall were found to have reached incipient melting, deduced from the presence of molten fuel adjacent to it. The outer surface of the cladding contained cracks, as shown in Fig. 32a; the slowly cooled, once-molten fuel is shown in Fig. 32b. It is evident from Fig. 32a that the cladding has been weakened, which may have led to the intergranular cracks seen in Fig. 31. The fuel shown in Fig. 32b is fairly dense and free of finely divided stainless steel. The large steel globules present probably froze after the fuel had cooled sufficiently.

Molten fuel also caused the small blowout, seen externally as a "blister" at ~8 in. from the bottom of the rod. This is shown by a transverse section in Fig. 33, and in magnified views of cladding and fuel in Fig. 34. A small amount of molten cladding was pushed out, which froze in layers between the inner and outer walls, as shown in Fig. 34a. The fuel in this region contained, in addition to the large globules, a more homogeneous mixture of finely divided stainless steel as shown in Fig. 34b.

Several other transverse sections were taken from positions corresponding to the middle and upper portions of the original fuel column. These sections essentially contained only layers of stainless steel frozen to the inner wall, with little or no fuel. Fuel in these areas was probably dislodged during the disassembly operation. Adherent fuel was found again above the original fuel-column location.

A longitudinal section was taken at the present location of the upper insulator pellets (see Fig. 35). 9.875 in.

Fig. 31. Transverse Section of Inner Wall at ~6.5 in. from Bottom of Rod. Mag. 7.75X. Neg. No. MSD–161693.
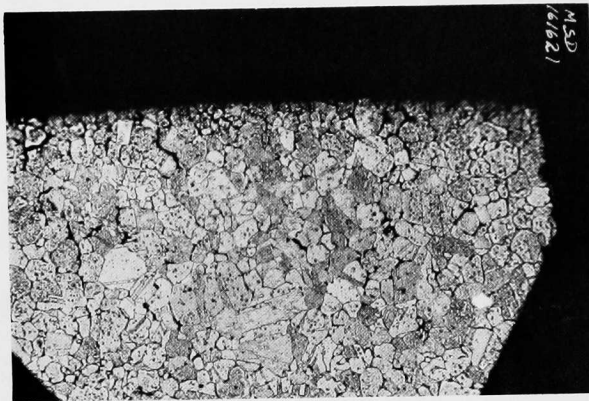
(a)
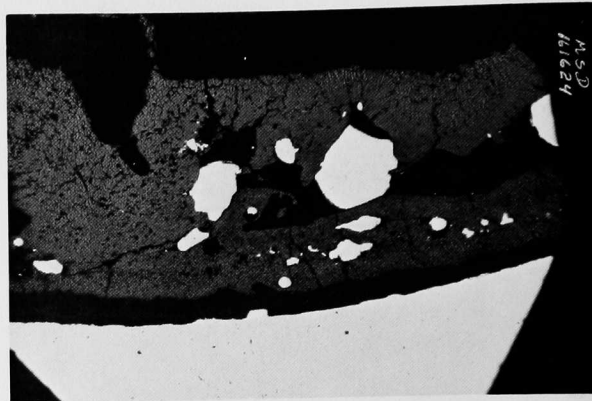
(b)

Fig. 32. High-magnification Views of Regions at ~6.5 in. from Bottom of Rod (OD of Cladding). Mag. (a) 92X; (b) 46X. Neg. Nos. MSD-161621 and -161624.

Fig. 33

Transverse Section of Inner Wall at ~8 in. from Bottom of Rod. Mag. 6X. Neg. No. MSD-161599.
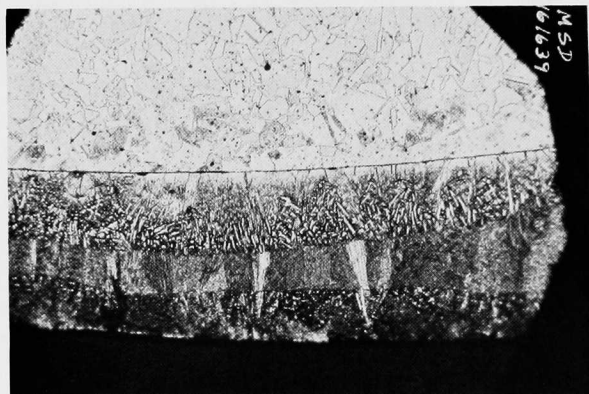
a. OD of Cladding. Mag. 92X. Neg. No. MSD-161639.
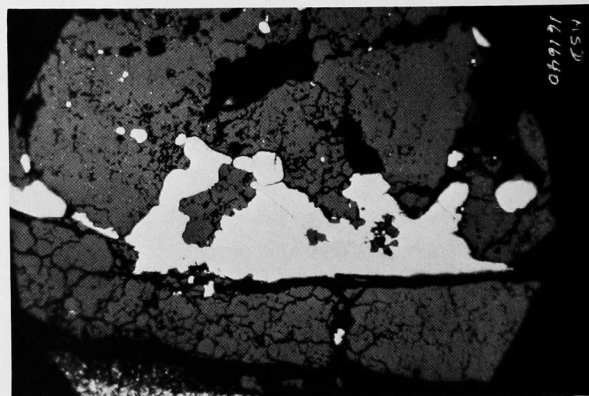
b. Adjacent Fuel. Mag. 60X. Neg. No. MSD-161640.

Fig. 34. High-magnification Views of Regions at ~8 in. from Bottom of Rod
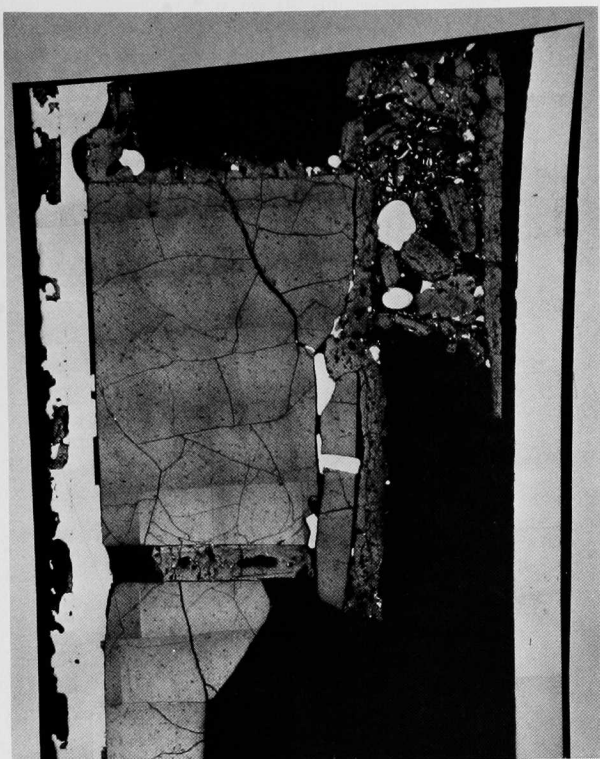
Fig. 35

Upper UO$_2$ Insulator Pellets Located
~19.875 in. from Bottom of Rod.
Mag. ~8X. Neg. No. MSD-161689.

from the bottom of the rod, which indicates that the insulator pellets had moved upward about 2 in. In the figure, intrusions of fuel and stainless steel into cracks in the pellets and between the two pellets are evident. One such region is magnified and shown in Fig. 36a. The cladding on the right side in Fig. 35 has completely melted. On the left side the cladding is still present, but melted steel and fuel can be seen on the outside of the cladding. At the upper left a washout is clearly defined at the cladding inner surface. Some fuel is present on the top surface of the upper insulator pellet, and a mixture of fragments of fuel and melted steel occupies the region on the upper right on Fig. 35, which is shown magnified in Fig. 36b. During the transient the molten fuel appears to have melted the cladding and spewed through the molten
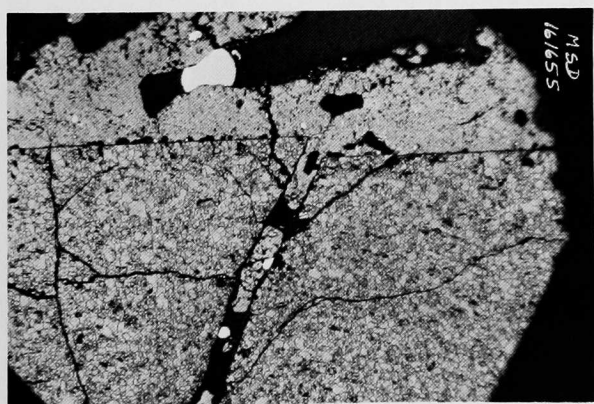
a. Fuel Intrusion. Mag. 46X. Neg. No. MSD-161655.
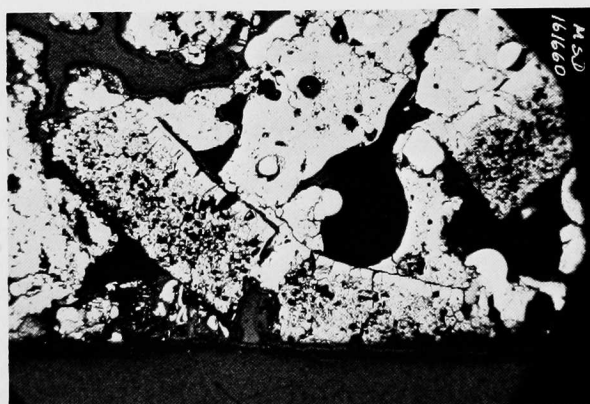
b. Fuel and Cladding Mixture. Mag. 46X.
Neg. No. MSD-161660.

Fig. 36. High-magnification Views of Upper Insulator Regions

cladding on one side, moving vigorously upward, mixing fuel and steel together until its force was spent and solidification occurred.

A transverse section ~0.5 in. above this section is shown in Fig. 37. Partially melted cladding with a section of partially melted fuel-pin spacer tube can be seen. Large amounts of fuel appear toward the outer part of the assembly between the cladding and the test-section tube. A section of thermocouple encased in melted steel is visible.
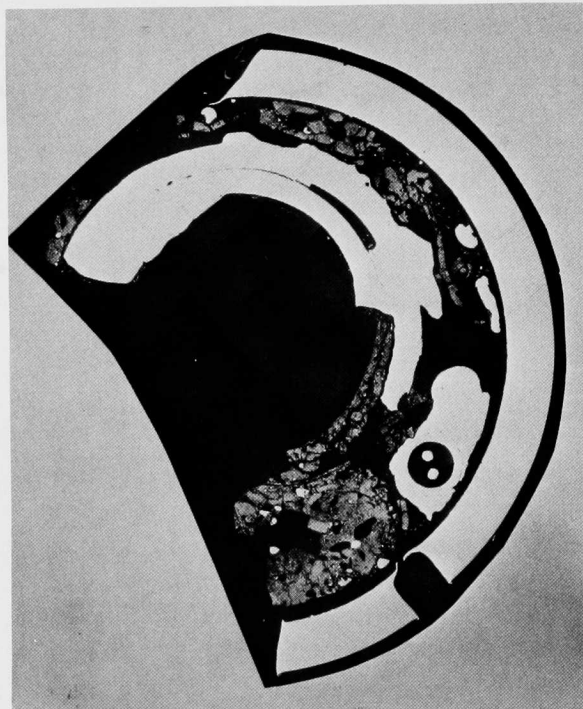
Fig. 37. Transverse Section of Inner Wall at ~18.5 in. from Bottom of Rod. Mag. 7.5X. Neg. No. MSD-161694.

4. Particle Characterization

As stated earlier, 64.4 g of cladding and fuel-particle debris were collected from the test section. This is to be compared with the 68.51 g of fuel loaded into the rod. The particles were sieved, after sodium removal, by reaction with alcohol. The sieve analysis is shown in Table IV. Photographs were taken of each size fraction. Figure 38 shows material collected on several sieves. Samples were taken of each size fraction for density determination and metallographic analysis.

Initial density determinations as shown in Table IV indicated the presence of low-density powders, most probably alumina (density of 3.5-3.9 g/cm^3) debris from the cutting operation. A partial separation was accomplished by flotation using methylene iodide, which has a density of 3.325 g/cm^3 at 20°C. The density measurements were repeated after separation. The results, shown in Table IV, indicate that some but not all of the suspected cutting was removed. Removal was easier for the larger-size fractions. Due to residual debris, the densities reported for the small particles are probably as low, was later substantiated by metallographic analysis. The density

TABLE IV. Characterization of H2 Powders

Sieve No.	Sieve Opening, mm	Total Weight, g	Powder Density, g/cm^3	
			Initial	After Separation
6	3.36	6.57	8.95	9.34
12	1.68	11.70	8.44	9.69
25	0.71	13.60	7.76	9.34
50	0.297	9.70	4.20	9.06
70	0.210	6.15	4.55	7.33
140	0.105	15.93	3.83	6.73
400	0.037	0.75	4.72	5.90
<400	<0.037	0.00	-	-
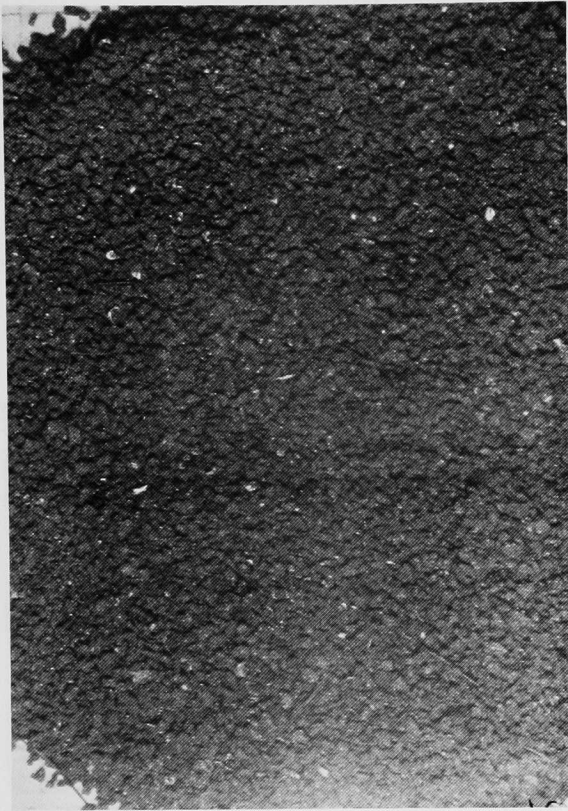
a. Sieve No. 50 Size Fraction. Mag. 2.75X.
Neg. No. MSD-166375.

b. Sieve No. 6 Size Fraction. Mag. 2.75X.
Neg. No. MSD-166378.

c. Sieve No. 25 Size Fraction. Mag. ~2X.
Neg. No. MSD-166377.
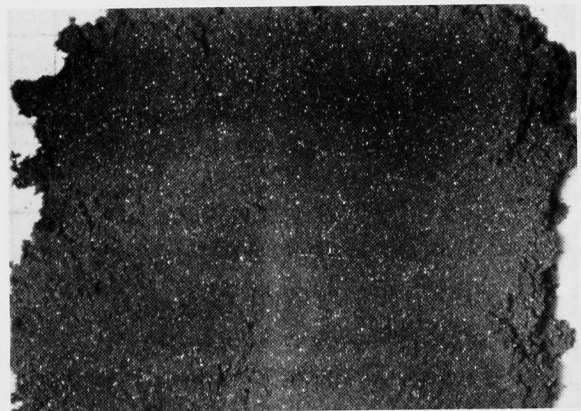
d. Sieve No. 140 Size Fraction. Mag. ~2X.
Neg. No. MSD-166381.

Fig. 38. Macroscopic Views of Particle Debris Retrieved from Test Section

average for the first four fractions in the table is probably greater than
9.3 g/cm^3. This is >84% theoretical density (TD) of oxide fuel and compares
favorably with a density of 10.13 g/cm^3 (or 91.6% TD) of the original pellets.
Hence, little reduction in density apparently occurred as a result of the fuel
ejection during the transient.

The appearance of the metallographically prepared particles qualitatively agrees with the density data. Particles from all size ranges were examined up to 500X. Particles from two sieve numbers under high magnification are shown in Fig. 39. The particles are fine-grained, had apparently been partially molten, and contain small globules, 0-5 vol. %, of stainless steel. The steel globules may account for some of the fuel-density difference. The larger particles contain the least molten fuel and stainless steel. They also appear slightly more dense, i.e., ~90% TD, whereas the smaller particles are 80-85% TD. As expected, the larger particles are more angular in shape; the smaller particles are more spherical and contain coalesced voids. This corresponds well with the degree of melting.
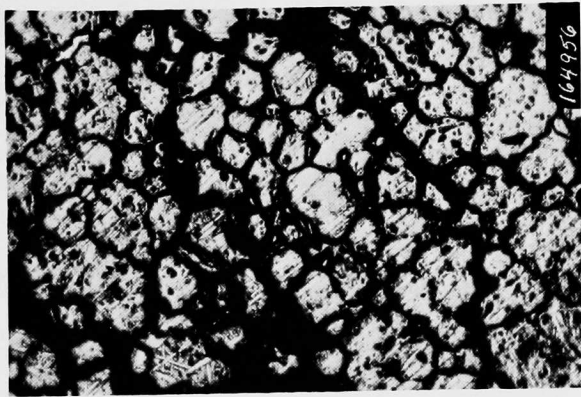
a. Sieve No. 12 Particle. Mag. 2.25X.
   Neg. No. MSD-164956.
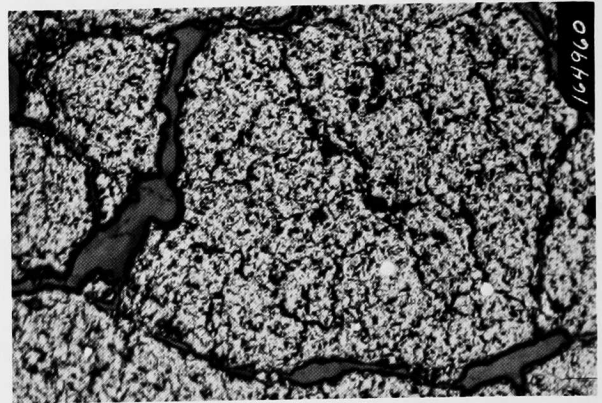
b. Sieve No. 12 Particle. Mag. 2.25X.
   Neg. No. MSD-164960.

Fig. 39. High-magnification Views of Fuel Particles Retrieved from Test Section

The loop sodium was also reacted with alcohol to reclaim any fuel or cladding debris. About 1 g of debris was collected, but the bulk of this appeared to be vermiculite contaminant and other light material that was floated off with methylene iodide.

5. Conclusions

Based on the macroscopic and microscopic examination of the inner wall, it is concluded that the initial failure in Test H2 was near the top of the fuel column. Some molten cladding at the lower end plug dropped downward, which, with some fuel, might have caused a partial inlet blockage. The inner wall was unaffected, except for a small blister near the bottom and the several burn-through holes above the original fuel column. (Between these regions little adherent fuel was found on the inner wall.)

The observed burn-throughs were probably caused by the hot fuel that moved upward and came to rest there. This hot fuel containing molten cladding spewed upward from below, past the insulator pellets, driven by either internal gas, rapid sodium vaporization, or stainless steel vapor. This force also moved the upper separated portion of the element upward.

Characterization of the fuel-particle debris from the test section revealed that it was composed of large, fairly dense, angular particles and smaller, slightly less dense, more spherical ones, containing small dispersed stainless steel globules. This corresponded well to the degree of melting. The loop sodium contained less than 1 g of fuel particles.

IV. TEST DATA FOR E4

Analog flow and power data from the magnetic tape were redigitized in time increments of 1 msec to provide better time resolution than was available from the earlier digitized data. The 60-Hz signal was removed by a least-squares fitting routine, the same as was done for Test H2. Uncertainty in the timing of the pressure pulses was ±1 msec for Test E4, but pulse-amplitude uncertainties were ±25 psi, the same as for Test H2.

Except for the timing and amplitude of the events during Test E4, the sequence and failure scenario is similar to that given for H2.

A. Prefailure Flow and Pressure Data

Pressure and flow data at the inlet and outlet for Test E4, including initial slug ejection and reentry, are shown in Fig. 40. Boiling began after 1.928 sec (most likely at 1.932 sec), and slug ejection at 1.975 sec. The last 10 msec of prefailure boiling was more active than observed in H2, and slug ejections were markedly more dynamic. For the initial fuel release in H2, the inferred time available for fuel fragmentation was ~5-10 msec. (Fragmentation time begins with initial positive acceleration of the outlet slug after failure and ends when the mixing zone at the point of failure is voided.) From
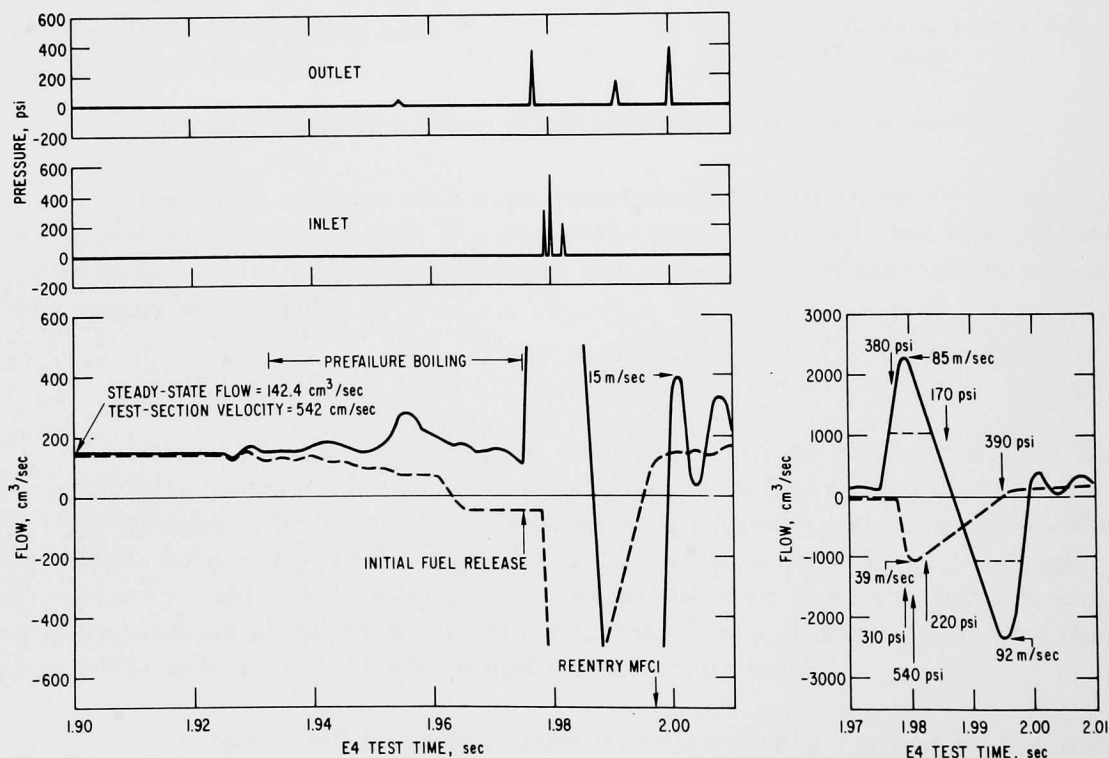
Fig. 40. Prefailure Flow and Pressure Data for Test E4. Steady-state flow at 1.90 sec is 142 cm^3/sec. The initial slug ejections are shown to the right on a compressed amplitude scale; the timing and amplitudes of inlet (bottom) and outlet (top) pressure pulses are shown with arrows. Detector saturation levels during initial slug ejection and reentry are shown by horizontal dashed lines. The zero shift in pressure-transducer baseline has been removed.

the E4 flow data, only a very short time (~1 msec) was available after failure before the sodium was voided, indicating a possibly more massive initial fuel release (calculations indicate the fuel pin was completely molten at this time) and a much shorter fragmentation time. Average accelerations (2.7×10^6 cm/sec^2 at the inlet; 2.2×10^6 cm/sec^2 at the outlet) were the largest ever observed in either the E or H test series.

Data for initial slug ejection and reentry are shown on a compressed scale to the right of Fig. 40. Full scale of the upper (outlet) flow detector was at 1050 cm^3/sec (dashed line), and peak slug velocities were estimated from the flow data and their time derivatives on either side of the peaks. The nearly constant prefailure reverse inlet flow (-50 cm^3/sec) from 1.966 to 1.978 sec can be accounted for by constant escape from the inlet of vapor produced by boiling in the mixing zone. Test E4 is the only fuel-dynamics test in which this flow condition existed. The observed difference of 3 msec between the time of slug ejection from the inlet and outlet can result from two-phase sonic-propagation time effects. This same effect would account for the observed 1- to 2-msec delay between the pressure pulses and the slug ejection.

There is evidence on the visicorder traces of very small outlet pressure pulses during the prefailure boiling. A small pulse of 10 ± 10 psi was noted at 1.955 sec and is attributed to vapor-bubble collapse in the outlet region.

The nearly simultaneous events (a 380-psi outlet pressure pulse at 1.977 sec; 85-m/sec outlet slug ejection beginning at 1.976 sec; a 310-psi inlet pressure pulse at 1.979 sec; and a 39-m/sec inlet slug ejection beginning at 1.978 sec) result from cladding failure at 1.975 sec and release of molten fuel into the flow stream. Coolant reentry from the top begins 10 msec later (1.986 sec) and with an acceleration of ~10^6 cm/sec^2. Reentry accelerations of this magnitude could be caused by rupture of the evacuated fuel holder. The second inlet pressure pulse (540 psi at 1.980 sec) corresponds to the holder-wall rupture. The third outlet pulse (390 psi at 1.995 sec) and the second slug ejection at the outlet were identified as a reentry MFCI. Absence of corresponding inlet activity during the reentry event suggests flow-channel blockage is complete by 2.000 sec and possibly as early as 1.987 sec.

Fuel release at 1.977 sec produced sufficient coolant vapor to drive the initial sodium slugs out of the test section. The fuel was carried upward with the vapor-liquid flow until 1.987 sec, at which time the inlet flow reversed. However, a positive (upward) driving force existed only during the period of positive acceleration (1.977-1.979 sec). Most, if not all, of the upward fuel sweepout must have occurred during this 2-msec period, and fragmentation time may have been as short as 1 msec. The voiding rate at the initial failure time was ~2 cm^3/msec. Delayed fuel release into voided regions would deposit on the holder walls and could cause holder failure by meltthrough. Some of the flow and pressure activity shown in Fig. 40 could be due to the effects of steel vapor (steel boiling temperature approximately equal to fuel-melting temperatures).

Both the integrated flow and the void for the prefailure portion of Test E4 are shown in Fig. 41. Flow data shown in Fig. 40 suggest that boiling began at 1.935 sec. The small growth rate of the void before boiling is most likely due to the effects of the expansion of the fuel pin and coolant due to heating. (A smaller effect is expected from heating of the flowmeters and a corresponding differential change in calibrations.) For comparison purposes, the void growth rate from Test H2 since the beginning of boiling (1.935 sec in E4, and 1.465 sec in H2) is shown with the E4 void in the lower curve of Fig. 41. During the first 30 msec of boiling, the void growth rates in the two tests were identical, indicating similar thermodynamic conditions during this time, despite the 16% higher flow rate in H2. A somewhat more active boiling began at 1.965 sec, when the void differences between Tests H2 and E4 became measurable. It is during this period that the constant negative inlet flow occurred. At the time of failure (1.975 sec), the vapor volume accounted for almost 6 cm^3 of flow-channel volume. If this were lumped as a single vapor bubble, it would extend over the top half of the fuel column. However, the level of refill following postfailure reentry suggests that only half the void is in the fueled region of the flow channel; the other half is in the outlet plenum region.
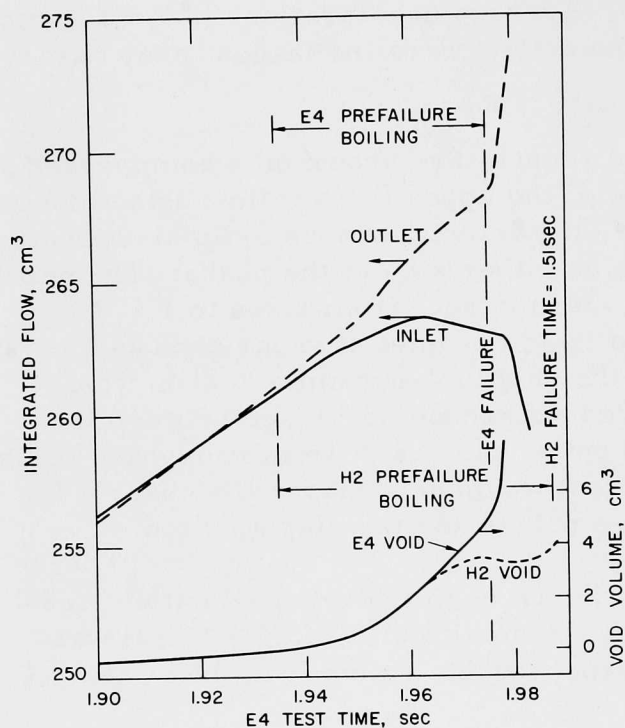
Fig. 41. Prefailure Integrated Flow and Void Volume for Test E4. H2 void data are shown for comparison.

B. Postfailure Flow and Pressure Data

Postfailure flow and pressure data are shown in Fig. 42. After flow recovery from initial ejection, there was a second and possibly a third ejection out of the inlet at 2.04-2.05 and at 2.07-2.08 sec. A train of small pressure pulses occurred at the inlet during these times. The correlation between inlet pressure and inlet flow was not sufficient to identify specific events. Outlet slug ejections after failure occurred at 1.995, 2.005, 2.015, and 2.03 sec. Each of the first three slugs was preceded (by ~5 msec) by pressure pulses (at 1.991, 1.999, and 2.009 sec). This delay between slug ejection and pressure pulse is probably due to the large volume of vapor in the flow channel. A delayed interaction is apparent at both the outlet and the sodium ejection between 2.03 and 2.05 sec. Thus, the delayed interaction in E4 occurred 65 msec after initial failure. In H2, it occurred 190 msec after failure.
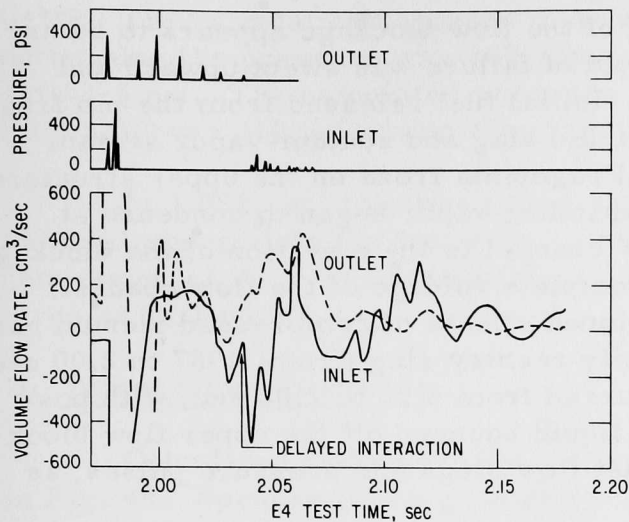
Fig. 42. Postfailure Flow and Pressure Data for Test E4. Details of the initial slug ejection after failure are shown in Fig. 40.

If fuel fragmentation and upward fuel sweepout can only occur during positive outlet flow, the fragmentation time is estimated as ~1 msec. Absence of significant inlet-outlet flow correlation after 2.00 sec suggests the flow-channel blockages were nearly complete. Posttest examination of the outlet blockage suggests it was porous enough for vapor to leak through to displace outlet sodium, as noted in the outlet flow from 2.03 to 2.08 sec.

Integrated flow and voiding history for Test E4 are shown in Fig. 43. After the initial reentry, liquid from the upper head cannot reenter the fueled region without a significant vapor interaction. This fixes the top of the fuel column with respect to the integrated flow at 279.5 cm³. The rest of the flow channel and the inlet and outlet plenums are located according to their respective volumes (see Fig. 8). After 1.986 sec, the entire fueled region of the flow channel was voided, and fuel-coolant (liquid or vapor) interactions were only loosely coupled to the pressure and flow instrumentation. The outlet reentry at 2.00 sec (see Fig. 41) accounts for the 370-psi outlet pressure pulse at 2.00 sec (see Fig. 42). The change in void growth rate from 2.03 to 2.05 sec is due to the delayed interaction. The abrupt inlet ejection at 2.04 sec and the corresponding inlet pressure pulses fix the delayed interaction at 65 msec after failure. Flow behavior after 2.08 sec is characteristic of local boiling (vaporizations and bubble collapses) at the surfaces of the blockages.

Fig. 43

Integrated Flow and Void History for Test E4. Relative locations of flow channel and fuel column are shown to the right. From the dimensions given in Fig. 8, it requires 4.84 cm³ of vapor to void the top of the flow channel, and 88 cm³ to void the region up to the pressure transducer.

A description of the formations of the flow blockage appears to be as follows: Molten cladding at the threshold of failure was swept upward and froze on the colder-pin plenum region. Initial fuel released from the pin fragments and was swept upward with the liquid slug and sodium-vapor stream within the first several milliseconds. Fragments froze on the upper structure of the flow channel and pin plenum. Expanding vapor began to condense at 1.985 sec, and liquid reentered the flow channel to the elevation of the blockage. Fuel released after 1.98 sec (time of complete voidage of the flow channel) burned through holder walls. The combined effects of compressed plenum gas* and holder rupture caused a high-velocity reentry slug (from 1.987 to 2.00 sec). Nearly steady-state flow recovery occurred from 2.00 to 2.02 sec, with possibly three identifiable interactions as liquid bounced off the upper flow blockage (2.00, 2.01, and 2.02 sec; from outlet flow slugs and pressure pulses, as shown in Fig. 42).

At 1.985 sec, the lower flow channel was voided (see Fig. 43) and the inlet blockage began to form. By 2.02 sec, liquid contacted the lower slug. At 2.037 sec, a delayed interaction displaced hot fuel/steel to create a series of pressure pulses and slugs for about 30 msec.

C. Mechanical Work

Bubble pressure and the various components of the work were calculated from the flow data in the same manner as for H2. Results of these calculations are shown in Fig. 44. Compared to H2 results, the work done by the expanding bubble took about one-fourth as long to maximize and was about five times as large in magnitude. The total P dV work was ~25 J, compared to ~10 J
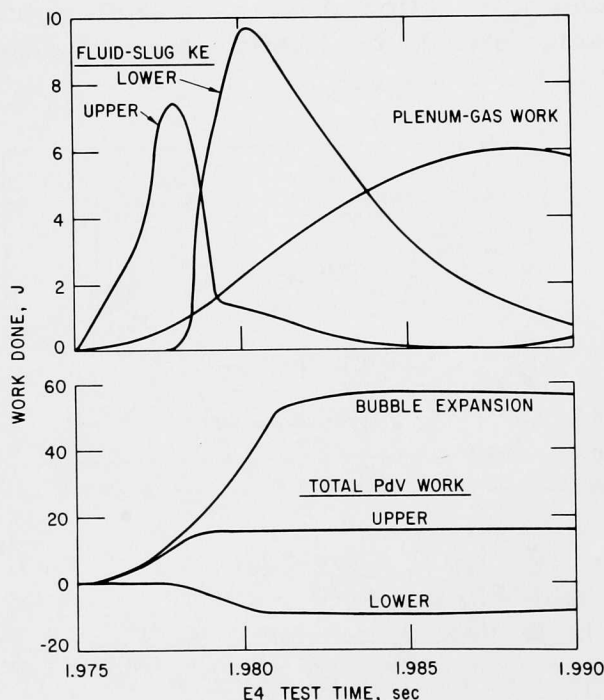
Fig. 44

Components of Work and Energy in Test E4. Kinetic energies of the ejected slugs at the time of the initial failure are shown in the top curves. The work done by the expanding bubble and the total P dV work are shown in the lower curve.

---

*Plenum pressure changes were small, since only ~30 cm³ of the 525 cm³ total volume were replaced by liquid.

in H2. The calculation suggests that during the maximum acceleration of the outlet slug the pressure was 2000 psi. The measured pulse at this time was only 375 psi. The calculated pressure during the maximum acceleration of the inlet slug was 210 psi, comparing favorably to the 220-psi pulse measured.

At 1.986 sec, the time of maximum work done by the bubble (57.1 J), the total energy into the test was 1.19×10^5 J. Accordingly, the efficiency for conversion of thermal to mechanical energy is 4.8×10^{-4}, about five times as large as in Test H2.

D. Temperature Histories

Calculated and measured temperature histories for Test E4 are shown in **Fig. 45**. Because of the greater energy into Test E4 (410 cal/g), the entire fuel pellet was above the liquidus temperature at the time of failure. Boiling at the cladding surface at the hottest axial node was expected to begin when peak cladding temperatures reached the sodium saturation temperature (at 1.93 sec). The calculations are in excellent agreement with the observed data.
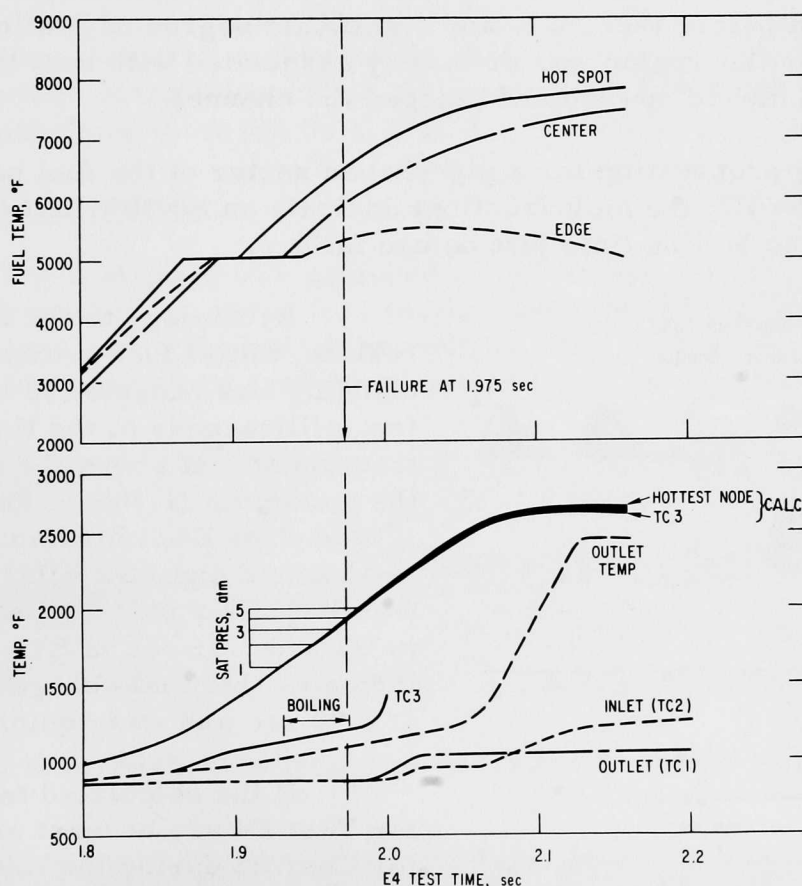
Fig. 45. Temperature Histories for Test E4. Top curves show calculated temperature at the edge, the center, and second radial nodes in from the edge (hot spot) of the fuel pin at the hottest (top) axial node. Cladding (calculated) and coolant (calculated and measured) temperatures are shown in the lower curves.

At most, there is a calculated temperature difference of 50°F between the cladding surface and the coolant at any axial node. Thermocouple TC3 was located at the hottest node (1 in. from the top of the top of the fuel column), but showed a disturbingly large difference (750°F at failure) between measurement and calculation. Better agreement was expected on the basis of Test H1 and H3 calculations. Twenty-five milliseconds after failure, TC3 failed, indicating deposition and solidification of fuel and cladding fragments during initial sweepout.

Measured inlet (TC2) and outlet (TC1) temperatures did not show much activity. Reverse inlet flow associated with initial failure occurred between 1.98 and 1.995 sec. A corresponding increase in temperature (~100°F) was noted between 2.00 and 2.02 sec. This corresponded to the mixing of a small amount of hot sodium being ejected from the flow channel with the colder inlet sodium.

Slug ejection at the outlet occurred between 1.975 and 1.985 sec. The absence of a corresponding increase in outlet temperature as this slug passed TC3 confirms the conclusion that initial fuel release ejected the upper flow-channel sodium before there was any significant degree of heating, and that heating in the outlet region was primarily associated with heat transfer from the fuel, which moved upward and plugged the channel.

Melting propagation for a pie-shaped sector of the fuel pellet is shown in Fig. 46. Like H2, the melt fractions indicate an equilibrium condition during the ~30-msec boiling time just before failure.

By analogy to the H2 hodoscope results, initial fuel motion within the cladding was expected to begin within a few milliseconds of the time the volume fraction of fuel above the solidus reached the maximum (1.38 sec for H2 and 1.90 sec for E4). Maximum internal motion was expected after the maximum fraction of liquidus was reached (1.48 sec in H2 and 1.95 sec in E4). Figure 45 indicates that fuel change of state began at 1.90 sec and was complete at 1.95 sec.

If the calculated temperatures for Test E4 are at least as good as these for Test H2 during the time in which the flow and void characteristics of the two tests are the same (see Fig. 41), prediction of 100% melt fraction at failure is probably good. If the thermal energy added between 1.965 sec and failure (1.975 sec) were added adiabatically, the average fuel temperature would rise

Fig. 46. Melting History for Test E4. Times at which solidus and liquidus temperatures are reached for each radial zone at the hottest axial node are shown at the top. Corresponding volume fractions are shown in the lower curves.

~40°F. From failure to the end of the transient, the additional 87 cal/g of energy added is sufficient to vaporize 10% of the fuel. It is sufficient to note that fuel vapor, if it existed in Test E4, did not significantly affect the post-failure fuel movement or the posttest nature and distribution of failed fuel.

E. Hodoscope Observations

During the pretest calibrations, oscillator pulses are multiplexed through each of the 334 counting channels of the hodoscope to test and verify their operation. During Test E4, this test signal was inadvertently left on, resulting in dead-time corrections varying from 40 to 80% during the transient. Efforts to remove or correct for the oscillator test signal have been unsuccessful, and the E4 hodoscope data were irretrievably lost.

F. Posttest Examination

The experiment disassembly and part of the macroscopic examination were performed at HFEF in an argon-atmosphere glovebox starting on June 19, 1972. The rest of the macroscopic examination and the microscopic examination were performed at the MSD Alpha-Gamma Hot Cell at ANL-East. The loop sodium was also recovered by HFEF and sent to MSD for fines retrieval by sodium dissolution. This operation was performed in a high-purity nitrogen-atmosphere glovebox by a joint RAS-MSD force.

1. Disassembly

The test train was removed directly from the loop body. No sodium drained from the bottom of the test section, and only 65 g of the expected ~150 g could be drained out of the top of the section. The test section is shown in Fig. 47, and the entire test train is shown in Figs. 48-51. No sodium or fuel
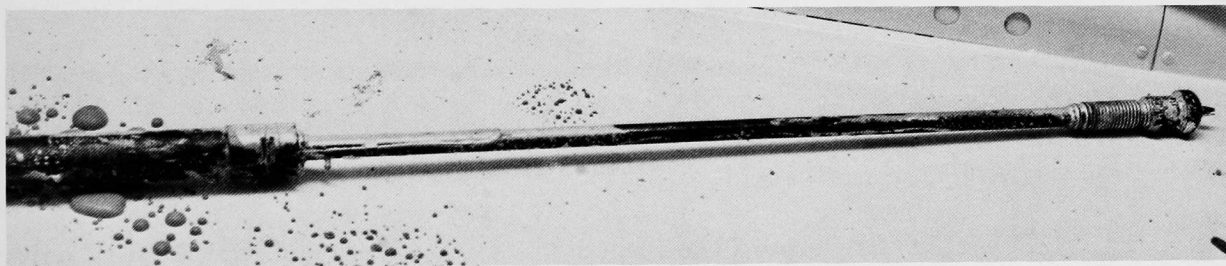
Fig. 47. Bottom Portion of Test Train Containing Test Section. ANL Neg. No. 103-A12320.
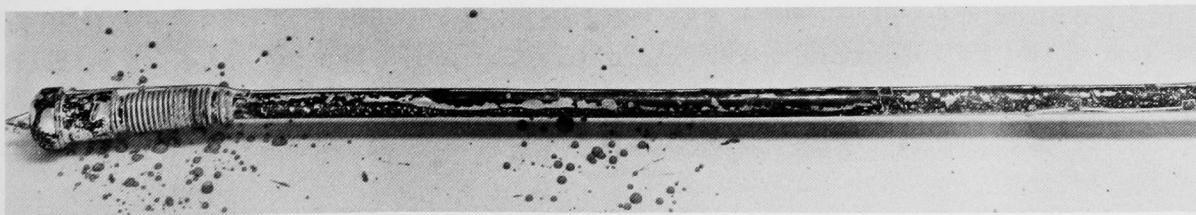
Fig. 48. Test Train Showing Most of Test Section. Mag. 0.3X. ANL Neg. No. 103-A12325.
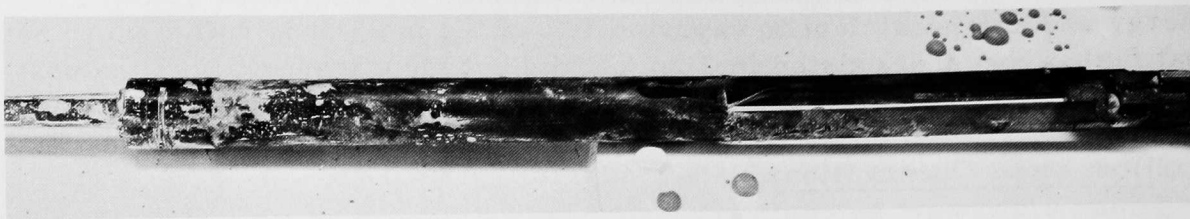
Fig. 49. Test Train Showing Remainder of Test Section and the Adapter
Tube. Mag. 0.3X. ANL Neg. No. 103-A12324.
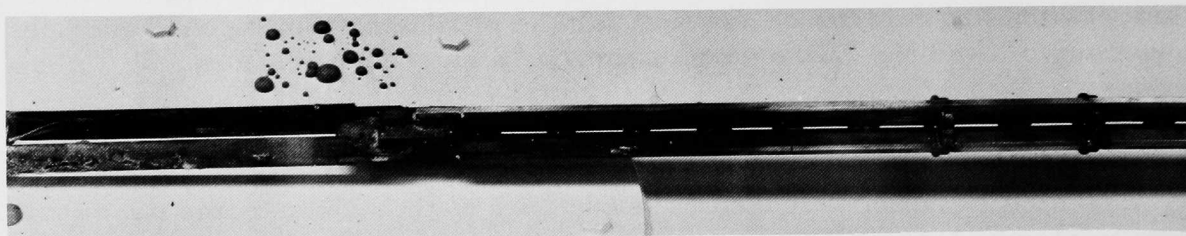
Fig. 50. Test Train Showing Adapter-tube Tee Connector and Bayonet
Assembly. Mag. 0.3X. ANL Neg. No. 103-A12322.
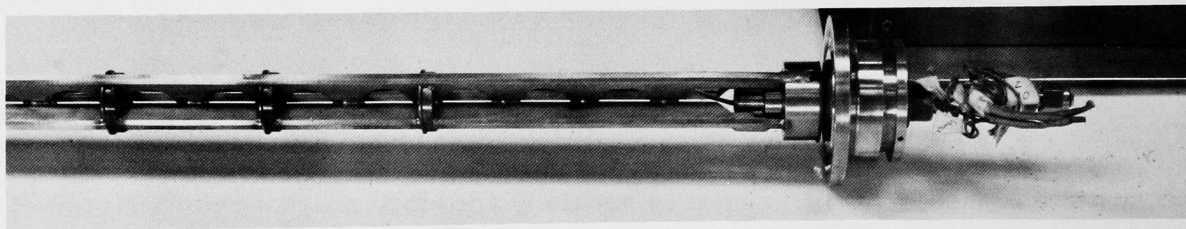
Fig. 51. Test Train Showing Bayonet Assembly and Upper Housing.
Mag. 0.3X. ANL Neg. No. 103-A12323.

is evident at the upper bayonet assembly. Measurements of the diameter of
the fuel holder before cleaning showed no bulges or out-of-roundness. As seen
in Fig. 48, the lower bellows was bent from its original position, but the rest
of the holder was fairly straight.

The clip that joined the upper instrument section to the fuel holder
and the pin supporting the fuel element were both easily removed. However,
the sections were not separable. Furnace heating permitted the upper adapter
to be slid off, and the remaining 90 g of sodium was reclaimed through the top
end of the fuel element, which was intact and externally unaffected. However,
a gap between the spacer wire and the element was evident. Figure 52 shows
the top of the fuel element extending above the fuel-element holder. A rather
large gap exists between the fuel element and the spacer wire where the ele-
ment protrudes from the holder.
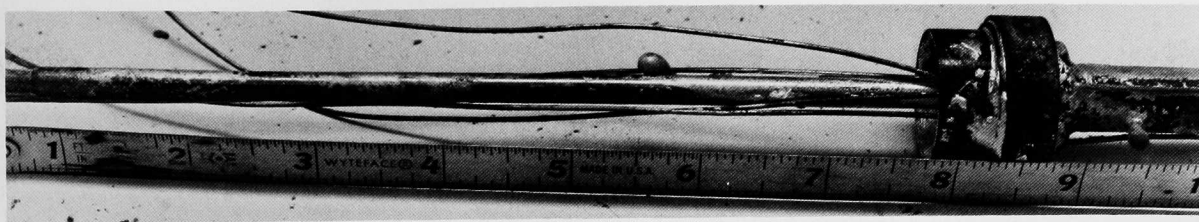
Fig. 52. Fuel Element above Fuel Holder after Removal of Adapter Tube. ANL Neg. No. 103-A12364.

2. Macroscopic Examination

The spherical seal was cut off with an abrasive cutoff machine just below the bellows. The surfaces obtained are shown in Fig. 53. Some fuel and cladding debris may be seen in the flow channel outside the end plug, which verifies the high radiation level found in this region by an axial gamma scan. Elsewhere the radiation levels were uniform. The lower portion of the test section was then longitudinally slit in two planes, 180° apart. (The depth of the cut could not be carefully controlled.) After these cuts were completed, a tubing cutter was used to cut through the outer wall of the fuel-element holder, slightly above the top of the original position of the uppermost insulator pellet. These sections are shown in Fig. 54. A slug of sodium containing debris was pulled out of the upper section. The debris was removed from the lower section and collected for later examination.

Fig. 53. Surfaces Exposed after Transverse Cut below Bellows. ANL Neg. No. 103-A12361.

Fig. 54. Surfaces Exposed after Transverse Cut above Top of Fuel Column. ANL Neg. No. 103-A12363.

The slit halves were then opened up, and the remains of the inner wall were removed. These are shown in Figs. 55 and 56. Several burned-through areas along the inner wall are evident along with a complete separation at 6.25 in. from the bottom cut. In addition, the inner wall at the upper end was melted nearly completely across its perimeter. Except for these regions, the OD of the inner wall was within ±0.001 in. of the original dimension. The surface, where it was not covered by sodium, looked fairly bright.

Fig. 55. Lower Portion of Inner Wall after Removal of Outer Wall. ANL Neg. No. 103-A12357.
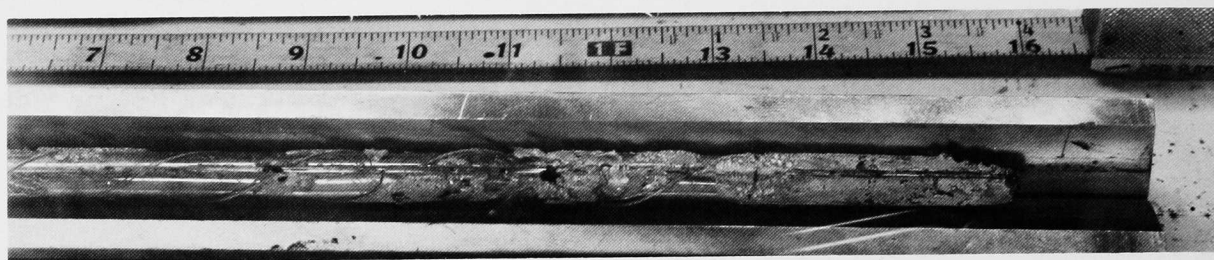
Fig. 56. Middle Portion of Inner Wall after Removal of Outer Wall. ANL Neg. No. 103-A12356.

Longitudinal cuts were then made in the inner wall of the fuel-element holder. Following the cuts, the inner tube was opened up to expose the interior. The bottom portion of the inner wall is shown in Fig. 57; the remaining (middle) portion is shown in Figs. 58 and 59, with the top at the left. Both figures, which are magnified 1.5 times, show some fuel and cladding debris covered by sodium (or sodium oxide). Large chunks of the lower insulator pellets appear to be present just above the bottom of the end plug.

Fig. 57. Bottom Portion of Inner Wall after Slitting. ANL Neg. No. 103-A12349.

Fig. 58. Upper Part of Middle Portion of Inner Wall after Slitting. ANL Neg. No. 103-A12343.
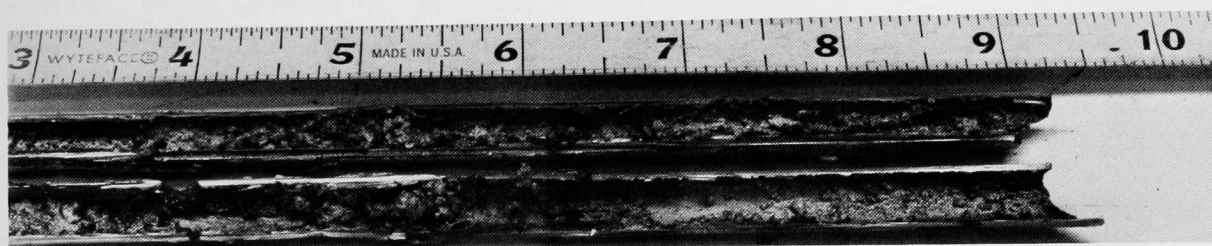
Fig. 59. Lower Part of Middle Portion of Inner Wall after Slitting. ANL Neg. No. 103-A12344.

Prior to sectioning the upper portion of the test section, diameter and other measurements were made and X-radiography was performed. The exposed part of the fuel rod (see Fig. 52) was found to be 0.2298 ± 0.0001 in., which is essentially unchanged from the pretest dimension. However, the fuel rod was found to be bowed ~0.19 in. and had moved upward ~2.25 in. as a result of the transient. The outer wall had increased in diameter by 0.016-0.019 in. (~3.5% $\Delta D/D$) over the pretest value of 0.495 ± 0.001 in. given in the detail drawings. The pretest value may be in error since the lower portion was also found to have increased uniformly. In addition, the inner wall had not increased in diameter.

The X-radiograph shown in Fig. 60 revealed that fuel material was impacted against the spacer cap and was extruded through the 1/16-in. hole in the cap toward the spring region. The spacer tube itself moved up 1.375 in. Also, the spring deformed and relaxed due to contact with masses of hot fuel extruded through the spacer cap. Fuel was evident along the inner surface of the spacer tube, and slugs of fuel were evident in the upper test-section portion. Steel from the cladding and the inner holder wall was found along with fuel impingement on the outer regions at the bottom of this section. These fuel slugs were apparently above the original position of the top of the fuel stack; however, this portion may have moved upward from a massive cladding failure lower down the rod.

The upper portion of the test section was cut open in stages. In the first stage, the large collar was removed by circumferential cutting, exposing
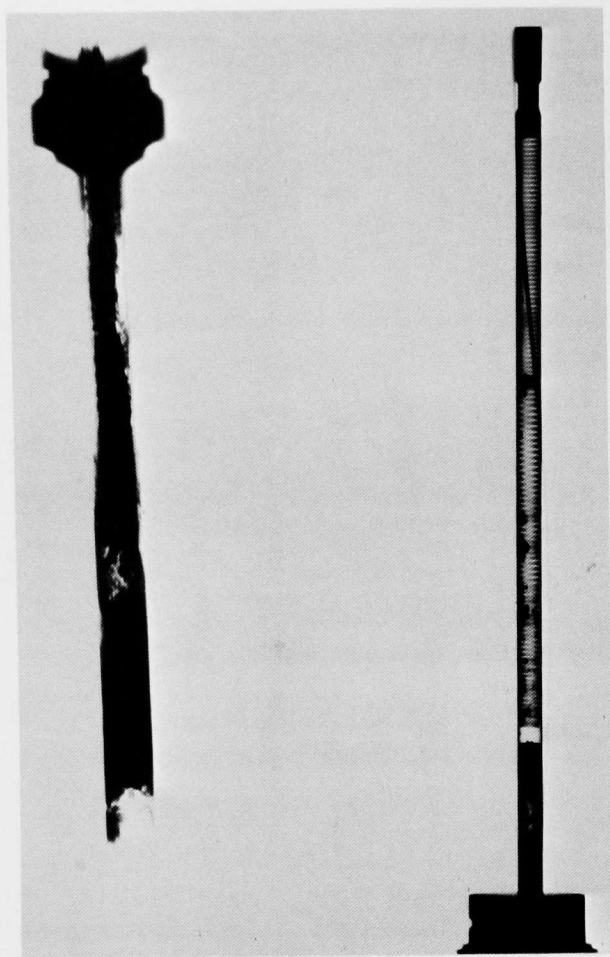
Fig. 60. X-radiograph of Upper Test Section Showing
Remaining Upper Intact Section of Fuel Rod.
Neg. No. MSD-164758.

a portion of the fuel cladding. The cladding was intact, but had a mixture of once-molten cladding and fuel deposited on ~40% of its surface, as seen in Fig. 61. The source of the mixture was the lower portions of the test section. Sections of the outer wall of the holder were then removed by circumferential cutting. In the upper sections, sodium, but no fuel, was evident. After the sodium was reacted away, the outer surface of the inner wall was found to be bright. About 2.5 in. of the outer wall was removed without difficulty. The next 0.5-in. section could not be removed, and a complete radial cut was made. A 0.25-in. slice was taken for metallographic examination.

The rest of the upper portion of the test section was slit longitudinally with a small abrasive cutoff machine. The longitudinal section is shown in Fig. 62. After dissolution of sodium, fuel and cladding debris were evident. Sections were taken for metallographic analysis.

The lower and middle portions of the test section were also cleaned of sodium by reaction with alcohol. Debris, loosened during this operation, was collected for later examination. The inside and outside of these sections are shown in Fig. 63. The outside of the lower section of the inner wall also was examined macroscopically, and several burned-through areas were present about 2 in. apart. These areas contained little fuel except for the upper 2 in. and the lower 1 in. The lower portion of the bottom end plug, also shown in Fig. 63, was examined further macroscopically at 5X. The macroexamination revealed a small amount of once molten fuel and cladding debris adhering to the plug adjacent to the wire wrap and the flat (see Fig. 64), but it covered only about one-fourth of the surface of the plug.

The upper plenum portion of the fuel rod containing the spacer and spring was sectioned. A longitudinal section was taken through the spacer tube and cap; the remaining plenum portion was slit longitudinally to recover the spring. Sodium was found condensed on the convolutions of the spring located above the spacer tube. This suggests that sodium vapor carried the fuel and

cladding mixture through the spacer tube to the spring region, after which the hole in the spacer tube cap was plugged by solidifying fuel. Sodium vapor did not condense below the spacer tube cap since this region was too hot. Portions of the spring containing large adhering fuel chunks were recovered for metallographic examination. Small fuel fragments were found distributed throughout the spring region and on the bottom surface of the upper end plug.

Fig. 61

Fuel and Cladding Debris Solidified on Cladding Plenum under the Collar. Mag. ~2.75X. Neg. No. MSD-164695.
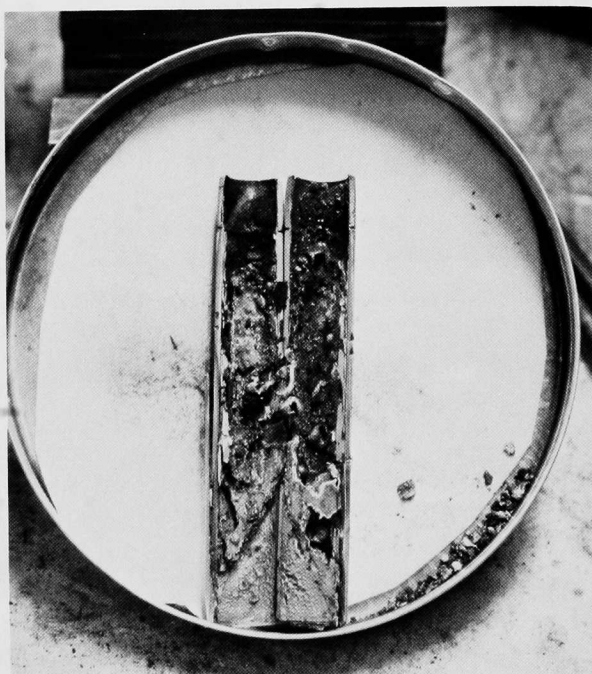
Fig. 62

Upper Portion of Inner and Outer Walls after Slitting. Mag. 0.75X. Neg. No. MSD-164837.
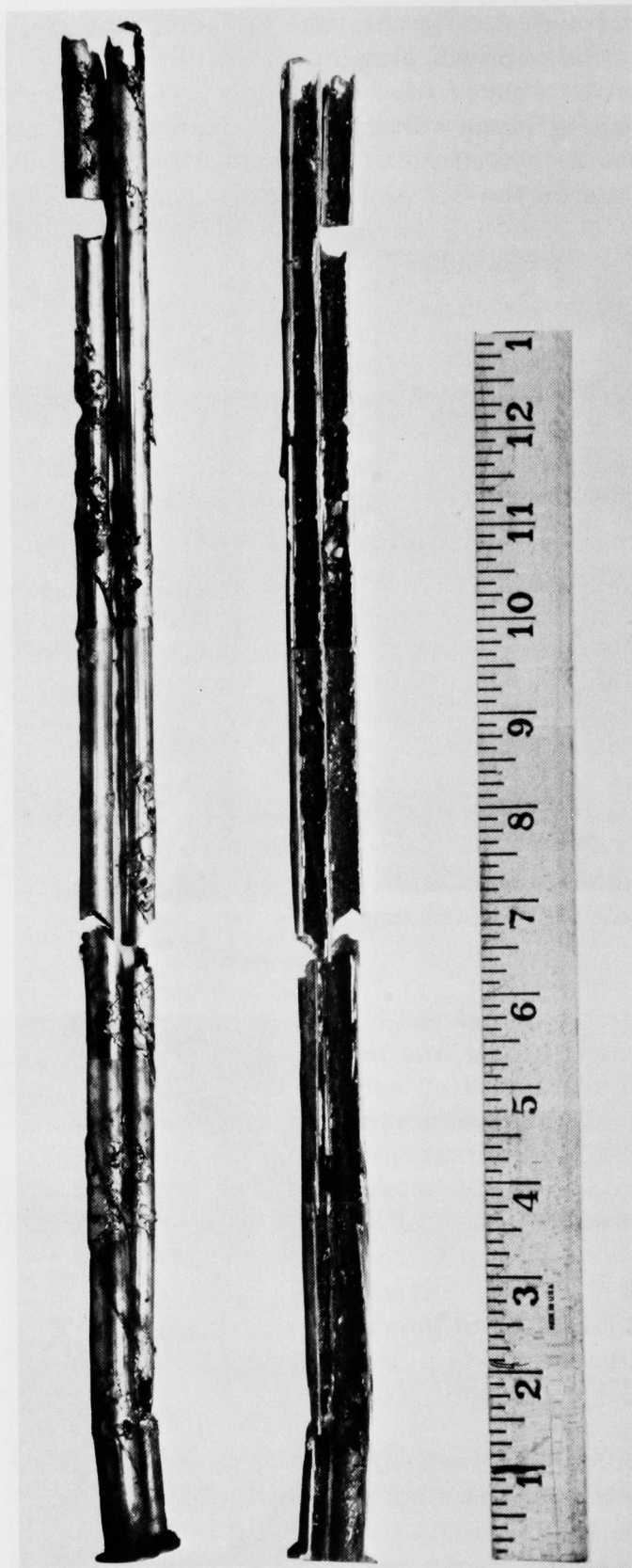
Fig. 63. Inside and Outside Views of Lower Portions of Inner
Wall after Sodium Dissolution. Mag. 0.5X. Neg.
No. MSD-165160.

Fig. 64. Debris Solidified on Lower Portion of Lower End Plug. Mag. ~5X. Neg. No. MSD-165211.

The sodium collected during the test-section removal at HFEF was reacted with alcohol and the debris collected. Essentially no fuel was found in these sodium samples. The remaining sodium samples containing debris from the disassembly operations were reacted, and the fuel and cladding debris collected and mounted for metallographic examination. The loop sodium was also reacted with alcohol to reclaim any fuel or cladding debris. About 1 g of debris was collected, but the bulk of this appeared to be vermiculite contaminant and other light material, which was floated off with methylene iodide. The likelihood that little fuel was carried out of the test section was partially substantiated by the cleanliness of the adapter tube and the fuel-rod cladding above the test section.

3. Microscopic Examination

Emphasis during the microexamination was placed on the upper and lower regions of the test section where fuel had concentrated. To aid the reader in following the microexamination, the results are presented from the bottom of the test section to the top.

A longitudinal and a transverse section were examined from the flow channel surrounding the bottom end plug, as shown in Figs. 65 and 66. The microexamination of the flow channel revealed fuel, insulator, and cladding particles ranging in size up to about 40% (0.02 in.) of the channel width (0.048 in.). These particles made up about one-third of the available channel in the longitudinal cross section and about half the channel in the radial cross section. The fuel and insulator particles in the channel had similar appearances from the top to the bottom. However, the stainless steel particles at the top had a more pronounced and directional dendritic pattern, whereas those at the bottom were just the reverse, i.e., weak and multidirectional. This indicates that the particles at the bottom cooled much slower than those at the top.

The next section examined was one taken from just below the original top of the fuel column, as seen in Fig. 67. The fuel adhering to the wall was made up of fairly dense grains bounded by large necklaces of pores. Little stainless steel was found in these boundaries. The exterior portion of the stainless steel inner wall had melted to a great degree when fuel abutted it.

Fig. 65. Transverse Section through Lower End Plug and Inner Wall. Mag. ~4.7X. Neg. No. MSD-165035.
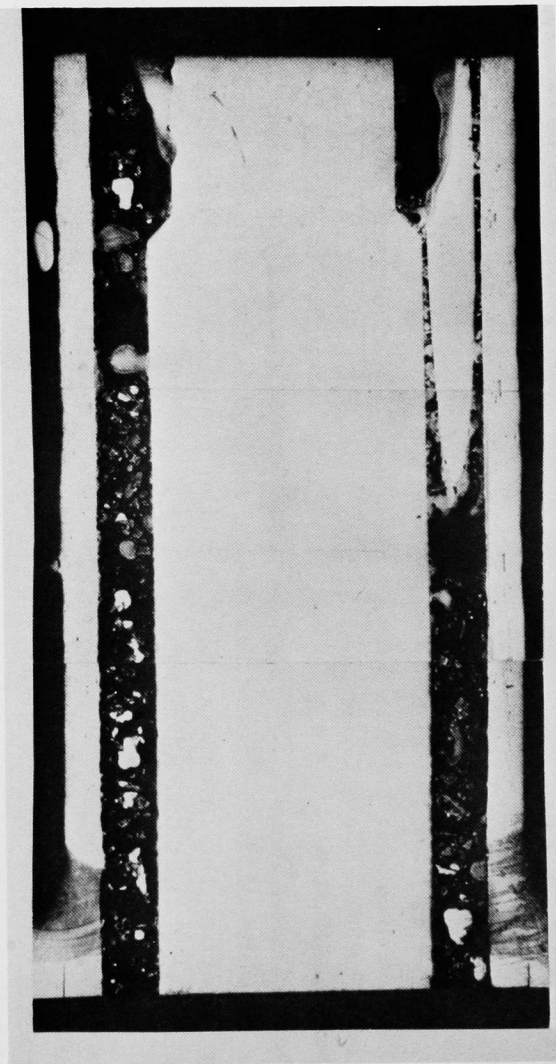
Fig. 66. Longitudinal Section through Lower End Plug and Inner Wall. Mag. ~6.75X. Neg. No. MSD-167417.

Fig. 67. Transverse Section of Inner Wall Just below Original Top of Fuel Column. Mag. ~13.5X. Neg. No. MSD-164898.

On the exterior of the inner wall, several layers of stainless steel from both the inner wall and fuel-element cladding were found. As seen in Fig. 67, these flows filled the gap between the inner and outer walls. The source of this material is probably the failure region above the top of the fuel column. Since the cladding was Type 316 stainless steel containing molybdenum, whereas the other walls were Type 304, microprobe examination was able to differentiate them.

The metallographic sample taken from the upper part of the test section near the flow blockage is shown in Fig. 68. This section was about 3.5 in. above the original top of the fuel column. Evident are the outer wall, a portion of the inner wall, an essentially whole insulator pellet, and once-molten cladding and fuel debris. At this elevation in the test section, molten fuel and cladding destroyed most of the inner wall and melted portions of the outer wall. Molten stainless steel was well distributed across this section and had infiltrated cracks in the whole insulator pellet. Microprobe examination has shown that much of the stainless steel on the inner holder wall is from the cladding, as well as the steel infiltrating the insulator pellet. The steel outside the inner wall was again layered like that found in the section shown in Fig. 67, and was made up to Type 316 and 304 with gradations of molybdenum content.
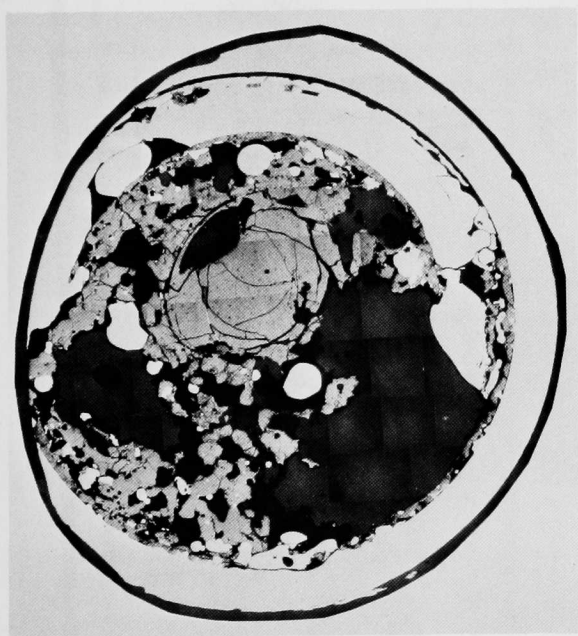
Fig. 68. Transverse Section near Flow Blockage 3.5 in. above Original Top of Fuel Column. Mag. ~5.5X. Neg. No. MSD-164897.

The nearly whole insulator pellet shown in Fig. 68 did not melt, but the adjacent fuel material was definitely molten and contained a uniform mixture of small stainless steel globules. The interface between nonmolten insulator and once-molten fuel is shown at 150X in Fig. 69. The missing portion of the insulator pellet was probably pushed upward with the ejected fuel.

A cladding section adjacent to the collar, which was previously noted to have had a mixture of once-molten cladding and fuel deposited on it (see Fig. 61), was metallographically examined. This section, shown in Fig. 70, had been about 2.5 in. below the spacer cap. Present are the cladding, spacer tube, fuel and cladding debris, and thermocouple and wrap wires. Hot fuel pushed up from below has melted and fused the spacer and cladding tubes. In contrast with Fig. 68, the annular fuel segments present in the section shown in Fig. 70 did not contain stainless steel; in some cases, a second layer of fuel containing steel was deposited. These segments probably originated from fuel just above the failure and were pushed up by either rapid sodium vaporization
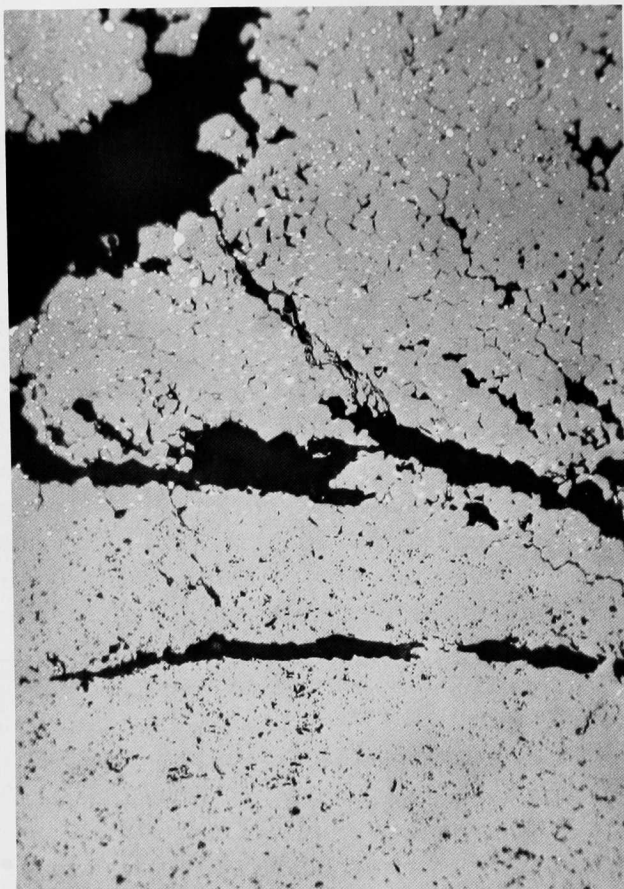
Fig. 69

Interface between Insulator and Once-molten Fuel. Mag. ~150X. Neg. No. MSD–164872.

Fig. 70

Transverse Section of Spacer Tube and Cladding, Showing Adhering Fuel and Cladding Debris. Mag. ~9X. (Same area as Fig. 61.) Neg. No. MSD–165161.

Figure 71 shows the longitudinal section of the upper plenum region containing the spacer tube and cap, against which fuel and cladding have impacted. The stainless steel was subsequently etched to reveal portions of the spacer tube that had melted after the molten fuel came to rest upon it. The more massive spacer cap did not melt, but was ablated by extrusion of hot fuel through it. The fuel in this region contained stainless steel globules distributed in it, as shown in Fig. 72, which indicates that the upward fuel motion occurred well after cladding melting. The once-molten fuel fragments found in the convolutions of the spring contained globules of stainless steel, which were identified by microprobe to be Type 316.

Samples of the small amounts of fuel and cladding fines collected during the disassembly operation were metallographically examined. Most of the fuel fines were nearly spherical, moderately porous, and contained small (up to 10 vol %) amounts of stainless steel. A sample of the fuel particles collected is shown in Fig. 73.

Part of the outer wall opposite a burned-through section of the inner wall, near the original top of the fuel column, was also examined metallographically. Fuel was adhering to the wall, but no obvious reaction other than an increase in grain size in the hot regions was noted.

4. Conclusions

Based on the metallographic examination of the upper part of the test section and the macroscopic examination of the inner wall, it is concluded that the major point of failure was within 2 in. of the top of the fuel column. The failure was probably initiated by sodium-film dryout that began near the top of the element and proceeded downward. The entire cladding melted, which, along with fuel, caused a flow blockage at the bottom of the fuel column. Fuel melting
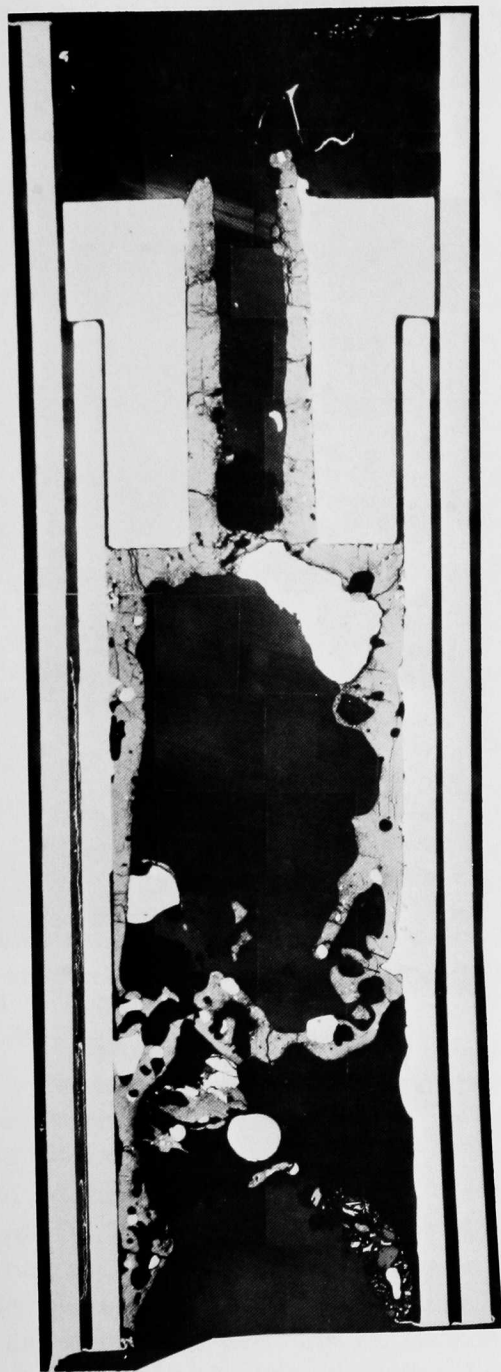
Fig. 71. Longitudinal Section of Plenum, Showing Spacer Tube and Cap. Mag. ~10X. Neg. No. MSD-164901.

followed cladding melting and produced a fuel-cladding mixture. The inner wall failed at this time at various locations due to the proximity of the molten cladding and fuel. The fuel-cladding mixture was then ejected upward, most probably by rapid sodium vaporization occurring both inside and outside the plenum region of the element cladding, causing a blockage in the upper region. This ejection also caused upward motion of the separated upper-plenum portion of the cladding, but was not an energetic FCI.

Fig. 72. Fuel and Cladding Impacted on Spacer Cap. Mag. 70X. Neg. No. MSD-164891.
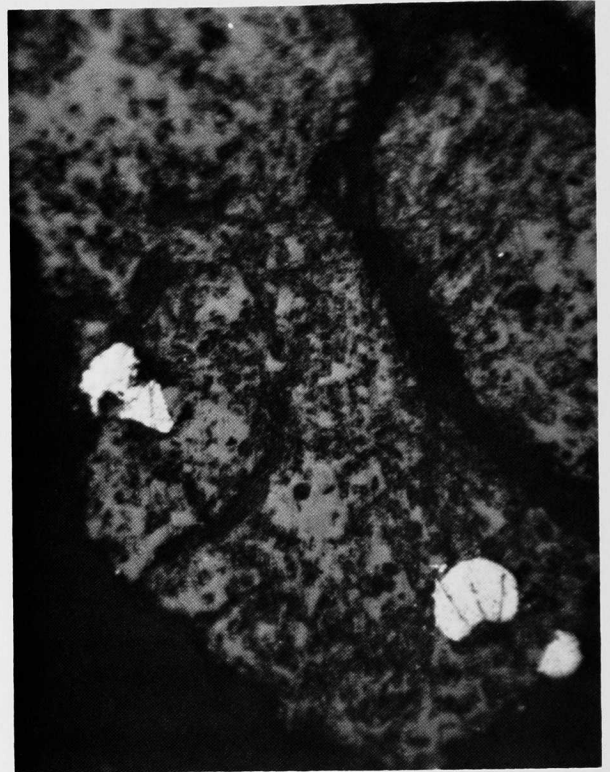
Fig. 73. Fuel Particles Collected From Test Section during Disassembly. Mag. 350X. Neg. No. MSD-165218.

V. SUMMARY AND INTERPRETATIONS

Test data from two failure experiments have been studied and compared. Thermal-hydraulic calculations were made to determine fuel, cladding, and coolant temperatures at locations where they could not be measured. The description of the events leading to and following fuel-element failure was based on the measured flow, pressure, and temperature data, with supporting evidence provided by the hodoscope and posttest examinations. The resulting failure scenario is useful in modeling studies of TOP accidents in the FTR at the beginning of life.

A. Rate Dependence

Fuel enthalpy and cladding temperatures at the time of initial failure were characteristic of an ~ $3/sec unprotected transient overpower accident in the FFTF. However, heating rates during the approach to failure were more characteristic of $6-10/sec accidents. Total energy in Test H2 exceeded the failure threshold by a small margin, and the failure phenomena were characteristic of scram-protected transient overpower accidents. Although failure in E4 occurred after the peak power in the transient, fuel and cladding temperatures as well as heating rates at the time of failure were characteristic of unprotected TOP accidents. Pin power increased exponentially with an 80-msec period in H2 and a 66-msec period in Test E4. Failure occurred 210 msec (H2) and 85 msec (E4) after peak power was reached. Failure was identified by sodium slug ejections from both ends of the flow channel. Cause of failure was cladding meltthrough from the inside. Concurrent with failure, a small amount of molten fuel was ejected into the flow stream. Sodium was displaced from the flow channel by coolant-vapor production resulting from transient heat transfer from the molten fuel to the two-phase coolant. No evidence suggests that the flow dynamics at failure was sensitive to the fuel heating rate.

Particle-size distribution in the fuel pins showed a limited sensitivity to rate dependence. During rapid transient heating, the cladding exhibited a low thermal inertia because of the high thermal conductivity of the cladding and coolant relative to the fuel and gap. As a result, the increases of cladding and coolant temperatures significantly lagged behind the fuel temperature rise. If the median fragment size decreases with increasing temperature (and hence increasing heating rates), the fines from H2 might be expected to be slightly larger than those found in the S test series. This was not the case, suggesting that the rate dependence of initial fuel release and fragmentation probably depends in some way on the flow dynamics and constraints at the mixing-zone boundaries, including the fuel-holder wall. For comparison purposes, the measured posttest particle-size distribution for a number of tests are shown in Fig. 74.

The combination of flow and heating rates for these tests was such that a 40- to 50-msec boiling time preceded failure by cladding meltthrough.
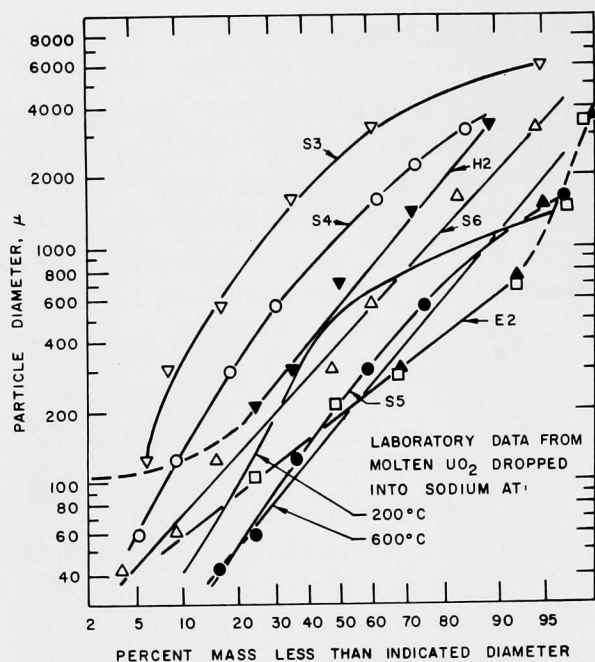
Fig. 74. Particle-size Distributions for
Zero-burnup Failure Test

This boiling regime occurred independent of the amount of heat energy generated in the pin during this time (22 cal/g in H2 and 60 cal/g in E4) as well as the amount of heat energy transferred to the coolant per unit length of fuel (6.9 cal/cm in H2 and 3.7 cal/cm in E4). Because of the difference in power transients, the retained energy in the fuel was significantly higher in E4 at the end of this prefailure boiling than in H2.

B. Thermal Conditions at Failure

Only a limited amount of the increase in specific volume of the fuel with heating and melting can be accommodated by the cladding. The specific volume of the fuel is shown by the solid line in Fig. 75. Also shown is the volume per gram of fuel contained within the cladding for 0, 3, and 6% elastic strain. These curves show that fuel with a volume-averaged temperature below 2140°C does not strain the cladding and that, up to the melting point, cladding strain is less than 3%. Above the fuel melting point, however, the cladding strain approaches 6% and would likely lead to rupture.
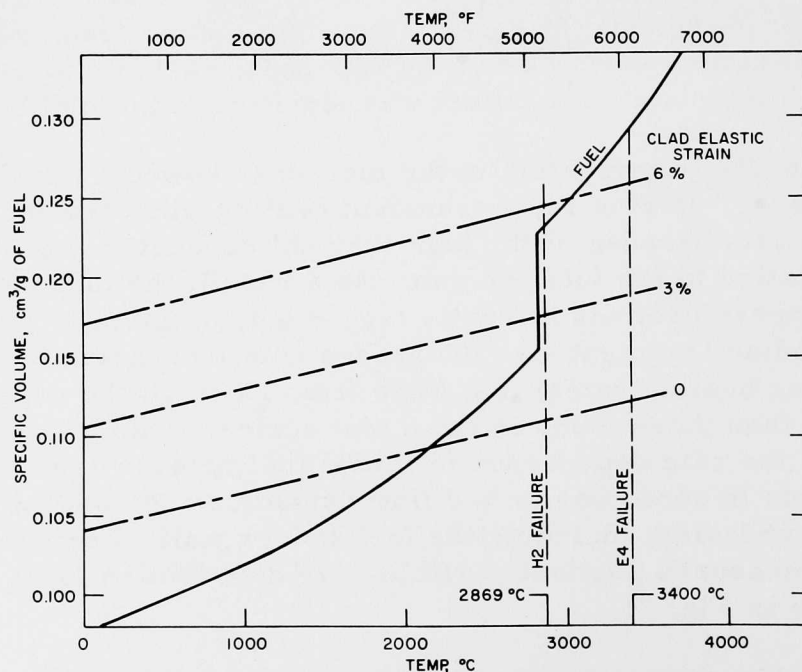
Fig. 75. Specific Volume of Fuel Pellets as a Function of Temperature.
The volume that can be contained by the cladding at 0, 3, and
6% strain is shown as the dashed line. The step increase in spe-
cific volume at 2840°C is due to the change from solid to liquid

Volume-averaged fuel temperatures were calculated at the time of failure. Volume fractions for each radial zone were used as weighting fractions for the calculated temperatures in each zone. For Test H2, the average fuel temperature at failure (1.51 sec) was 2870°C, just above the liquidus point (2840°C). In the same way, the volume-averaged fuel temperature at the time of failure in E4 was 3400°C. Both temperatures are indicated as the failure points in Fig. 75. Although this averaging technique may not accurately account for the expansion resulting from melting, excessive cladding strain will result at this time if the increase in fuel specific volume is not accommodated by internal motion into the pin-plenum region.

Calculated thermal histories of the fuel just before failure illustrate some interesting features shown in Figs. 14 and 46. After about 80% of the fuel that melts is above the liquidus, boiling begins at the cladding surface. Coolant boiling continues, for 40-50 msec, until the liquid film dries out. During the final 20-25 msec, a stable fuel state at maximum liquidus seems to exist. A thin outer shell of fuel, about 100°F below the solidus temperature, remained during failure in H2. At failure in E4, the entire cross section of the fuel was above the liquidus.

C. Failure Sequence

A sequence of failure events, based on available data and calculations, is summarized in Table V. A "zero" time for each test was defined by backward exponential extrapolation of the power trace (see Figs. 4 and 5) to 1 MW. Relative times listed in Table V are in milliseconds after this zero time. The sequence is described below. Where data from only one of the two tests apply, this fact is noted.

1. Prefailure Pin Bowing (H2 Hodoscope Data)

As the solidus temperature is approached at the hottest axial node in the fuel pin, differential expansions in fuel, cladding, and spacer wire cause the pin to bow locally. With increased fuel along the axis at the solidus, more of the pin participates in the bending process and the pin assumes a bow over the entire fuel-column length.

2. Prefailure Internal Fuel Flow

H2 hodoscope data showed upward fuel motion began at the time calculation indicated that the cross section of fuel at the solidus or above extended from the centerline out to about 75% of the oxide cross section. This motion left behind a region of low density--little or no fuel extending across the region within the cladding. Upward motion continued until failure and appeared to be at a constant rate proportional to the volume-averaged fuel temperature. Most of the fuel that moved came from the upper third of the fuel column.

TABLE V. Failure Sequence[a]

	H2[b]			E4		
Event	Time[c]	Energy	Enthalpy	Time[d]	Energy	Enthalpy
Cladding gap closes at hottest node	720	264	195	560	238	210
Fuel melting begins	690	220	195	528	229	201
Max solidus %	720	270	230	560	280	230
Fuel liquidus begins	740	284	239	564	290	240
Max liquidus %	840	357	282	610	270	310
Sodium at saturation temp (1 atm)	782	325	267	615	352	303
Prefailure boiling						
Mild	820	347	279	590	330	280
Bubble collapse	845-855	360-368	284-288	623-635	365-410	315-335
Film dryout	865	360	280	630	400	325
Failure	870	363	284	635	410	335
Fragmentation and sweepout	870-890	363-371	284-289	635-648	410-427	335-338
First slug ejection[e]						
Outlet	870-882	363-372	284	635-639	410-416	335-338
Inlet	870-884	363-372	284	638-641	419-424	337-345
Reentry						
Outlet	883-943	385-388	289	641-645	424-430	345-358
Inlet	885-910	385-388	289	642-656	426-444	348-361
Second slug ejection						
Outlet	f			715-740	482-504	396-410
Inlet	1060-1084	400	290	700	465	387
Total energy in test	1260	400	290	870	520	410

[a]Energy is total energy into the pin, and enthalpy is retained energy in the pin, both in units of cal/g of fuel.
[b]Cooling began at fuel edge at 950 msec (max enthalpy was 290 cal/g).
[c]Zero time in table corresponds to 640 msec in H2 test time.
[d]Zero time in table corresponds to 1310 msec in E4 test time.
[e]Peak outlet slug acceleration = 4.3×10^5 cm/sec in H2, 27×10^5 cm/sec in E4.
  Peak inlet slug acceleration = 1.2×10^5 cm/sec in H2, 10×10^5 cm/sec in E4.
[f]Not observed.

Postmortem examinations indicate that the pressure of molten (or slushy) fuel against the upper insulator pellets not only moved these pellets upward, but also forced liquid fuel into the cracks and between the pellets.

3. Prefailure Boiling

Boiling began when the fraction of fuel at the liquidus reached ~80% of its maximum and lasted 40-50 msec. Calculations of peak cladding temperature have correctly predicted the onset of initial boiling. A likely location for boiling to begin is just behind or under the spacer wire at or near the top of the fuel column. Only a small amount of the measured prefailure void (~1 cm^3) in the flow channel can be attributed to fuel-pin expansion; most of the measured void is believed to be sodium vapor.

The vapor was swept downstream with the flow. Some condensation occurred when the vapor reached the upper cold surfaces of the pin and flow channel, and mixed with the cold upper sodium. Evidence of bubble collapse

was seen in small but detectable pressure pulses at the outlet starting about
20 msec after boiling began. (It was assumed that the vapor was either several
large bubbles that incoherently collapsed or a large number of small bubbles
that coalesced to form large bubbles.)

4. Failure

After a 40- to 50-msec period of mild boiling, the liquid film on
the cladding surface dried out and failure followed by meltthrough from inside.
The maximum fuel fraction above solidus was reached 20-25 msec before
failure.

It is concluded from H2 hodoscope data that, during prefailure
fuel flow within the cladding, molten fuel contacted the cladding tube and melted
a hole through the cladding in the region of the top insulator pellet. The mech-
anism of contact was molten fuel moving against the cladding near or around
the insulator. Following meltthrough, molten fuel issued through the hole,
increasing the hole size and carrying some molten cladding dispersed within
it. Initial release of fuel or fuel/cladding produced the observed rapid vapor-
ization of the coolant. At some time during Test E4, this region of the cladding
tube did melt, but there is no evidence available as to when this happened.
Posttest examination suggests that the plug in the upper flow channel may have
originated at the top, and subsequent debris was packed and molded together
to form the relatively long plug extending below the upper insulator pellet. If
initial fuel release were in the insulator region, the top of the plug might be
expected to be at or close to this region.

5. Fuel Fragmentation

A 20- to 30-msec period existed before failure, during which time
coolant vapor pressures did not allow any liquid to enter the flow channel.
(Inlet flow was zero or negative.) This would suggest that the flow in the failure
region was largely vapor with a bubbly flow above and mostly liquid below.

Fuel released into the vapor zone can thermally interact with the
liquid films and droplets on the holder surface. This interaction leads to
fragmentation on freezing. The smaller difference between fuel temperature
and the steel boiling point is not apt to lead to fragmentation from a fuel-steel
interaction, although it is a likely thermal sink to accelerate fuel freezing.

Initial heat-transfer rates are somewhat slower than calculated
by current FCI models. Energetic shock waves, at "acoustic" pressures of
~100 atm, were not observed. No deformation of the upper holder and pin
structure was noted in the posttest examinations.

Vapor pressures generated in the coolant were sufficient to retard
or momentarily stop further fuel ejection from the hole. Fragmentation times
inferred from pressure and flow data at the time of initial fuel release appear

to be rate-dependent. This would be the case if very hot fuel completely dried out the liquid film on the mixing zone surfaces to prevent further transition boiling and fragmentation.

6.   Fuel Sweepout

In addition to a general upward fuel motion "seen" by the hodoscope in Test H2, the fragmented fuel was carried upward with the sodium vapor. The major heat sinks leading to cooling of the fuel fragments being carried upward (some fragments must also go downward) by the vapor were the holder walls, the pin cladding in the upper plenum region, the spacer wire, and the thermocouple sheath. Fragments froze to these surfaces about 3 in. above the upper insulator to start an outlet flow blockage. No macroscopic quantity of these fragments was swept completely out of the flow channel into the remainder of the loop.

Cushioning effects of the adiabatic fuel holder tend to limit the magnitude of an FCI and, hence, of the initial velocity of fragments that can be swept out of the flow channel.

From pressure-equilibrium consideration, fuel release from within the pin was limited by mixing-zone pressures outside the cladding breech. As the external pressure was reduced by slug ejection, additional molten fuel and cladding could be released into the mixing zone. This suggests that, initially, fuel was released as a jet or squirt that produced the major observable pressure and flow transients. This was followed by a slower release into an essentially dry channel, and the amount of fragmentation and solidification was limited. The later-released fuel, being hotter then that first released, was probably the fuel that first reacted with the upper flow-channel structure to start the outlet flow blockage.

7.   Axial Failure Propagation

After initial sodium pressures were reduced by slug ejections, the entire length of the fuel column became vapor-blanked with the downward motion of the lower liquid interface. This took 20 msec and was followed in another ~20 msec by film dryout and cladding melting. During this period of fuel ejection, the flow channel was voided, and some of the fuel was deposited on the inner holder wall, causing it to fail by melting. The extent of holder-wall melting depended on the temperature of released fuel and the amount of liquid film remaining rather than on the amount of fuel initially released.

8.   Reentry

After the fuel holder failed, the mixing-zone volume was increased by about two and one-half times, and the loop wall became available as a potentially very large heat sink for cooling. In E4, all the fuel was molten during

the failure process, and large portions of the inner holder wall were destroyed. In the less energetic Test H2, only small meltthrough holes were found in the inner wall. In both tests, the large increase in mixing-zone volume favored reentry.

There was no evidence that reentry from the top (outlet) led to a secondary FCI of any substantial magnitude. At most, a small amount of liquid may have interacted with the outlet plug. The pressure of residual vapor and a small amount of noncondensable bond gas from the fuel pin did not allow a sodium hammer.

The outlet blockage appears to have formed first, and some liquid entered the mixing zone from the inlet. In the mild threshold-failure situation of H2 this sodium vaporized at approximately the same rate as it entered. Some liquid film remained on the mixing-zone wall surfaces to prevent excessive holder melting. During the cooling process, some liquid reentered to cause a later, rapid coolant vaporization, but no energetic FCI.

In the more severe failure situation of E4, postfailure reentry was limited, the mixing-zone walls remained dried out, and released fuel deposited on the holder walls melted through them. The major heat sink for cooling was the structure, and little heat was transferred to the coolant. In a multipin environment, it is not clear that the mixing zone would dry out as completely as appeared to be the case in E4. This would account for the substantial delayed FCI's in H2 and the S-series, but not in E4.

The principal fuel motion appeared to be radially outward, with some upward moving particulate contributing to the flow blockage. Median particle size was found to be large, and the particles contained homogeneous mixtures of steel (both cladding and holder wall) and fuel. Where insufficient liquid existed for transition boiling and fragmentation to occur, the particle size was probably too large to move very far in the flow channels.

D. Postfailure Fuel Motion

Pressure pulses were noted between 200 and 400 msec after failure in most of the S-series of tests. In S4, a major inpulse was recorded as late as 2.4 sec after failure. Significant pressure and flow transients were recorded in Test H2 about 200 msec after failure. Small flow transients accompanied by a train of pressure pulses between 100 and 25 psi were recorded in Test E4 between 60 and 100 msec after failure. Power levels in Test H2 at these late times were too low to provide any statistically reliable hodoscope data on delayed fuel movement. Some late fuel motion can be inferred from the flow data and posttest examination.

The inlet flow blockage in each test included a relatively large volume fraction of steel. Little, if any, melting of the fuel-pin end cap was noted,

despite the presence of once-molten fuel in that region. Both observations tend to suggest downward cladding motion before significant fuel melting, as well as a relatively cool fuel-steel mixture that was once quite hot.

The relatively small amount of fusion of the holder wall with the flow-channel plugs suggest that the walls in the plug region were melted by a liquid film during formation of the plugs. The oscillating nature of the flows during this time is an indication of film dryout by boiling. After initial fuel release and fragmentation, the hodoscope showed a predominantly upward and a general outward movement of fuel, starting near the top of the fuel column and progressing downward. It is concluded that, after the flow channel became voided, the remaining lower half of the fuel column squirted or broke off in slushy chunks that were deposited on the holder walls as clinkers. Analysis of clinker samples showed a nearly homogeneous distribution of 2-μ steel particles, which suggests that molten cladding or cladding vapor was dispersed within the fuel at the time of ejection. In the process of cooling, some of these chunks may have cracked and broken loose from the walls, and fell downward to add to the inlet blockage. Fuel near the bottom of the pin that never got hot enough to melt may have broken up under thermal stresses and contributed to the inlet plug. Some molten steel seems to have acted as a binder for parts of this plug.

Reliable postfailure thermodynamic calculations cannot be made without a complete description of the fuel, coolant, and vapor distribution. Estimates of transient heat transfer to the loop wall for a uniform posttest deposition of fuel essentially in contact with the wall indicated that cooling began about 100 msec after failure. At this time, the steel in solution with the fuel was at its maximum temperature. Since the boiling point of steel is close to the fuel liquidus temperature, it is not unreasonable to assume the delayed events were interactions between fuel and steel vapor. Such interactions could lead to the final fuel distributions observed in the postmortem examinations.

VI. CONCLUSION

A single failure criterion of fuel-cross-section area fraction at solidus or above does not appear to be satisfactory to predict the failure thresholds in Tests H2 and E4. Some criterion based on heating rate appears more appropriate, but none is obvious from the available test data. However, both tests exhibit a threshold fuel-liquidus fraction for prefailure surface boiling (~75%) and a fixed period of boiling (50 msec) before failure. Hence, these two criteria are suggested as improvements on a single areal-fraction criterion. The apparent constant prefailure-boiling period may be due to the characteristics of film dryout and, in an approximate manner, account for the higher threshold energy for failure in the faster transient.

Fuel motion internal to the pin began as the maximum fuel fraction above solidus was reached and continued at a nearly constant rate up to the time when significant portions of the cladding failed. Most of the molten cladding was swept upward and froze on the upper pin structure to start an outlet blockage. Some molten cladding dripped toward the inlet and appeared to have solidified without substantial attachment to the lower pin structure.

Initial fuel release involved only a small amount of fuel, which was fragmented into a 50- to 1000-μ particle-size group and carried with the ejected vapor/liquid slugs. Primary motion was upward. Hot fuel mixed with cladding material in the upper structure region of the flow channel, and froze in place to complete the outlet blockage. Few, if any, fragments were swept out into the rest of the loop. For higher fuel enthalpies at failure (as in E4), no macroscopic collections of fuel fines were found after the test.

Subsequent fuel release may splatter or sputter onto the holder walls, to produce the large-particle-size group (~1 mm). Some fuel may break off the holder surfaces with cooling and contribute to the inlet blockage. Particles of this size are too large to undergo any extensive movement within the confines of the flow channel. There was little evidence of massive slumping of either fuel or cladding. Clearly, some of the initial fuel fragments were swept downward and contributed to the inlet blockage, but the quantity was small compared to the amount swept upward. Cladding or structural steel that reached the inlet served as a binder for fuel fragments and chunks.

The nature of the redistributed fuel does not seem to be strongly dependent on either the rate of heating at failure or the total energy in the test. There is an obvious dependence of the total fuel moved upon total energy in the test. Both tests showed chunks or clinkers of fuel/steel debris deposited on and frozen to the holder wall. Both tests showed relatively complete, through porous, flow-channel blockages of comparable size at the inlet and outlet. The outlet blockage contained relatively large concentrations of fuel, whereas the inlet plug was diluted with steel.

Timing of the observed phenomenon can be quantitatively explained in terms of liquid films. Incoherent failures in multipin tests are likely to have more areas wetted by such films. The flow dynamics would be better characterized by the Test H2 results. In very rapid transients in which fuel temperatures approach the boiling temperature, complete dryout of liquid films on the mixing-zone surfaces is possible, and postfailure fuel movement may be more benign.

In both tests, an apparent postfailure event appeared to occur at or near the inlet. Flow and pressure data suggest this event might have been a fuel-steel interaction in the inlet blockage. Such an interaction would redistribute fuel to the state found in the posttest examination. It would also be expected to blow material, including fuel, out of the inlet into the lower bend and drain line of the loop. Although these parts of the loop have not been examined in detail, there is no evidence from the radiographs, the gamma scans, or the loop sodium of significant quantities of fuel outside the flow channel. The delayed events probably correspond to the delayed events observed in the S test series and possibly the so-called "eructation" in the loss-of-flow tests.

Finally, it is observed that no energetic FCI events approached the thermodynamic limits. Thermal-energy conversion to work done on coolant was < 1 J/g of oxide.

APPENDIX

Thermal-Hydraulic Calculations

Detailed fuel, cladding, coolant, and duct-wall temperatures were calculated by the ANL-modified version of the COBRA-IIIB code,[48] originally developed by Rowe.[49] Crossflow (due to pressure gradients and the wire wrap) and turbulent mixing were also calculated. Only radial heat transfer was considered in the fuel and cladding; axial heat transport was modeled through the coolant flow. The thermal conductivity of the fuel-cladding gap was taken to be proportional to the conductivity of the gas in the gap, k, and to the increase of the gap size; i.e.,

$$h_{gap} = \frac{k}{c + \Delta r},$$

where c is a parameter reflecting the residual gap and Δr is the time-dependent gap calculated from differential thermal expansion between fuel and cladding. Values of h_{gap} were bounded by initial and maximum values read as input.

Subsidiary calculations included the average energy density and enthalpy of the fuel, and the average of the coolant temperature at the onset. These results are shown in Figs. 1, 4, 5, 13, and 45.

Sodium properties were taken from Golden and Tokar[50] and are listed in Table A.1. Cladding and duct-wall properties, assumed to be the same, were taken from the SAID Document[51-53] and are listed in Table A.2.

In the geometric modeling of the test, the fuel pin was divided into six 60° azimuthal sectors, each with its own flow channel. Each azimuthal sector was divided into eight equally spaced radial nodes and 14 equal axial nodes; seven in the fueled region of the pin and seven above the fuel column.

Relative radial and axial power shapes were taken from Ref. 24 and are listed in Table A.3. Use of a nonzero gap conductance in the axial node of the insulator pellet allows for some axial heat loss from the top of the column. Miscellaneous physical and thermal input parameters are listed in Table A.4. The power-driving function for the fuel is given in Fig. 4 for Test H2 and in Fig. 5 for Test E4.

A sensitivity study reported by Hughes showed that the outlet temperature is sensitive to the duct-wall thickness, but not to heat transfer between the fuel holder and loop wall. COBRA allows but one input value for each parameter. As a consequence, the heat losses in the upper structure of the flow channel are underestimated, and the average calculated outlet temperature is higher than that measured. This could account for at least a part of the difference noted in the experiments (see Figs. 13 and 46). High operating pressures are used to suppress boiling because of the difficulty in treating two-phase heat transfer (see discussion in Sec. III.D).

TABLE A.1. Sodium Properties

Press. (psi)	Temp. (°F)	Liquid Specific Volume (ft³/lb)	Vapor Specific Volume (ft³/lb)	Liquid Enthalpy (btu/lb)	Vapor Enthalpy (btu/lb)	Liquid Viscosity (lb/hr-ft)	Liquid Thermal Cond. (btu/ft-°F)	Liquid Surface Tension (lb/ft)
0.000	590.00	0.01825	999999.0000	331.90	2220.52	0.81430	43.95000	0.01204
0.001	650.00	0.01842	409866.C000	350.49	2227.58	0.75580	42.98000	0.01181
0.003	700.00	0.01856	178122.0000	365.88	2234.13	0.71380	42.17999	0.01162
0.007	750.00	0.01870	83102.0000	381.19	2240.18	0.67670	41.39000	0.01143
0.014	800.00	0.01885	41266.0000	396.43	2245.77	0.64370	40.62000	0.01124
0.024	840.00	0.01897	24533.0000	408.58	2249.94	0.61980	40.00000	0.01109
0.040	880.00	0.019C9	15060.0000	420.69	2253.87	0.59800	39.39000	0.01094
0.065	920.00	0.01921	9519.0000	432.77	2257.57	0.57750	38.78999	0.01078
0.082	940.00	0.01927	7645.0000	438.80	2259.35	0.56830	38.50000	0.01071
0.100	960.00	0.01933	6180.0000	444.83	2261.09	0.55920	38.20000	0.01063
0.130	980.00	0.01940	5026.0000	450.85	2262.78	0.55040	37.90999	0.01056
0.160	1000.00	0.01946	4111.0000	456.86	2264.44	0.54190	37.60999	0.01048
0.200	1020.00	0.01952	3382.0000	462.87	2266.06	0.53380	37.42000	0.01040
0.240	1C40.00	0.01959	2798.C000	468.88	2267.65	0.52590	37.03000	0.01033
0.290	1060.00	0.01965	2326.0000	474.88	2269.22	0.51830	36.73999	0.01025
0.350	1080.00	0.01971	1944.0000	480.88	2270.75	0.51100	36.45999	0.01017
0.470	1100.00	0.01978	1632.0000	486.88	2272.27	0.50390	36.17000	0.01010
0.540	1120.00	0.01985	1376.0000	492.87	2273.76	0.49700	35.89000	0.01002
0.610	1140.00	0.01991	1166.0000	498.87	2275.24	0.49040	35.60999	0.00995
0.720	1160.00	0.01998	992.0000	504.86	2276.70	0.48400	35.32999	0.00987
0.850	1180.00	0.02005	847.0000	510.86	2278.15	0.47780	35.04999	0.00979
1.000	1200.00	0.02011	727.C000	516.85	2279.60	0.47170	34.78000	0.00972
2.100	1300.00	0.02046	356.0000	546.85	2286.72	0.44420	33.42000	0.00934
4.200	1400.00	0.02082	189.1000	576.95	2293.86	0.42040	32.10999	0.00896
7.800	1500.00	0.02119	107.4000	607.21	2301.10	0.39950	30.84000	0.00857
14.000	1600.00	0.02157	64.6300	637.70	2308.47	0.38110	29.60999	0.00819
22.000	1700.00	0.02197	41.2500	668.49	2316.95	0.36470	28.42000	0.00781
34.000	1800.00	0.02238	27.4000	699.65	2325.24	0.35010	27.26999	0.00743
51.000	1900.00	0.02281	18.8700	731.24	2333.38	0.33680	26.17000	0.00705
320.000	2500.00	0.02575	3.4400	933.78	2371.86	0.27850	20.42000	0.00476

TABLE A.2. Fuel and Cladding Properties

Temp, °F	Thermal Conductivity, Btu/hr-ft-°F	Specific Heat, Btu-lb-°F	Temp, °F	Thermal Conductivity, Btu/hr-ft-°F	Specific Heat, Btu-lb-°F
	Cladding and Duct Wall			**Fuel**	
70	8.32	0.108	77	4.10	0.0419
300	9.35	0.120	800	2.08	0.0573
600	10.70	0.128	1520	1.42	0.0707
700	11.15	0.130	2060	1.18	0.0797
800	11.60	0.132	2780	1.03	0.0902
900	12.05	0.134	3500	0.99	0.0991
1000	12.50	0.137	4040	1.03	0.1046
1100	12.95	0.139	4400	1.09	0.1078
1200	13.40	0.141	4760	1.17	0.1106
1300	13.85	0.144	5000	1.23	0.1122
1400	14.30	0.147	5100	1.50	0.1200
2500	14.30	0.147	8000	1.50	0.1200

Cladding-expansion Coeff. $= 9.0 \times 10^{-6} + 1.17 \times 10^{-9}T$ Fuel-expansion Coeff. $= 3.764 \times 10^{-6} + 9.15 \times 10^{-10}T$

TABLE A.3. Pin Power Shapes and Gap Conductance

r_{inner}, in.	r_{outer}, in.	Relative Power	r_{inner}, in.	r_{outer}, in.	Relative Power
0	0.0125	0.804	0.0875	0.1	1.109
0.0125	0.025	0.822	0.1	0.103	0
0.025	0.0375	0.850	0.103	0.106	0
0.0375	0.05	0.896	0.106	0.109	0
0.05	0.0625	0.942	0.109	0.113	0
0.0625	0.075	1.016	0.113	0.115	0
0.075	0.0875	1.072			

Axial Node	Z_{lower}, in.	Z_{upper}, in.	Material	Relative Power	Gap Conductance, Btu/hr-ft²-°F Initial	Maximum
1	0	1.928	Fuel	0.861	750	5500
2	1.928	3.857	Fuel	0.956	750	5500
3	3.857	5.786	Fuel	0.976	750	5500
4	5.786	7.714	Fuel	1.00	750	5500
5	7.714	9.643	Fuel	1.013	750	5500
6	9.643	11.571	Fuel	1.033	750	5500
7	11.571	13.5	Fuel	1.995	750	5500
8	13.5	15.429	Insulator	0	750	5500
9-14	15.429	27.0	Pin plenum	0	0	0

TABLE A.4. Miscellaneous Physical and
Thermal Input Parameters

Flow area[a]	0.0068 in.^{2}
Wetted perimeter[a]	0.3121 in.
Heated perimeter[a]	0.1204 in.
Hydraulic diameter[a]	0.0871 in.
Fuel density[b]	605 lb/ft^3
Holder-wall thickness[a]	0.031 in.
Heat transfer to wall	100 Btu/hr-ft^2-°F
Crossflow resistance factor	0.5 lb/sec-ft
Gap-jump distance[c]	0.0006 in.
Operating pressure[d]	300 psi

[a]Per channel. See Figs. 7 and 8.
[b]Fuel-pellet density ($r_0 = 0.097$ in.) is 642 lb/ft^3;
  smeared density ($r_0 = 0.100$ in.) is listed. See Table II.
[c]Effective average gap with fuel pellet in contact with
  cladding.
[d]A high value is chosen to suppress early boiling. These
  amounts for high outlet temperatures shown in Figs. 13
  and 45.

ACKNOWLEDGMENTS

REFERENCES

1. *Reactor Development Program Progress Report: April-May 1970*, ANL-7688, p. 226 (July 14, 1970).

2. *Reactor Development Program Progress Report: June 1970*, ANL-7705, p. 179 (Aug 4, 1970).

3. *Reactor Development Program Progress Report: July 1970*, ANL-7726, p. 150 (Aug 27, 1970).

4. *Reactor Development Program Progress Report: October 1970*, ANL-7753, p. 147, p. 154 (Nov 24, 1970).

5. *Reactor Development Program Progress Report: February 1971*, ANL-7783, p. 104 (Mar 22, 1971).

6. *Reactor Development Program Progress Report: April-May 1971*, ANL-7825, p. 8.16 (June 23, 1971).

7. *Reactor Development Program Progress Report: August 1971*, ANL-7854, p. 8.16 (Sept 23, 1971).

8. *Reactor Development Program Progress Report: December 1971*, ANL-7900, p. 8.16 (Jan 28, 1972).

9. *Reactor Development Program Progress Report: July 1973*, ANL-RDP-18, p. 7.42 (Aug 29, 1973).

10. *Reactor Development Program Progress Report: August 1970*, ANL-7737, p. 168 (Sept 29, 1970).

11. *Reactor Development Program Progress Report: October 1970*, ANL-7753, p. 150 (Nov 24, 1970).

12. *Reactor Development Program Progress Report: December 1970*, ANL-7765, p. 94 (Jan 19, 1971).

13. *Reactor Development Program Progress Report: January 1971*, ANL-7776, p. 107 (Feb 19, 1971).

14. *Reactor Development Program Progress Report: March 1971*, ANL-7798, p. 126 (Apr 19, 1971).

15. *Reactor Development Program Progress Report: June 1971*, ANL-7833, p. 817 (July 26, 1971).

16. *Reactor Development Program Progress Report: March 1973*, ANL-RDP-15, p. 9.35 (Apr 26, 1973).

17. *Reactor Development Program Progress Report: July, 1973*, ANL-RDP-18, p. 7.36 (Aug 29, 1973).

18. A. W. Cronenberg, *A Thermodynamic Model for Molten UO_2-Na Interaction Pertaining to Fast-reactor Fuel-failure Accident*, ANL-7947 (June 1972).

19. A. B. Rothman et al., Trans. Am. Nucl. Soc. *13*, 652 (1970).

20. R. C. Doerner et al., Trans. Am. Nucl. Soc. *14*, 279 (1971).

21. C. E. Dickerman et al., "Fuel Dynamics Experiments on Fast Reactor Oxide Fuel Performance under Transient Heating Condition Using the TREAT Reactor," *Am. Nucl. Soc. Proc. Fast Reactor Fuel Element Technology*, April 13-15, 1971, New Orleans, La, p. 643 (1971).

22. *Reactor Development Program Progress Report: August 1974*, ANL-7845, p. 8.4 (Aug 20, 1971).

23. R. E. Henry et al., *Cladding Relocation Experiments*, Trans. ANS *18*, 209 (June 1974); M. A. Grolmes et al., *Flooding Correlation for Sodium and Cladding Motion in Subassembly Voiding*, ibid., p. 209.

24. E. P. Hicks and D. C. Menzies, "Theoretical Studies on the Fast Reactor Maximum Accident," *Proc. of the Conf. on Safety, Fuels, and Core Design in Large Fast Power Reactors: October 11-14, 1965*, ANL-7120, pp. 654-670 (1965).

25. A. M. Judd, *Calculations of the Thermodynamic Efficiency of Molten Fuel Coolant Interactions*, Trans. Am. Nucl. Soc. *13*, 369 (1970).

26. A. Padilla, *Energy Release Mechanisms*, BNWL-SA-3093, XVII, 1-49 (Mar 1970).

27. A. Padilla, *Transient Analysis of Fuel-Sodium Interaction*, Trans. Am. Nucl. Soc. *13*, 375 (1970).

28. R. B. Duffey, *Channel Voiding due to Fuel-Coolant Interaction in Sodium Cooled Fast Reactors; A Theoretical Model*, Central Electricity Generating Board, RD/B/N1609, Berkley, England (1970).

29. D. H. Cho and R. W. Wright, *A Rate-Limited Model of Molten Fuel-Coolant Interaction*, Trans. Am. Nucl. Soc. *13*, 658 (1970).

30. R. W. Wright and D. H. Cho, *Acoustic and Initial Constraint in Molten Fuel-Coolant Interaction*, Trans. Am. Nucl. Soc. *13*, 658 (1970).

31. A. W. Cronenberg and H. K. Fauske, UO_2 *Solidification Phenomena and Fragmentation During Quenching in Sodium Coolant*, Trans. ANS *18*, 213 (June 1974).

32. R. W. Ostensen et al., *Fuel Flow and Freezing in the Upper Subassembly Structure Following an LMFBR Disassembly*, Trans. ANS *18*, 214 (June 1974).

33. A. E. Waltar to L. W. Deitrich, *private communication* (June 1974).

34. G. A. Freund, P. Elias, D. R. MacFarlane, J. D. Geier, and J. F. Boland, *Design Summary Report on the Transient Reactor Test Facility (TREAT)*, ANL/6034 (June 1960).

35. C. E. Dickerman, *Kinetics of the Transient Reactor Test Facility (TREAT)*, *Reactor Kinetics and Control*, AEC Symp. Ser. 419, USAEC, Oak Ridge (1964).

36. F. Kirn, J. Boland, H. Lauroski, and R. Cook, *Reactor Physics Measurements in TREAT*, ANL-6173 (Oct 1960).

37. H. P. Iskenderian, *Post Criticality Studies on the TREAT Reactor*, ANL-6115 (Feb 1960).

38. L. E. Robinson, R. T. Purviance, and K. J. Schmidt, *The Mark-II Integral Sodium TREAT Loop*, ANL-7692 (Nov 1971).

39. L. E. Robinson, R. T. Purviance, and K. J. Schmidt, *The Mark-II Integral Sodium TREAT Loop*, Trans. Am. Nucl. Soc. *13*(1), 354 (1970).

40. L. E. Robinson and R. D. Carlson, *The Development of Pumps for Use in Fast-reactor-safety Integral-loop Experiments*, ANL-7369 (Apr 1968).

41. *Reactor Development Program Progress Report: December 1969*, ANL-7655, p. 133 (Jan 29, 1970).

42. A. B. Rothman et al., *Neutron Filter for TREAT Safety Studies on Fast Reactor Fuels*, Trans. Am. Nucl. Soc. *13*, 356 (1970).

43. *Reactor Development Program Progress Report: January 1970*, ANL-7661, p. 126 (Feb 25, 1970).

44. *Reactor Development Program Progress Report: March 1970*, ANL-7679, p. 154 (Apr 27, 1970).

45. L. E. Robinson and R. T. Purviance, "Transient Response of Stand-off Pressure Transducer Assemblies on the Transient Reactor Test (TREAT) Facility Integral Sodium Loop," *Reactor Physics Division Annual Report: July 1, 1965 to June 30, 1966*, ANL-7210, p. 254 (Dec 1966).

46. L. W. Deitrich, *Evaluation of Energy Conversion in TREAT Mark-II Loop Experiments*, Trans. Am. Nucl. Soc. *14*, 278 (1971).

47. J. C. Carter, *Reactor Development Program Progress Report: January 1974*, ANL-RDP-24, p. 7.23 (Feb 27, 1974).

48. W. W. Marr and R. M. Crawford, *Thermal-Hydraulic Analysis of Multipins In-Pile Experiments*, Trans. Am. Nucl. Soc. *12*, 868 (1969).

49. D. S. Rowe, *COBRA-IIIB: A Digital Computer Program for Steady-State and Transient Thermal-Hydraulic Analysis of Rod Bundle Nuclear Fuel Elements*, BNWL-B-82.

50. G. H. Golden and J. V. Tokar, *Thermophysical Properties of Sodium*, ANL-7323 (Aug 1967).

51. Hanford Engineering Development Laboratory, unpublished information (1971).

52. *Design Guide for LMFBR Sodium Piping*, SAN-781-1, C. F. Brown and Co. Report CFB-4122-1 (Feb 1, 1971).

53. B. F. Rubin, *Summary of (U, Pu)O$_2$ Properties and Fabrication Methods*, GEAP-13582 (Nov 1970).